Spring 2012

# Nonosecond Pulsed Electric Field Induced Changes in Dielectric Properties of Biological Cells

Jie Zhuang
*Old Dominion University*

# NANOSECOND PULSED ELECTRIC FIELD INDUCED CHANGES

# IN DIELECTRIC PROPERTIES OF BIOLOGICAL CELLS

by

Jie Zhuang
B.S. June 2004, Xiamen University, China
M.S. December 2006, Peking University, China

A Dissertation Submitted to the Faculty of
Old Dominion University in Partial Fulfillment of the
Requirements for the Degree of

DOCTOR OF PHILOSOPHY

ELECTRICAL AND COMPUTER ENGINEERING

OLD DOMINION UNIVERSITY
May 2012

Approved by:

Juergen F. Kolb (Director)

Karl H. Schoenbach (Member)

Ravindra P. Joshi (Member)

Ali Beskok (Member)

# ABSTRACT

## NANOSECOND PULSED ELECTRIC FIELD INDUCED CHANGES IN DIELECTRIC PROPERTIES OF BIOLOGICAL CELLS

Jie Zhuang
Old Dominion University, 2012
Director: Dr. Juergen F. Kolb

Nanosecond pulsed electric field induced biological effects have been a focus of research interests since the new millennium. Promising biomedical applications, e.g. tumor treatment and wound healing, are emerging based on this principle. Although the exact mechanisms behind the nanosecond pulse-cell interactions are not completely understood yet, it is generally believed that charging along the cell membranes (including intracellular membranes) and formation of membrane pores trigger subsequent biological responses, and the number and quality of pores are responsible for the cell fate. The immediate charging response of a biological cell to a nanosecond pulsed electric field exposure relies on the dielectric properties of its cellular components. Conversely, intense nanosecond pulses will change these properties due to conformational and functional changes. Hence, an understanding of biodielectric phenomena is necessary to explain the underlying interaction mechanisms between nanosecond pulses and biological materials.

To this end, we have investigated the changes in dielectric characteristics of biological cells and tissues after exposure to multiple nanosecond pulses. Significant differences have been observed in dielectric properties and membrane integrity of Jurkat cells for exposures to nanosecond and microsecond pulsed electric fields despite delivery of the same energy, suggesting different pore formation and development mechanisms. The effect of nanosecond pulsed electric fields on the dielectric properties of Jurkat cells is

long-lasting which is consistent with predictions of much longer pore resealing times for shorter pulses. Strong correlation between short-term plasma membrane conductivity and long-term cell survival has also been observed for different nanosecond-exposure conditions. Together with the studies on tissues, we demonstrate that dielectric spectroscopy is capable of assessing conformational and possibly functional changes of cells after exposure to nanosecond pulsed electric fields on biologically relevant time scales, and in turn, evaluate and compare the efficacy of chosen pulse parameters.

To my parents Jihua Zhuang and Shufeng Zhao,

and my wife, Xiaoyan Sun

# ACKNOWLEDGMENTS

I am sincerely and heartily grateful to my advisor, Dr. Juergen F. Kolb, for his patience and guidance through the course of my study at the Center for Bioelectrics. His insight and enthusiasm in research has set a great example for me follow. I would like to acknowledge all of my committee members, Dr. Karl H. Schoenbach, Dr. Ravindra P. Joshi and Dr. Ali Beskok, for their suggestions and advice on my research. This dissertation would not have been accomplished without their efforts.

I am truly appreciative to Ahmet C. Sabuncu for the inspiring discussions and friendship which has been invaluable on both an academic and a personal level. I thank James T. Camp, Dr. Yu Jing and Dr. Wei Ren for their support on my research. Special thanks to Barbara Carroll for all the help she has provided starting from my first day at Center for Bioelectrics.

I am indebted to my parents and my wife for their supports and understanding.

# TABLE OF CONTENTS

# LIST OF TABLES

# LIST OF FIGURES

# CHAPTER 1

## INTRODUCTION

### 1.1    Overview

Pulsed electric fields (PEFs) are capable of inducing significant conformational and functional changes in biological cells and tissues when the pulse parameters reach certain criteria. After exposure to PEFs of a few kV/cm for durations of microseconds or milliseconds, the cell membrane becomes permeable to ions and large molecules, which are generally excluded from cells with an intact membrane. The phenomenon is often described by the formation of pores and the method as electroporation, accordingly [1]. For moderate field strengths the change in membrane permeability is transient and eventually reversible, i.e. reversible electroporation. Hence, the technique has been used to enable and facilitate the transport of large molecules, drugs and proteins into the cell [1-5]. New therapeutic approaches targeting solid tumors in particular are currently being developed on this principle [6-13]. Stronger electric fields of similar duration will result in the irreversible loss of membrane integrity, i.e. irreversible electroporation, and consequently, cell death [14]. Applications of these more intense electroporation conditions have also been explored as a method for decontamination and sterilization [15] and are under investigation as a tissue ablation alternative [16]. For even higher field strengths, but exerted for shorter durations in the nanosecond range, the creation of smaller nanopores has been predicted for cell and organelle membranes [17]. Recent experiments support these findings at least for the plasma membrane [18-20]. Furthermore, observations, such as the release of calcium from internal stores [21, 22] and dye uptake into the nucleus [23], agree with a similar effect on subcellular

membranes. As a possible consequence or concurrent outcome, such nanosecond pulsed electric fields (nsPEFs) are capable of manipulating cellular mechanisms and trigger apoptosis [24]. Accordingly, this approach has demonstrated remarkable potential for the treatment of solid tumors [25]. An overview of different biological effects that have been observed and studied in response to pulsed electric fields is presented in Figure 1.
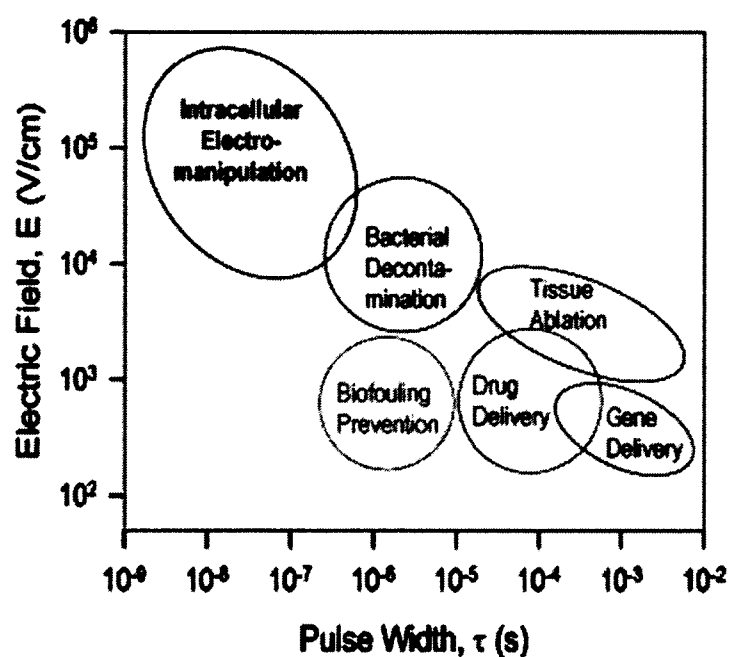


**Figure 1.** Biological effects for exposures to pulsed electric fields of different durations and amplitudes. All indicated applications rely on the administration of multiple pulses.

Any response to an electric field is fundamentally promoted by polarization mechanisms along interfaces of different dielectric properties, foremost along membranes. It has been shown both theoretically and experimentally that longer duration pulsed electric fields of microseconds ($\mu$sPEFs) with slow rise times and lower field

strengths primarily affect the plasma membrane, while nsPEFs can effectively reach into a cell and also charge the membranes of organelles [26]. Such difference in membrane charging is mostly determined by the charging time constant of cell membranes, which strongly depends on the dielectric properties of the cell and its constituents [27]. In other words, the initial charging behavior of a cell to a pulsed electric field may be predicted when the cell geometry and the dielectric properties (conductivity and permittivity) of all constituents (supernatant, membrane, and cytoplasm) are known [28-32]. If the applied pulse electric field is strong enough, transmembrane voltages will be charged above a critical value which results in conformational changes to the membranes, e.g. formation of membrane pores. These conformational changes will inevitably change the dielectric properties [33, 34]. Accordingly, measurements of these parameters, particularly the temporal development of changes, can help to predict the effect of exposures and assess possible outcomes. This offers the possibility to evaluate and optimize treatment modalities, for example for tumor therapies, and develop disease-specific or even patient-specific protocols. Thus far, a lot of modeling and simulation approaches predicting the interactions between pulsed electric fields and biological materials require values of the sample's dielectric properties as input [35, 36].

## 1.2    Motivations for This Research

Although PEFs are now commonly used in applications, exact mechanisms of the interactions between cells and pulsed electric fields are still not totally understood. Theoretical models have been established to predict the charging and poration of cell membranes when the cell geometry and the dielectric properties of all constituents are known [28-32]. However, there are still significant gaps between theoretical simulations

and PEF-related biomedical applications: 1. Biological studies almost exclusively rely on the applications of multiple pulses, while mechanisms are mostly only discussed for single exposures. 2. Analytical and numerical models fail to describe the evolution of pores or membrane reassembly for the exposure to multiple pulsed electric fields. 3. Unknown dielectric characteristics of cells don't allow theoretical models and discussions of effects on cell membranes to be conducted with respect to differences in cell lines. Therefore, protocols for pulsed electric field treatments are still optimized empirically [37].

A deeper understanding of the responses of biological cells and tissues to multiple exposures with nsPEFs requires experimental approaches. The investigations of this research will pick up theoretical predictions and test them on cell suspensions and tissues. Instead of relying on generic parameters, we will be able to determine the specific dielectric parameters of different cells and hence account for differences in membrane compositions and configurations. The knowledge of the dielectric parameters of cell constituents and their changes after nsPEF-exposures would be crucial to explain the observed differences in charging characteristics. In this study the dielectric evolution of cells and tissues to multiple pulses, which are mostly used to study biological responses, will be recorded. Measurements of membrane permeability and cell viability will also be conducted as they would help associate the cell dielectric modifications with the conformational and functional responses [27]. These investigations in turn can provide important benchmarks for modeling and simulation studies. Theoretical models will benefit from these results and may eventually be able to predict the most effective delivery parameters with pulsed electric fields for different applications.

## 1.3    Objectives and Scope

The objectives of this research include: 1. Develop a comprehensive approach which can be used to obtain the dielectric properties of cell constituents. Experimental techniques and theoretical models, including time domain dielectric spectroscopy, measuring sensor design, sample preparation and dielectric spectrum analysis, will be combined into this approach. This way we will be able to derive the dielectric characteristics of several different cell lines and perform comparison. 2. Record the dielectric evolution of biological cells after multiple nsPEF-exposures by means of aforementioned approach. The changes in dielectric properties of mammalian cells exposed to pulses of different pulse duration, pulse amplitude will be studied. 3. Correlate nsPEF-induced changes in dielectric properties of cells with the changes in plasma membrane integrity and long-term cell survival. The feasibility of using dielectric spectroscopy as a non-invasive and fast monitoring technique to predict the efficacy of PEF-related treatment will be discussed. 4. Probe the effect of nsPEFs on the dielectric properties of tissues and explore the relationship with conformational changes of cells.

In Chapter 2 of this dissertation, the fundamental knowledge to understand the dielectric phenomena in biological materials is introduced. Selected experimental results of nsPEF-induced biological responses are presented. A review of existing studies regarding the effects of PEFs on the impedance and dielectric properties of biological cells and tissues is also included in this chapter. The detailed descriptions of experimental methods and data analysis strategies are given in Chapter 3, including the technical details of performing time domain dielectric spectroscopy on biological materials and derivation of complex permittivity of cellular structures using dielectric mixture and cell

models. Chapter 4 contains experimental results obtained in this research. In Chapter 5, the outcomes of this study are compared with previous studies and the possible indications are discussed. Finally, conclusions of this study and future directions are provided in Chapter 6.

# CHAPTER 2

## BACKGROUND AND LITERATURE REVIEW

### 2.1 Dielectric Characteristics of Biological Cells and Tissues

In this section, a short overview of the linear passive dielectric properties of biological materials, i.e. properties which are independent of the assessing magnitude of the fields, is provided. First, basic concepts of the dielectric theory and widely adopted relaxation functions, such as the Debye relaxation function, are introduced. The typical dielectric phenomena and fundamental dielectric mechanisms of biological cells and tissues are covered. Then the commonly used dielectric measurement techniques are discussed and dielectric spectroscopy is highlighted. Finally, previous studies on dielectric properties of biological cells and tissues are briefly reviewed.

### 2.1.1 Introduction

The term "dielectric" was first introduced by William Whewell after a request from Michael Faraday to describe a material through which (greek—"dia" = through) an electric field passes. Maxwell laid a firm theoretical foundation of dielectric theory [38]. The dielectric properties of a material are characterized by conductivity ($\sigma$, in S/m) and permittivity ($\varepsilon$, in F/m), both are intrinsic properties. Conductivity describes the material's ability to conduct electric current, whereas permittivity, often referred as dielectric constant, is the material's ability to polarize or to store electric charges. The dielectric properties, permittivity and conductivity, of a dielectric material depend on many factors such as temperature, pressure and frequency. The frequency dependence, or dielectric spectrum, of a dielectric material is usually modeled by relaxation functions.

For instance the dielectric spectrum of water up to microwave frequencies can be

expressed by a single Debye relaxation function [39] as

$$\varepsilon^*(\omega) = \varepsilon_h + \frac{\varepsilon_l - \varepsilon_h}{1 + j\omega\tau_r} + \frac{\sigma_{dc}}{j\omega\varepsilon_0}$$

,                                                                                          (1)

where $\omega$ is the angular frequency, $j$ is $(-1)^{1/2}$, $\varepsilon^*(\omega)$ is the complex permittivity of water,

$\varepsilon_h$ is the high frequency relative permittivity, $\varepsilon_l$ is the low frequency relative permittivity,

$\varepsilon_0$ is the permittivity of free space, $\tau_r$ is the so-called relaxation time of water dipoles and

$\sigma_{dc}$ is the ionic conductivity which is very small for pure water. Figure 2 shows the

dielectric spectrum of water derived from equation (1).
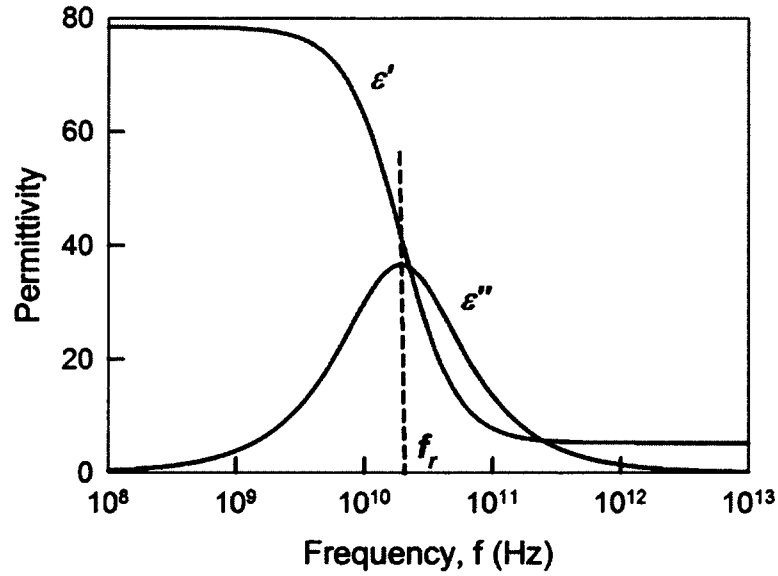


**Figure 2.** A typical Debye Relaxation response for deionized water. $\varepsilon_l = 78.36$ $\varepsilon_h = 5.2$, $\tau_r = 8.27$ps.

Typically the dielectric properties of biological materials display extremely high permittivities at low frequencies, which fall off in relatively distinct steps as the excitation frequency is increased. These dispersions were first observed by Schwan and named $\alpha$-, $\beta$- and $\gamma$-dispersion [40]. Each type of dispersion can be attributed to a different polarization mechanism. Cell suspensions usually exhibit a significant $\beta$-dispersion in the frequency range from 10 kHz to 100 MHz. This is explained by the combined response of bound and free charges at the interface between the plasma membrane and intra- or extracellular electrolyte as described by the Maxwell-Wagner effect, which links the suspension dielectric spectrum to the dielectric properties of the supernatant and individual cells [41]. By combining the Maxwell-Wagner mixture model with descriptions for the cell, properties of fundamental cell constituents, such as the membrane and cytoplasm, can be determined. In the single shell model, the cell is described as a homogeneous conducting sphere enclosed in a highly resistive thin shell. By fitting a measured cell suspension dielectric spectrum to the mixture and shell model, the dielectric properties of the plasma membrane and cytoplasm can be obtained as fitting parameters. The characteristics of subcellular structures can be assessed by expanding the method further and include organelles such as the nucleus, for example, in a double shell model.

### 2.1.2 Measurement Techniques

A number of methods have been developed to study the dielectric properties of cell suspensions and cellular structures, including patch-clamp[20], electromechanical techniques[42], optical techniques [43], voltage-current method [44] and dielectric spectroscopy [45]. Dielectric spectroscopy has certain advantages over the other

techniques: 1. Permittivities and conductivities are frequency dependent and can be measured over a wide range from $10^{-6}$ Hz to $10^{12}$ Hz [46]. The frequency dependent characteristic is especially of interest for an understanding of effects caused by different rise times of a PEF exposure. 2. The analysis of a large number of cells (typically $10^6$-$10^7$) provides well-defined averages for specific cell lines and conditions. 3. The method is especially sensitive to interfacial polarization at membranes, which is determined by the dielectric characteristics of cell membranes. 4. Measuring sensors can be designed purposefully for different sample types and characteristics (e.g., cell suspensions or tissues), allowing measurements to be conducted non-invasively both in vitro and in vivo [47]. Hence, cells and cell parameters are not altered by the diagnostic method and are available for further investigations on the characterized cells.

Dielectric spectroscopy can be performed in either frequency domain or time domain. In frequency domain, impedance analyzer and LCR meter are mostly used for lower frequency and vector network analyzer is suitable for higher frequency range. For time domain measurement, a time domain spectrometer capable of generating fast rise time step function is usually used. Figure 3 shows an overview of the equipments and test fixtures required in dielectric spectroscopy covering a wide frequency range [48].
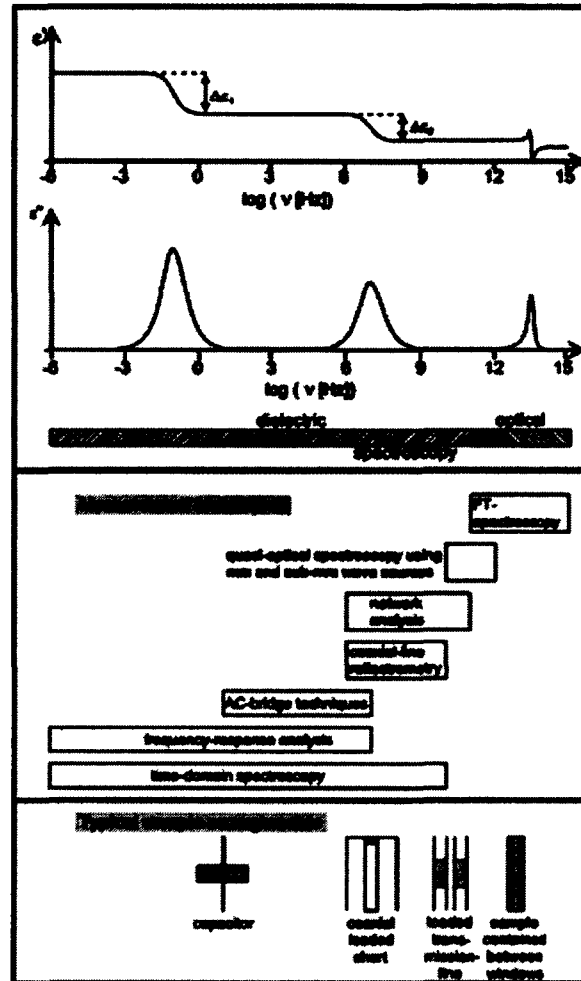
**Figure 3.** Survey of experimental techniques used in the frequency range from $10^{-6}$ to $10^{15}$ Hz [48].

## 2.1.3 Experimental Studies

The dielectric properties of biological cells and tissues have been studied extensively for more than a century. Dielectric properties of cell and tissue can give important information about a cell's physiology, in particular the properties of the membrane and the cell interior [49, 50]. Historically, measurements of the dielectric properties of biological materials play a significant role in physiology and biophysics areas. Hobner

measured the electrical impedance of erythrocyte cell suspensions up to 10 MHz. He found that the impedance decreased with increasing frequency and concluded that the cells were composed of a cytoplasm of relatively low resistivity surrounded by a poorly conducting membrane [51]. Fricke conducted a theoretical and experimental analysis of the dielectric properties of red blood cell suspensions and obtained a value of 0.81 $pF/cm^2$ for the erythrocyte membrane capacitance [52]. He also used a value of 3 for the relative permittivity of the membrane and derived a value for its thickness of 3.3 nm which is within a factor of two of the values currently accepted [53-55]. Likewise, Cole and Baker observed an inductance during measurements of the AC electrical properties of squid axons [56]. This observation led to the concept of voltage-gated membrane pores which was the crucial mechanism of neurotransmission and was included in the Hodgkin-Huxley treatment [55, 57]. Schwan also made great contributions to the dielectric measurement and interpretation of cell suspensions and tissue after World War II [51]. He laid the foundation in this field and most of his experimental designs are still widely used today. Schwan's 1957 review on cells and cell suspensions is one of the earliest and most studied texts on the subject [40]. Thereafter the study of the dielectric properties of biological materials has been a very active and continuously expanding field of research. Studies in this field are increasingly leading to practical and commercial applications. For instance, the possible physiological effects caused by the absorption by tissues of non-ionizing electromagnetic radiation are becoming an area of intensive research. Hence the dielectric properties which determine the ways in which electromagnetic energy interacts with cells and tissues are also of importance. Abundant data on the dielectric properties of biological cells and tissues has been reported by many researchers, such as Pethig et al.

[51, 58], Stuchly et al. [59], Schwan and Foster [60, 61], Gabriel et al. [47, 62, 63]. Books containing the basic knowledge and data treatment theory of this subject are written by Cole [55], Grant et al. [64], Schanne and Ceretti [53], Pethig [65], Grimnes and Martinsen [66].

As an example, Feldman et al. investigated the dielectric properties of normal and malignant cell and derived the dielectric properties of each cellular structure using a double shell model [50]. The results are listed in Table 1, where $\varepsilon_m$ is the plasma membrane permittivity, $\sigma_m$ is the plasma membrane conductivity, $\varepsilon_{ne}$ is the nuclear envelope permittivity, $\sigma_{ne}$ is the nuclear envelope conductivity, $\sigma_{cp}$ is the cytoplasm conductivity, $\sigma_{np}$ is the nucleoplasm conductivity, $\varepsilon_{cp}$ is the cytoplasm permittivity, $\varepsilon_{np}$ is the nucleoplasm permittivity, $d_m$ is the thickness of the plasma membrane, $d_n$ is the thickness of the nuclear envelope, $R_n$ is the radius of the nucleus and $R_c$ is the radius of the cell.

Table 1. Dielectric Parameters of Cell Structural Parts [50]

| | $\varepsilon_m$ | $\sigma_m$ $10^{-6}$ S/m | $\varepsilon_{ne}$ | $\sigma_{ne}$ $10^{-3}$ S/m | $\sigma_{cp}$ S/m | $\sigma_{np}$ S/m |
|---|---|---|---|---|---|---|
| B-cells | | | | | | |
| B-normal | 12.8 ± 1.6 | 56 ± 29 | 106 ± 35 | 11.1 ± 7.2 | 1.31 ± 0.08 | 2.04 ± 0.29 |
| Magala | 11.4 ± 2.4 | 8.8 ± 0.7 | 72.5 ± 11.6 | 3.7 ± 0.9 | 0.55 ± 0.2 | 1.08 ± 0.03 |
| Farage | 9.8 ± 1.1 | 9.1 ± 1.4 | 60.3 ± 22.6 | 4.4 ± 2.5 | 0.48 ± 0.14 | 1.07 ± 0.43 |
| Raji | 8.8 ± 1.1 | 8.2 ± 0.6 | 79.9 ± 34.4 | 4.0 ± 1.6 | 0.58 ± 0.02 | 1.02 ± 0.25 |
| Bjab | 8.0 ± 0.7 | 11.0 ± 5.3 | 108 ± 35 | 2.1 ± 0.7 | 0.88 ± 0.11 | 1.39 ± 0.54 |
| Daudi | 7.2 ± 0.7 | 9.5 ± 1.4 | 66.1 ± 7.5 | 2.7 ± 0.3 | 0.85 ± 0.09 | 1.44 ± 0.35 |
| T-cells | | | | | | |
| T-normal | 11.1 ± 1.4 | 27.4 ± 6.2 | 85.6 ± 16.7 | 8.8 ± 0.6 | 0.65 ± 0.13 | 1.26 ± 0.27 |
| Peer | 9.5 ± 0.7 | 12.9 ± 3.6 | 61.6 ± 17 | 2.1 ± 0.6 | 0.81 ± 0.09 | 1.42 ± 0.2 |
| HDMAR | 7.4 ± 1.2 | 14.5 ± 4 | 101.2 ± 55.3 | 3.0 ± 0.2 | 0.88 ± 0.25 | 1.58 ± 0.28 |

Fitting procedure was performed on the assumption that $\varepsilon_{cp} = 60$, $\varepsilon_{np} = 120$, $d_m = 7$ nm, $d_n = 40$ nm, $R_n = R_c (0.6)^{1/3}$.

## 2.2 nsPEF-induced Conformational and Functional Changes in Biological Cells and Tissues

There are concrete experimental evidences that nsPEF is capable of inducing significant conformational and functional changes to biological cells and tissue such as poration of cell and organelle membranes, triggering intracellular calcium release and induction of apoptosis. However some mechanisms are extremely difficult to investigate with current experimental techniques. Fortunately valuable information regarding the PEF-cell interactions, e.g. generation, distribution and evolution of membrane pores, may be provided by theoretical models which promotes not only deeper understanding of underlying mechanisms but also better experimental designs. In this section, experimental evidences of nsPEF-induced conformational and functional changes in biological cells

and tissues are briefly reviewed. Theoretical models and predictions of the PEF-cell interactions are also introduced.

### 2.2.1 Selected Experimental Observations

The conformational changes in plasma membrane induced by nsPEFs are significantly different from that induced by longer pulses in microsecond or millisecond range. In order to detect the formation of membrane pores, membrane integrity markers, such as trypan blue, propidium iodide (PI), and ethidium homodimer, are usually used. When exposed to relatively long (microsecond) pulses, the uptake of membrane integrity markers typically follows the onset of the pulsed electric fields rapidly, suggesting large pores are formed in plasma membrane. The resealing time of reversible electroporation is generally on the order on milliseconds to seconds. Conversely the effects of nanosecond pulses on the plasma membrane are often delayed. For instance, Chen et al. studied the uptake of PI by HL-60 cells after exposure to a single 60 ns, 65 kV/cm pulse [23]. Figure 4 shows the time course of the PI fluorescence intensity of a HL-60 cell after exposure [23]. It is interesting that the increase in fluorescence is observed only after approximately 12 minutes and then completed in one minute. This indicates that the formation of pores large enough to allow passage of PI is a secondary effect, following the formation of nanopores, which occurs on a nanosecond timescale. It is likely that the nanopores are too small to allow PI uptake immediately and the delayed PI uptake is due to membrane failure as in-vitro-necrosis, secondary to apoptosis. Other studies on Jurkat cells and HCT116 cells showed that the delayed formation of large membrane pores might be "reversible" and the recovery time could be as long as 5 hours [67, 68].

Therefore uptake of these membrane integrity dyes may not necessarily indicate cell death when cells are exposed to nanosecond pulses.
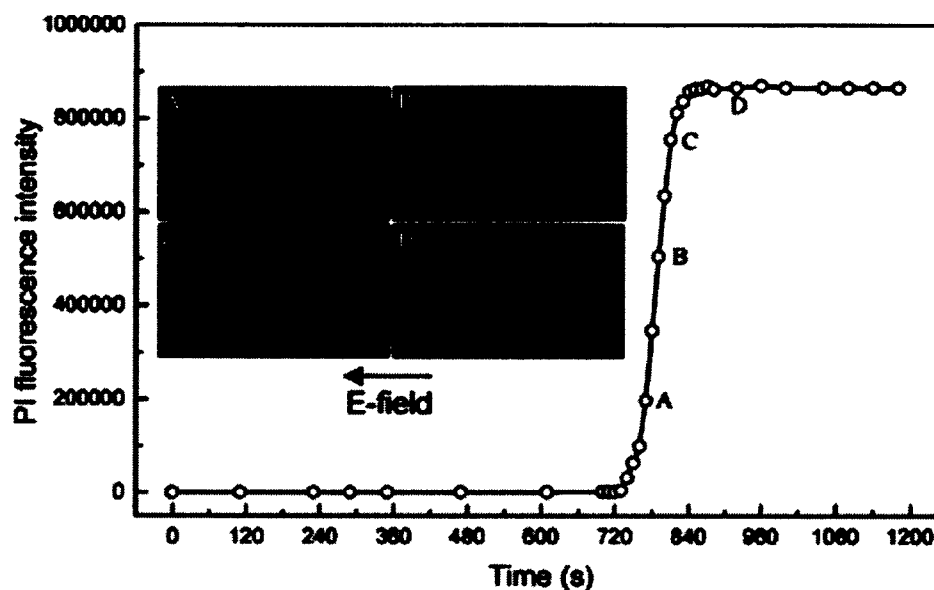


**Figure 4.** Microscopic real-time image tracings of a typical cell undergoing PI uptake. Images were taken at (A) 770 s, (B)790 s, (C) 810 s, and (D) 920 s following a 60 ns, 26 kV/cm electric pulse. The porated cells saturated quickly by PI bound to DNA. Electric field orientation is marked. PI uptake is randomly nonpolarized [23].

The first experimental evidence that nsPEFs can selectively porate the intracellular membranes without severely compromising the plasma membrane integrity was reported by Schoenbach and co-workers at Old Dominion University [26]. They found that 60 ns pulses with 50-kV/cm or higher field strength could breach the granule membranes while the plasma membrane remained impermeable to cytoplasmic calcein molecules. Later on researchers from the same group further explored the effect of short electrical pulses on the cell nucleus [23]. In this study, HL-60 cells stained with acridine orange (AO), a vital nuclear acid fluorescent dye, were exposed to a single 10 ns, 65 kV/cm pulse. The results

in Figure 5 show a decrease in fluorescence in the nucleus and an increase in fluorescence in the entire cytoplasm [69]. These results suggest that a single nanosecond pulse can cause an increase in the permeability of the nuclear envelope, with a subsequent outflow of labeled DNA. The outflow of DNA after nsPEF-exposure was also observed by Stacey et al. in Jurkat cells after exposure to a single 60 ns, 60 kV/cm pulse [70].
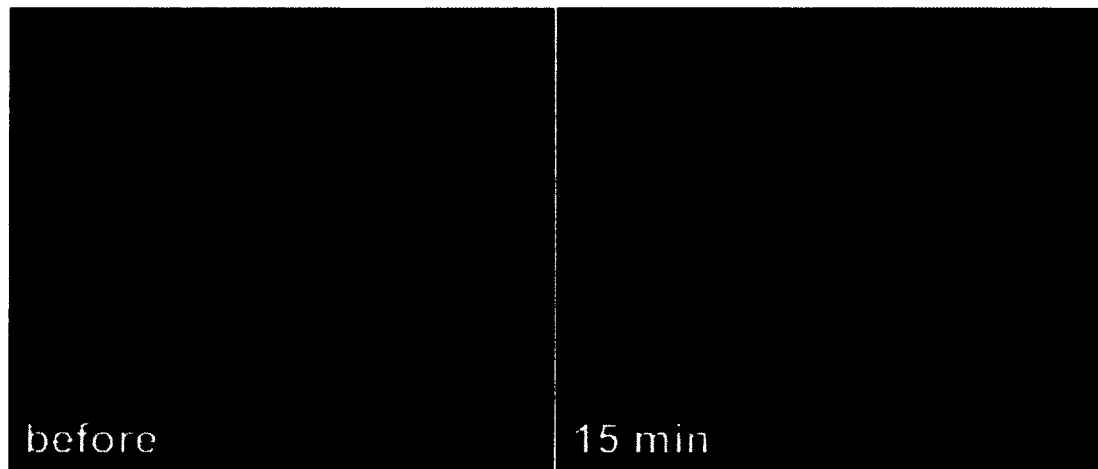
before                    15 min

**Figure 5.** Images of HL-60 cells before (a) and 15 min after (b) applying a 10-ns, 60-kV/cm pulse. The cells were stained with acridine orange (AO) a vital nuclear acid fluorescent dye [70].

The release of intracellular calcium triggered by nanosecond pulses has been reported by researchers from Old Dominion University and University of Southern California [21, 71, 72]. Scarlett et al. took a series of images of Jurkat cells, stained with the fluorescent marker Fluo-4 AM, before and after exposure to a 60-ns pulse of 100 kV/cm [21]. As shown in Figure 6a to Figure 6d, the temporal resolution was 18 ms and the spatial resolution was high enough to resolve the increase in $Ca^{2+}$ concentrations and identify

potential intracellular sources. The location of the endoplasmic reticulum (ER) was indicated by staining with Bodipy Brefeldin A 558/568 (Figure 6e). In the absence of extracellular $Ca^{2+}$, there was a continuous increase in calcium fluorescence intensity. A peak value 1.9 times higher than the baseline level was reached in approximately 2.4 s. About 15–20 s after pulse application the fluorescence intensity showed a sudden drop meanwhile the uptake of PI was significantly enhanced, suggesting formation of large membrane pores [21].
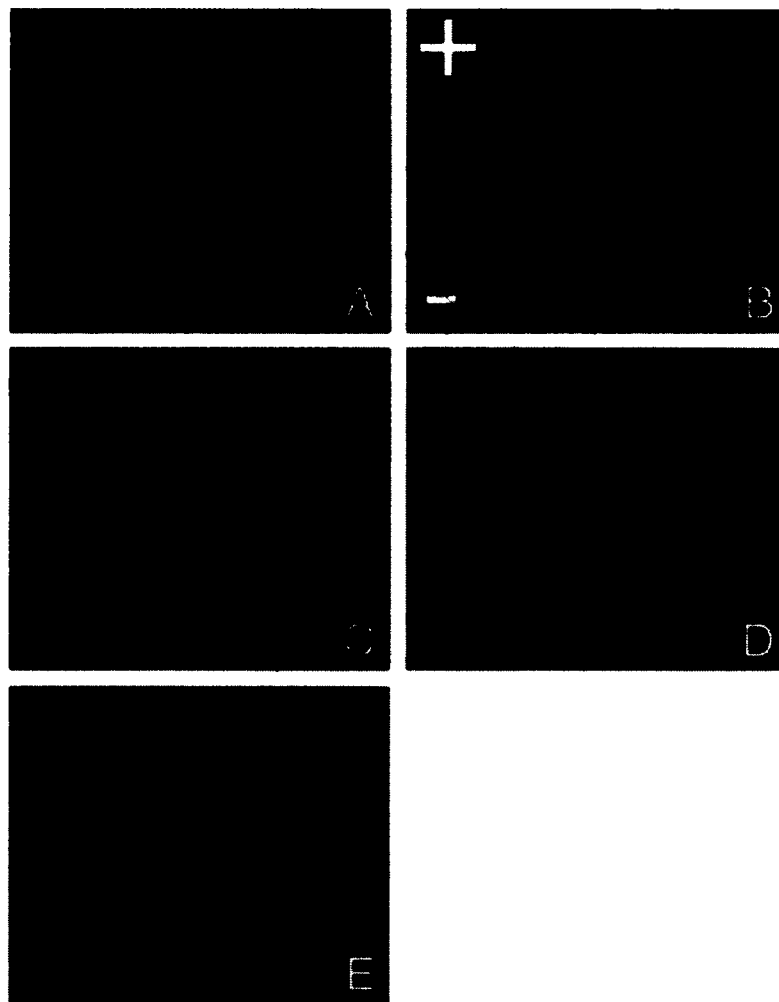
**Figure 6.** Jurkat cells loaded with fluo-4 were imaged every 18 ms after application of a 60-ns pulse of 100 kV/cm. Images were taken before exposure (a), at 18 ms (b), at 36 ms (c) and at 54 ms (d). Cells in (e) were stained with brefeldin A, 558/568 to locate the endoplasmic reticulum [21].

Apoptosis is one of the most remarkable biological responses that can be triggered by exposure to nsPEFs. The first report of apoptosis induction by nsPEFs appeared in 2001 [24] and extensive studies have been done thereafter. As an example, Table 2 shows that caspase activity, a marker of apoptosis, was significantly increased in cells that were exposed to nsPEFs. Each of these exposures provided similar energy input into the cells. In agreement with caspase activation determined in intact cells by flow cytometry,

caspase activation was greater as the pulse duration increased. Cycloheximide, a chemical that inhibits protein synthesis and is known to induce apoptosis, also increased caspase activity.

**Table 2.** Activation of Caspase Activity in Jurkat Cells after Exposure to nsPEFs [67]

| Condition | Caspase activity<br>Pmol AcDEVD-afc<br>hydrolyzed/min/mg protein |
|---|---|
| Control | $33.8 \pm 6.8$ |
| 10 ns, 150 kV/cm | $53.0 \pm 7.2$ |
| 60 ns, 60 kV/cm | $100.4 \pm 25.7$ |
| 300 ns, 26 kV/cm | $208.4 \pm 46.3$ |
| cycloheximide | $187.0 \pm 48.1$ |

## 2.2.2 Modeling and Simulation Predictions

Equivalent circuit model is the most straightforward and simplest approach to predict the charging of a cell when subjected to a pulsed electric field. Figure 7 shows a simplified equivalent circuit of a cell containing a nucleus between two electrodes [69]. Each cell component is represented by either a capacitor or a resistor according to its dielectric properties and geometry. This way the voltage distribution among each cellular structure can be determined analytically. When exposed to a pulsed electric field, the changes in transmembrane voltage, $\Delta V(t)$, is readily described by the widely used Schwan's equation

$$\Delta V(t) = 1.5 ER(1 - e^{-t/\tau_c})$$

(2)

where $E$ is the electric field strength, $R$ is the radius of the cell, $\tau_c$ is the charging time constant of the plasma membrane. As the pulse duration shortens to sub-microsecond range which is shorter than the charging time of the plasma membrane, the intracellular structures are affected by the pulsed electric field. Numerous studies have been conducted by means of this analytical approach to study the charging of cells when exposed to various pulsed electric fields.
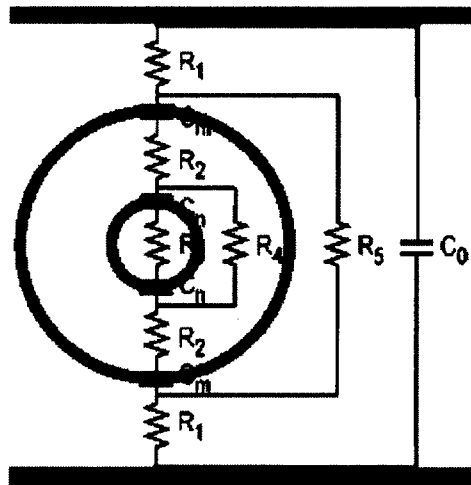


**Figure 7.** Equivalent circuit of a cell with a nucleus between two electrodes. The plasma membrane is represented by a capacitor, $C_m$, the nuclear envelope by a capacitor, $C_n$, $R_2$, $R_3$ and $R_4$ are determined by the conductivity of cytoplasm and nucleoplasm, $R_1$, $R_5$ and $C_0$ are dependent on the electrical properties of the medium [70].

However the above analytical model cannot predict and follow the non-linear changes of cells, e.g. membrane poration, stimulated by application of intense pulsed electric fields over a certain threshold of amplitude and duration. Therefore more sophisticated modeling schemes capable of predicting the creation and evolution of pores are employed to describe electric field-cell interactions. So far several numerical approaches have been

established, e.g. the transport lattice model developed by Weaver's group at Massachusetts Institute of Technology and the distributed circuit model together with a coupled Smoluchowski equation proposed by Joshi's group at Old Dominion University. As an example, Figure 8 shows the characteristics of membrane pores when exposed a 180 kV/cm trapezoidal pulse with a 10 ns on-time and 1.5 ns rise and fall times obtained from the above distributed circuit approach. Details of the modeling scheme can be found in literature. The temporal development of the transmembrane voltage at the poles is shown in Figure 8a. A transient peak of about 1.6 V is predicted during the membrane charging phase which slightly exceeds the conventional 1.0 V threshold for electroporation, About 9.2 ns after onset of the pulse, poration occurs which is indicated by the drop in transmembrane voltage. The continuous decrease in membrane potential is due to the dynamic increase in membrane conductivity. The model yields the time dependent generation, growth and dynamic expansion of pores. Figure 8b shows the distribution of pore size when exposed to 1, 2, 5, 10, and 50 pulses. For a single pulse application, the median pore radius is about 0.55 nm. As the pulse number increases, the pore distribution shifts to larger values of radius. The dependency of total area of pores on the number of applied pulses is shown in Figure 8c. The entire area of pores across the whole plasma membrane increases monotonically with the number of pulses. For the highest pulse number, the total area of pores is about $11 \ 10^{-11}$ m$^2$ which is equivalent to 7% of the entire surface area.
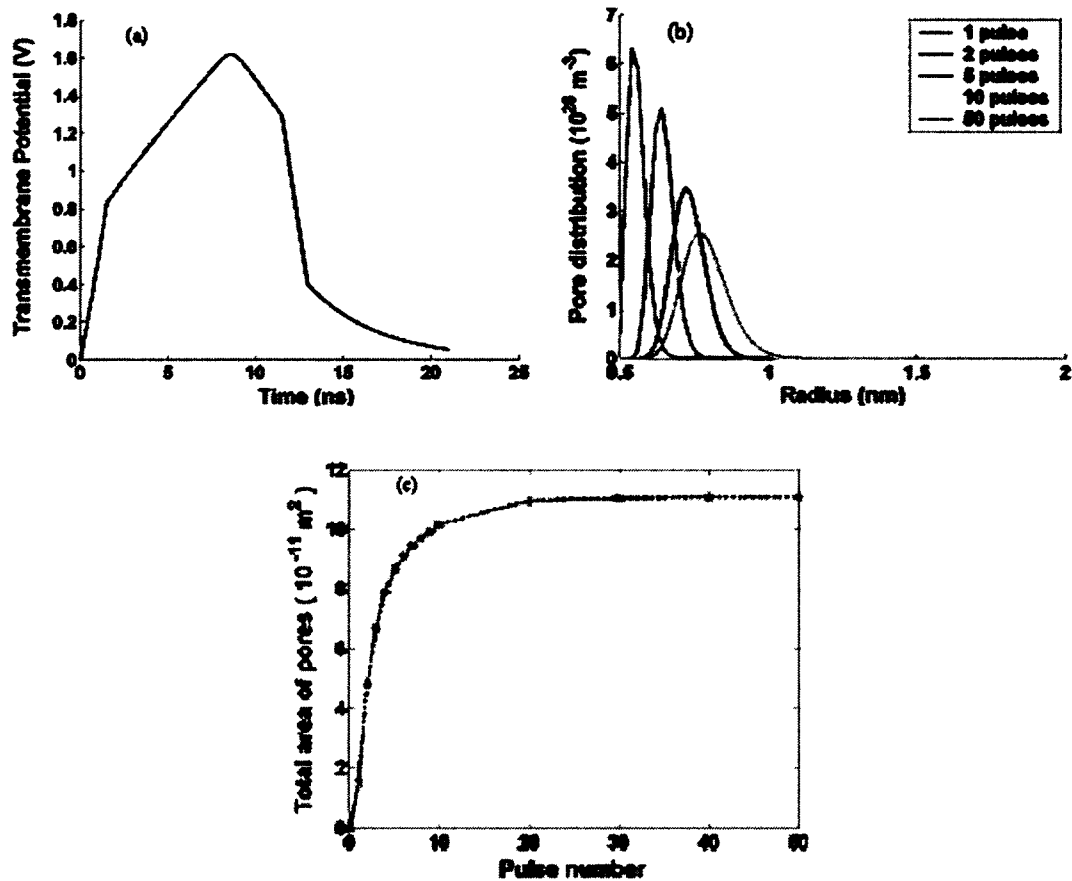
**Figure 8.** Characterization of membrane pores when exposed a 180 kV/cm trapezoidal pulse with a 10 ns on-time and 1.5 ns rise and fall times. Results are obtained from the distributed circuit approach proposed by Joshi et al [70]. (a) Temporal development of the transmembrane voltage across the cell membrane. (b) Pore distribution functions at the pole. (c) Dependence of the total pore area at the plasma membrane on applied pulse numbers.

In order to better understand the underlying mechanisms of the interactions between PEFs and biological cells at molecular level, molecular dynamics (MD) simulations have been introduced as the most basic and fundamental modeling approaches by a number of research groups in the field of bioelectrics since last decade [73-79]. In general molecular dynamics is a time-dependent, many-body, kinetic scheme relying on the application of classical Newtonian mechanics for the dynamical movement of every particle in the

simulation region. In the case of modeling a cell membrane, the DPPC (Dioleoyl-phosphatidyl-choline) molecules that form the lipid bilayer are considered as a collection of interacting particles. For every single molecule the Newton's equation is solved, with the force on each charge and dipole within the molecular structure generated by the surrounding charges and dipoles. MD simulations permit visualization of the structural details of the cell membrane on the nanoscale, both spatial and temporal, during exposure to external electric fields. The critical electric fields for membrane changes, e.g., pore formation, can also be determined. The detailed description of the advantages and modeling procedures of molecular dynamics can be found in a review by Schoenbach et al. [69] and in other publications [74, 75, 77, 78]. It is worth noting that MD simulations require extensive computation efforts due to the immense number of particles considered and the small time steps. Thus MD simulations, at current stage, are only suitable for tracking the changes of small parts of a cell such as a patch of plasma membrane up to several tens of nanoseconds when subjected to electrical pulses [69]. Figure 9 shows typical results of a MD simulation demonstrating nano-pore formation by Joshi's group at Old Dominion University [75], with a fixed field of 0.5 V/nm across the membrane. The patch of membrane used for this simulation is composed of 164,000 particles and the time steps is on the order of one femtosecond [74, 75] The pre-pulse configuration (t = 0 ns) of the lipid bilayer with water on both sides is shown in Figure 9a. Figure 9b shows a membrane pore formed by lining of the head groups after about 3.3 ns. The pore is about 1.5 nm in diameter, and has a funnel-shaped opening and each end. Figure 9c shows the top view of the membrane pore. Membrane pores with similar forming time, pore

geometry and pore size have been reported by other research group under similar exposure conditions using MD simulations [73, 76-78].
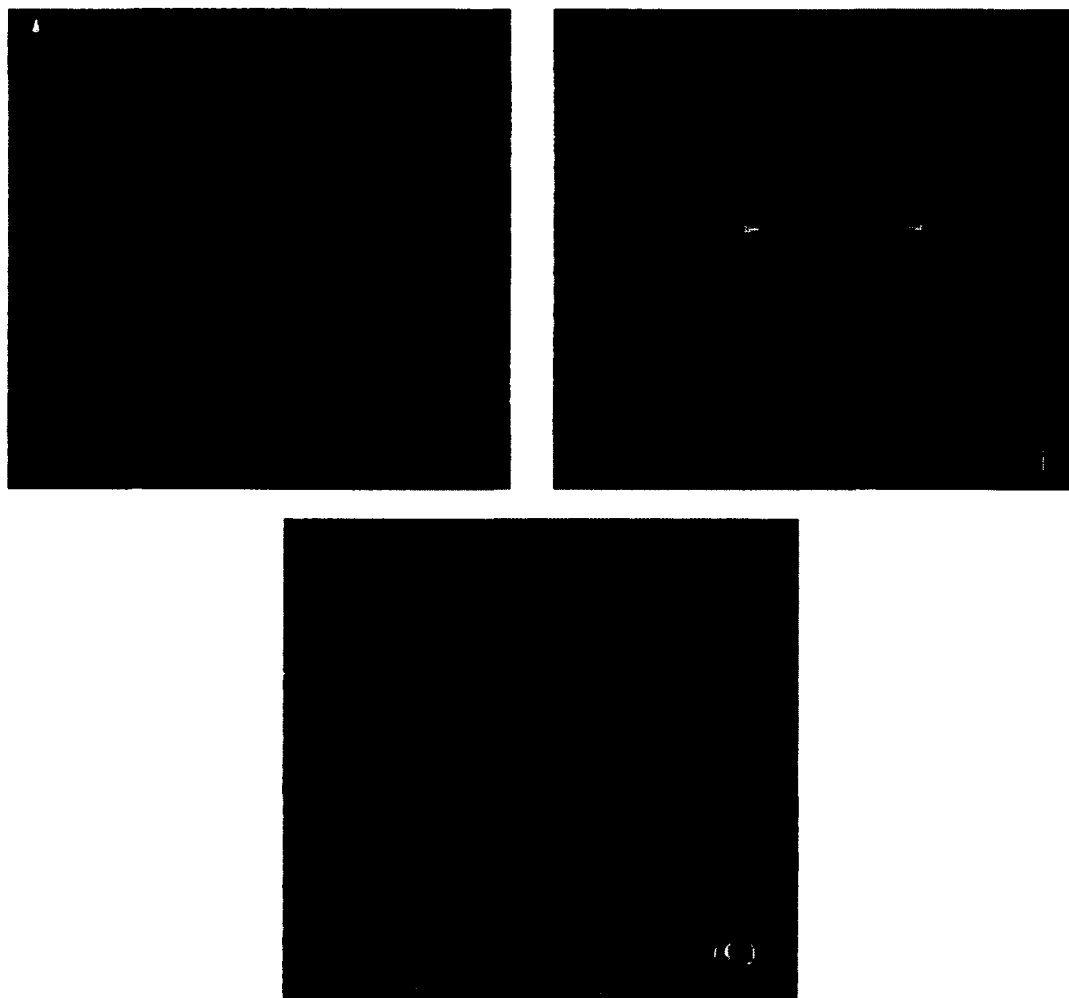


**Figure 9.** MD results showing formation of a nanopore in a patch of membrane by an external 0.5 V/nm pulsed electric field. (a) Initial configuration at t = 0 ns; (b) A view of the cross-section slice; (c) Top view of the membrane pore. The positively polarized choline groups are blue, and the negatively polarized phosphatidyl group brown, the glycerol green, the tails cyan. The oxygens in water molecules are red and hydrogens are white [77].

## 2.3    PEF-induced Changes in Impedance and Dielectric Properties of Biological Cells and Tissues

### 2.3.1    Changes Induced by Electroporation Pulses

Starting from 1977, Kinosita and Tsong conducted a series of studies investigating the hemolysis of human erythrocytes induced by microsecond pulsed electric fields (2 μs and 80 μs) [44, 80, 81]. By recording the current and voltage across the erythrocyte sample, they found that the conductivity of the erythrocyte suspension exhibited a time-dependent change when the applied electric field is greater than a threshold of about 1.5 kV/cm [44]. The increase in suspension conductivity during pulse application was attributed primarily to membrane conductance increase which corresponds to the formation of pores in the cell membrane. The changes in suspension conductivity after removal of the applied field were measured by switching the exposure chamber to a sinusoidal voltage of 10 kHz using a relay. This method covered a time range of 1 ms to 10 s. The authors observed recovery of the suspension conductivity towards its initial value, indicating a resealing process of the membrane pores. A second suspension conductivity increase was observed 10 seconds after pulsed electric field exposure, which was attributed to the efflux of intracellular ions through the pores in the membrane. Based on the conductivity measurement, the number of pores per cell was estimated to be in the order of 100. For cells suspended in high conductivity buffer (NaCl buffer), the final stage of suspension conductivity development was a slow decrease which was explained as the colloid osmotic swelling of porated cells. By means of the same current-voltage method, Teissie and Tsong found that the increase in red cell membrane conductance induced by electroporation pulses can be partially blocked by a specific inhibitor, ouabain [82].

Abidor and co-authors measured the conductance of compact cell pellets centrifuged in a special chamber [83]. The advantage of using compact cell pellets over cell suspensions is that the electric current through the extracellular medium is minimized and the resolution of conductance measurements is increased. For all the cell lines they examined (L-929, NIH3T3, HeLa, CHO and E2 cells), a significant increase in cell pellets conductance was observed when the voltage of applied 30-$\mu$s pulse was over a 'critical' value. This instant conductance increase was attributed to the poration of cell membranes. The conductance of cell pellets increased with increasing pulse amplitude which was suggested as a sign of higher level of membrane poration. The resealing process of membrane was also investigated by applying a series of test pulses (10 V, 10 $\mu$s, 50-$\mu$s period). At least 3 stages of pellet conductivity decrease were identified after exposure to reversible electroporation pulses (50-$\mu$s pulses of 100, 200 and 300 volts). The first stage was a fast decrease of pellet conductivity (0.5 ms $-$ 1 ms). In the second and third stages, the cell pellet conductivity gradually decreased to its initial value, which took several minutes. Both membrane recovery and colloid-osmotic swelling were suggested to be responsible for the slow conductivity relaxation. Similar temporal development of conductivity was also observed in rabbit erythrocyte pellets with the same experimental setup [84].

Pliquett et al. studied the changes in the resistance of heat stripped human cadaver stratum corneum (SC) when exposed to exponential pulses of 1-ms duration [85, 86]. The pulse amplitude ranged from 40 V to 130 V. The resistance of the skin ($R_{skin}$) after pulsed electric field exposure was determined by low voltage rectangular pulse with a peak to peak voltage of 150 mV. The resistance of the skin changed rapidly and significantly if

the amplitude of applied exponential pulse exceeds 40 V. The changes in $R_{skin}$ were reversible for pulses with voltage ranging from 40 V to 90 V. On the other hand changes for pulses with voltage higher than 110 V were irreversible. The changes in $R_{skin}$ were attributed to pulsed electric field-induced formation of new aqueous pathways or pores across SC lipid regions, which is consistent with the electroporation theory. Permanent changes in the SC were suggested responsible for the irreversible changes in $R_{skin}$. The authors proposed that the skin resistance can serve as an indicator of changes in the skin barrier and electrical measurements may serve as a rapid monitoring means for reversible electroporation conditions. Gowrishankar et al. further recorded the time course of changes in heat stripped skin impedance between and after exposure to high voltage pulses of 3-ms duration up to 2 hours [87]. The skin impedance was measured by a LCR meter. In this study, a series of 200 pulses of 500 V and, spaced 5 s apart, were applied across the skin. The prepulse skin impedance was over 200 k$\Omega$ which dropped rapidly to less than 3.8 k$\Omega$ after exposure to the first 10 pulses. After application of next few pulses, the skin impedance decreased to only 2.1 k$\Omega$ and stayed stable for the following pulses. An immediate recovery of 200 to 400 $\Omega$ was observed within the first 60 seconds following the termination of pulsed electric field application. The long-term recovery of skin impedance was rather slow and reached only 3 k$\Omega$ after 2 hours. The fast drop in skin impedance was explained by creation of small aqueous pathways in the skin. The fast shrinkage and closure of these pathways after pulsed electric field exposure was considered responsible for the immediate recovery of skin impedance. The long-lasting low skin impedance (or high skin conductance) was attributed to the existence of stable larger pathways which remain opening for a rather long time after termination of pulsed

electric field application. Later Vanbever et al. compared the effects of short (1 ms), high-voltage (1.5 kV) and long (300 ms), medium-voltage (100 V) pulses on skin resistance and transport properties [88]. They found that long pulses of medium-voltage appeared to be more efficient in transporting molecules across skin. The authors suggested that the recovery of skin resistance might reflect pathway resealing with water/ion entrapment.

Gallo et al. studied the changes in the resistance of porcine skin when exposed to electroporation pulses of 1, 4, and 10 ms and 10-300 V [89]. The pre-pulse and post-pulse skin resistance was determined by a continuous low-voltage (300 mV), 1000-Hz bipolar square wave, and the in-pulse skin resistance was determined by recording the current and voltage across the skin sample simultaneously. The authors observed significant decrease in skin resistance when the applied pulse exceeded a threshold voltage. The threshold voltage decreased with increasing pulse length. The maximum decrease of in-pulse skin resistance was about 10% - 20% the pre-pulse value. They found that the decrease seemed to be proportional to the dosage of applied electric pulses (voltage pulse width). For a single pulse application, the post-pulse skin resistance recovered to almost 90% of its pre-pulse value within seconds after exposure. For multiple pulse application, the skin resistance underwent a slow and incomplete recovery which took tens of minutes to hours. The structural alterations caused by repeated breakdown of the stratum corneum were suggested to be responsible for the changes in skin resistance. The authors suggested that electrical measurements can be used to augment human in vivo transdermal drug or gene delivery. Researchers from the same group also studied the influence of temperature on the skin resistance and transport of macromolecules across

porcine skin during and after exposure to electroporation pulses [90, 91]. They found that the threshold voltage that induces significant drop in skin resistance decreases with increasing temperature, i.e., the skin was more susceptible to permeabilization at high temperature [90]. At temperature over 40 °C the rate of increase in post-pulse resistance was significantly less and the transdermal delivery of macromolecules was considerably higher than those observed at temperatures lower than 37 °C. On the other hand, the resistance drop during pulse application was less sensitive to temperature (10 - 50 °C). The results suggest that electroporation at mild hyperthermia temperature is more efficient for transport of molecules [91].

Davalos et al. simulated the changes in conductivity of a liver induced by 60-ms electroporation pulses [92]. The authors suggested that impedance measurement can be a noninvasive method which would allow us to know if the cells in treatment area have become permeable during electroporation, in real time.

Pavlin et al. correlated microscopic membrane changes induced by pulsed electric field to macroscopic changes in conductivity of a suspension [93]. The effect of different cell parameters, e.g., cell volume fraction, membrane and medium conductivity, critical transmembrane potential and cell orientation, on suspension conductivity was discussed. Their analysis showed that the effective medium theory can be used for the calculation of the effective conductivity of a suspension of permeabilized cells. In a series of subsequent studies [33, 94, 95], Pavlin and co-workers tried to connect the theoretical analysis on increased membrane conductivity due to electroporation with experimental observations of changes in cell suspension conductivity during and after pulsed electric field application. They quantitatively related the changes in cell suspension conductivity

to enhanced transport of ions and molecules, and also the development of membrane pores. In these studies, a concentrated cell suspension was exposed to a train of 8 consecutive 100-μs conventional electroporation pulses. The conductivity of the cell suspension was recorded by either current-voltage method during or a LCR meter before and after pulsed electric field exposure. In addition to the electrical measurements, the percentage of permeabilized and survived cells was determined and the extent of osmotic swelling was measured. The experimental results showed a transient increase in the suspension conductivity during pulsed electric field exposure when the electric field strength was over the electroporation threshold. The in-pulse suspension conductivity increased with increasing pulse amplitude for both low-conductive and high-conductive medium conditions [96]. The elevated suspension conductivity exhibited complete relaxation in less than 1 second following exposure [96]. The membrane conductivity derived from electrical measurements also dropped towards the initial level in a range of a millisecond after exposure [94]. The post-pulse suspension conductivity showed continuous changes within 2 minutes after exposure. Based on the temporal development of cell suspension conductivity during and after pulsed electric field application, the authors proposed existence of two types of pores: short-lived pores and long-lived pores. The short-lived pores are created during exposure to electroporation pulses and are responsible for the transient increase in suspension conductivity. These short-lived pores shrink and close within 10 ms once the applied pulse is removed, leading to the fast relaxation of suspension conductivity. The long-lived pores stay stable after pulse application for a period of time and result in the transport of ions and molecules, and colloid-osmotic swelling. The long-lasting change in post-pulse suspension conductivity

is a sign of the existence of the long-lived pores. The authors concluded that measuring electric conductivity enabled detecting the permeabilization threshold during pulse application and estimating the fraction of long-lived pores after pulse application.

In 2007, Ivorra et al. reported the effect of reversible and irreversible electroporation pulses on the conductivity of rat liver and skeletal muscle tissue ex vivo [97]. A train of 8 pulses of 100 µs with a repetition frequency of 10 Hz was applied to the sample tissue sandwiched between two annular surface electrodes. The in-pulse tissue conductivity was measured by current-voltage method. The pre-pulse and post-pulse tissue conductivity was measured by an impedance analyzer. The in-pulse tissue conductivity showed significant increase for both exposure conditions. The increase for irreversible electroporation (1500 V/cm) is higher than for reversible electroporation (450 V/cm). Fast recovery of tissue conductivity was observed and was attributed to the resealing of membrane pores. The long term recovery in tissue conductivity after electroporation was tissue specific and showed complex patterns. The differences in post-pulse conductivity evolution between liver and muscle were suggested due to the differences in the blood perfusion impediment phenomenon. In another study by Ivorra and Rubinsky, in vivo electrical measurements were conducted on rat liver with the same exposure conditions [98]. An important conclusion of this study was that measuring the dielectric properties of electroporated tissues might provide real time feedback on the outcome of the treatment. This hypothesis was further confirmed by in vivo conductivity measurements on irreversibly porated rat tumors [99]. The authors found that post-treatment conductivity measured 30 minutes after exposure was correlated with treatment outcome in terms of reversibility. Researcher from the same group further explored the possibility

of using impedance imaging to predict the efficacy of tissue ablation with irreversible electroporation [100].

### 2.3.2 Changes Induced by Nanosecond Pulses

Benz and Zimmermann recorded the temporal development of the conductance of black lipid bilayer membranes after exposure to a high intensity pulse of short duration [101]. The membrane conductance was derived by applying a low intensity voltage pulse of longer duration (50 μs) with voltage and current recorded simultaneously. They found that the membrane conductance returns to unexposed value quickly after the exposure to high voltage 500-ns pulses. The resealing time estimated from the conductance measurements is on the order of 10 microseconds and strongly depends on the temperature. This initial pore size calculated from the conductance data is about 4 nm in radius. The mechanical breakdown of the membrane is attributed to the formation of large pores which occur at a longer time scale (microseconds to seconds).

Using time domain dielectric spectroscopy, Chen et al. measured changes in conductivity of Jurkat cell suspensions exposed to 50-μs electroporation and 10-ns ultrashort pulses [102]. A single 10-ns, 150 kV/cm pulse did not induce noticeable change in suspension conductivity while a 50-μs, 2.12 kV/cm pulse with the same energy caused an appreciable conductivity rise. Such difference was claimed consistent with the hypothesis that the 10-ns pulses primarily interact with the intracellular organelles instead of the plasma membrane. A cumulative effect on the plasma membrane was observed for multiple ultrashort pulse application - with five 10-ns pulses a gradual rise in conductivity was observed up to ten minutes post-pulsing. With the same exposure conditions and a cell dielectric model, Garner et al. further showed that a 50-μs pulse

caused a much larger rise in membrane conductivity than a 10-ns pulse with the same electrical energy [34]. This study confirmed that 10-ns pulses have less effect on the cell membrane than 50-μs pulses. Though single 10-ns pulse showed insignificant effect on the electrical properties of cell suspension and cells, application of multiple 10-ns pulses induced noticeable changes to conductivity of cell suspension [102], cytoplasm and nucleoplasm [34]. These results further confirmed that nanosecond pulses have a cumulative effect on cells.

Pliquett and co-workers studied the conductivity of Jurkat cells in a low conductive buffer during and after application of 300-ns high voltage pulses by means of time domain dielectric spectroscopy and current-voltage method [103, 104]. Significant increase in suspension conductance during pulse application and fast relaxation after pulse cessation was observed [103]. Calculations with a dielectric cell model showed that the conductivity of the plasma membrane returned to almost pre-pulse values within less than 10 ms [104]. When the electric field strength was over 20 kV/cm, the post-pulse suspension conductance showed continuous increase up to 5 minutes. The authors suggest that both the significant conductance increase and the fast conductance relaxation cannot be explained by simple membrane electroporation alone. Localized membrane rupture and fragmentation on the "nanoscale" at high electric fields are proposed to account for the conductance changes [103]. The continuous increase in post-pulse suspension conductivity was attributed to cell killing as tested by trypan blue exclusion [105]. In addition Pliquett et al. explored the limits of cell concentration and organelle size for the recognition of changes due to high voltage treatment using dielectric

spectroscopy [103]. The conclusion of this study is that cell volume fraction of at least 5% is recommended for dielectric characterization of cellular dielectric properties.

Using patch-clamp method, changes in membrane resistance of several cell lines (GH3, PC-12, and Jurkat cells) after application of nsPEFs were recorded by Pakhomov and co-workers [20, 106]. Their measurements show that even a single 60-ns pulse at 12 kV/cm can caused a profound and long-lasting (minutes) reduction of the cell membrane resistance ($R_m$), accompanied by the loss of the membrane potential. The membrane resistance measured in 80–120 s after nsPEF exposure was decreased about threefold, and its gradual recovery could take 15 min. Enhanced permeabilization was observed for multiple nsPEF-exposures. The change in membrane resistance was attributed to opening of stable conductive-membrane pores. These conductive membrane pores were permeable to Cl and alkali metal cations, but not to larger molecules such as PI. Later on, using the same patch-clamp technology, Ibey et al. found that similar membrane resistance decrease in both CHO cells and GH3 cells after exposure to single or multiple 60-ns and 600-ns pulses [107, 108]. These results suggest that pores created by nsPEFs may stay open for times that could extend up to several minutes.

Silve and co-authors studied the effect of frequency of both microsecond and nanosecond pulses on the impedance of potato tissue [109]. The impedance showed significant decrease after exposure to PEFs. The changes in impedance showed dependency on both pulse duration and frequency. The permeabilization level in potato was directly related to the value of the impedance drop. An interesting finding of this study is that the permeabilization level on potato tissue seems to be much higher at very low frequencies for both microsecond and nanosecond exposures [109].

# CHAPTER 3

## MATERIALS AND METHODS

In this study, the dielectric characteristics of several cells were investigated by means of time domain reflectometry (TDR) dielectric spectroscopy. This method delivers the dispersion relations for permittivity and conductivity of a dielectric sample from the information contained in the reflection of a known electric signal. This way, the frequency spectrum for the electric parameters can be obtained in a single or several, relatively short measurement, which will not heat samples or induce effects that are associated with the exposure of cells to oscillating electromagnetic fields. Combined with mixture models, averaged dielectric properties of individual cells can be derived and, with appropriate models for the cell, its constituents as well. Since several of the invoked parameters of the models are dependent on each other, solutions for dielectric parameters are pursued iteratively to determine the values that describe the measured spectra best. The approach requires taking into account interfering mechanisms, such as electrode polarization, changes in the conductivity of the suspending medium, and variation of geometrical parameters. Jurkat cells were chosen to demonstrate how nsPEFs affect the dielectric properties of cellular structures. The response of this cell line to both nanosecond and microsecond pulsed electric fields is studied extensively and well-documented. Also the spherical shape of Jurkat cells is ideal for dielectric modeling. The changes in plasma membrane integrity and viability were recorded for various exposure conditions. In addition, the dielectric response of tissues, e.g. blood and potato, to nanosecond exposures was probed.

## 3.1    Dielectric Spectroscopy of Biological Cells and Tissues

### 3.1.1    Time Domain Reflectometry (TDR) Dielectric Spectroscopy

Details of the TDR dielectric spectroscopy method used in this study can be found in the literature [110, 111]. As shown in Figure 10, an incident voltage pulse $V_0(t)$ of known rise time and amplitude is sent into a transmission line of characteristic impedance $Z_0$. The transmission line is terminated with a coaxial sensor that contains the sample. Permittivity and conductivity of the sample determine the impedance of sensor, $Z_x$. The change in impedance at the termination will result in a reflected pulse $R_x(t)$. The impedance of the sensor holding the sample, $Z_x$, can then be calculated by

$$Z_x = Z_0(v_0 + r_x) / (v_0 - r_x)$$

(3)

$v_0$ and $r_x$ are the Fourier transforms of the time-domain incident and reflected signals, $V_0(t)$ and $R_x(t)$. In practice, the reflected signal, $R_r(t)$, obtained for an open circuit, i.e., the empty sensor, is used instead of the incident signal $V_0(t)$. The signal is as well defined but easier to correlate in time with the signals obtained for samples being tested. From the comparison of both responses, i.e., signals, the frequency dependent apparent complex permittivity of the sample can be derived:

$$\varepsilon^* = \frac{1 + \rho / j\omega Z_0 C_0}{1 + \rho j\omega Z_0 C_0}$$

(4)

where

$$\rho = (r_r - r_x) / (r_r + r_x)$$

(5)

$C_0$ is the geometric capacitance of the empty sensor, and $r_r$ is the Fourier transform of the empty sensor reflection. Finally, the relative permittivity, $\varepsilon_r$, and conductivity, $\sigma$, of the sample can be determined through the apparent complex permittivity, $\varepsilon^*$:

$$\varepsilon^* = \varepsilon_r - j\sigma / \varepsilon_0 \omega , \qquad\qquad (6)$$

In this study, we used an Agilent 86100C TDR oscilloscope together with a 54754A differential plug-in. The latter generates an incident voltage pulse with a rise time of 35 ps and an amplitude of 200 mV. The same module also includes the sampling head and receives the reflected signal with an 18-GHz detection bandwidth. Samples, such as cell suspensions and blood, are contained in a cut-off type termination-sensor with gold plated stainless steel electrodes. The sensor is connected to the TDR oscilloscope with a semi-rigid 3.5-mm cable of 1 m length with a characteristic impedance of 50 Ω (Agilent 8120-4948). To exclude temperature effects, we immersed the sensor in a water bath and maintained the temperature at 25°C with a thermostat (Julabo, San Diego, CA). The time-domain response was collected using non-uniform sampling and subsequently brought into the frequency domain by a running Laplace transform as suggested by Hager [110].
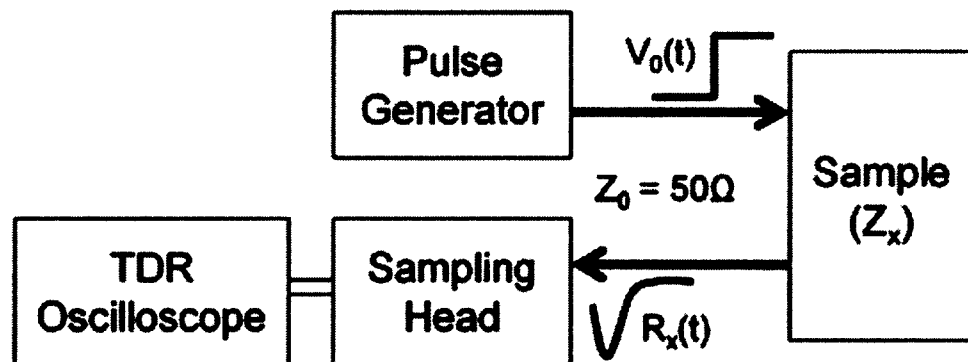


**Figure 10.** Block diagram of the TDR dielectric spectroscopy system. A fast rising voltage pulse, $V_0(t)$, is generated by a pulse generator and applied to the sample through a coaxial cable with a characteristic impedance of $Z_0$. The reflected signal, $R_x(t)$, is digitized by a sampling head and stored in a TDR oscilloscope.

## 3.1.2 Sensor Design

The design of the measuring sensor, i.e. the sample holder, has to accommodate the mechanical characteristics and phase of the dielectric under test and also be appropriate for the frequency range that is to be investigated. For dielectric spectroscopy of a cell suspension in the $\beta$-dispersion range, the cutoff type coaxial sensor has become preferred [46]. Our sensor is constructed on a SMA adaptor as shown in Figure 11. The sensor contains a coaxial line section and a circular waveguide section. Such configuration has been widely used and extensively studied both analytically and numerically [46, 49, 112]. The derivation algorithm used in this study takes into account the stray electric field and has been validated in dielectric measurements of conductive samples [111, 113]. The inner diameter of the outer conductor is 4 mm which ensures the cutoff frequency of the circular waveguide section to be much higher than 100 MHz. The length of the inner conductor is 2.5 mm, which avoids quarter-wave resonance effects in $\beta$-dispersion range. The diameter of the inner conductor of 2.65 mm provides an empty sensor capacitance of 400 fF. Inner and outer conductors are made of stainless steel and plated with gold. In order to minimize the electrode polarization effect, a layer of platinum black was further plated onto the electrodes. Cell suspensions being tested are contained in the space formed by these two sections, which holds about 50 μl.
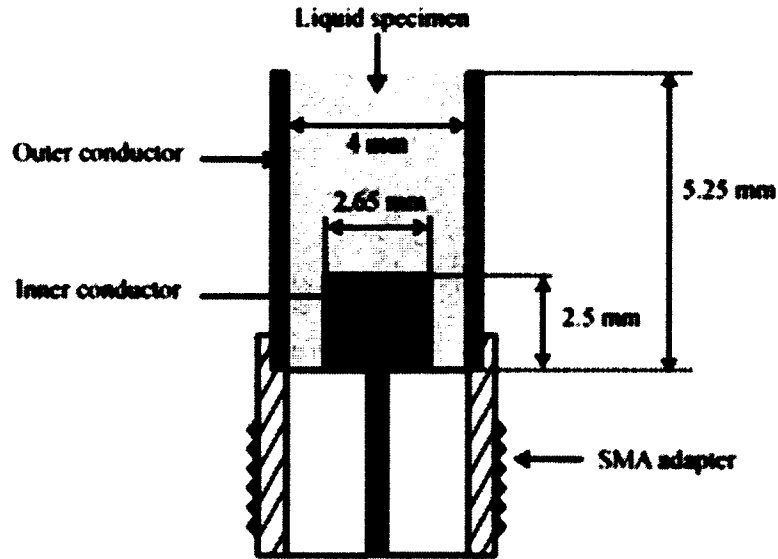
**Figure 11.** Measuring sensor constructed on an F/F SMA adapter. The chamber formed by the outer and inner conductors accepts cell suspension volumes of 50 µl.

### 3.1.3 Correction of Electrode Polarization

The apparent complex permittivity of a conductive sample, $\varepsilon^*$, derived from equation (4) contains contributions from both the sample's bulk dielectric properties and electrode polarization. The formation of an electric double layer at the electrode, i.e. electrode polarization, dominates measurements in the audio to radio frequency range, which is especially a problem for conductive samples. To correct the measurements for the effect, electrode polarization can be modeled as a constant-phase-angle (CPA) element in series with the cell suspension [114]. The corresponding impedance, $Z_{EP}$, can be described as:

$$Z_{EP} = K^{-1}(j\omega)^{-\eta}$$ 
(7)

where $K$ is a constant and $0 \le \eta \le 1$ [114].

The $\beta$-dispersion of a cell suspension and a tissue is usually described by a single Cole-Cole relaxation function [115]

$$\varepsilon^*(\omega) = \varepsilon_h + \frac{\varepsilon_l - \varepsilon_h}{1 + (j\omega\tau_r)^\alpha} + \frac{\sigma_l}{j\omega\varepsilon_0},$$ (8)

where $\varepsilon^*(\omega)$ is the complex permittivity of the sample, $\varepsilon_h$ is the high frequency permittivity, $\varepsilon_l$ is the low frequency permittivity, $\varepsilon_0$ is the permittivity of free space, $\sigma_l$ is the low frequency conductivity, $\tau_r$ is the relaxation time and $0<\alpha<1$. Cole-Cole model has an advantage over Debye model that the distribution of cell size is accounted by parameter $\alpha$, leading to better modeling of $\beta$-dispersion. Hence, the terminating impedance measured by TDR dielectric spectroscopy can be written as

$$Z(\omega) = Z_{EP}(\omega) + \frac{1}{j\omega\varepsilon^*(\omega)C_0},$$ (9)

By fitting equations (7)-(9) to the measured apparent complex permittivity, the $\beta$-dispersion of a cell suspension can be parameterized by a Cole-Cole function in terms of $\alpha$, $\varepsilon_h$, $\varepsilon_l$, $\tau_r$, $\sigma_l$, etc. The contribution of electrode polarization can be quantified by $K$ and $\eta$, which lays the foundation for subsequent derivation of cellular dielectric properties.

## 3.2 Derivation of Cell Dielectric Parameters

The intrinsic complex permittivity of a cell suspension, $\varepsilon^*$, comprises contributions from the bulk dielectric properties of the supernatant and contributions from suspended cells. The dielectric spectrum of the mixture can be described by the Maxwell-Wagner mixture model [50] as:

$$\varepsilon^* = \varepsilon^*_{sup} \frac{2(1-p)\varepsilon^*_{sup} + (1+2p)\varepsilon^*_{cell}}{(2+p)\varepsilon^*_{sup} + (1-p)\varepsilon^*_{cell}},$$ (10)

where $\varepsilon^*_{sup}$ is the complex permittivity of the supernatant; $\varepsilon^*_{cell}$ is the complex permittivity of a single cell; $p$ is the volume fraction of cells in the suspension.

The contribution from a cell can be broken down further into shares from individual cell structures. Contributions depend on the assumed organization of the cell. Both single shell and double shell models were used in this study for cells with and without a nucleus, respectively. Accordingly, the complex permittivity of the cell is determined by parameters for the cell membrane and overall values for the cellular content:

$$\varepsilon^{*}_{cell} = \varepsilon^{*}_{m} \frac{2(1-v_0)+(1+2v_0)R_0}{(2+v_0)+(1-v_0)R_0} \quad , \tag{11}$$

with $\varepsilon^{*}_{m}$ describing complex permittivities of plasma membrane. The parameter, $v_0 = (1-d_m/R_c)^3$, accounts for the cell-geometry, where $d_m$ represents membrane thickness and $R_c$ the cell radius. In the case of the single shell model,

$$R_0 = \frac{\varepsilon^{*}_{cp}}{\varepsilon^{*}_{m}} \quad , \tag{12}$$

where $\varepsilon^{*}_{cp}$ is the complex permittivity of the cytoplasm.

In case of the double shell model, a nucleus inside the cell with the nucleoplasm covered by the nuclear envelope is taken into consideration and the parameter $R_0$ is described as

$$R_0 = \frac{\varepsilon^{*}_{cp}}{\varepsilon^{*}_{m}} \frac{2(1-v_1)+(1+2v_1)R_1}{(2+v_1)+(1-v_1)R_1} \quad , \tag{13}$$

where $v_1 = ((R_n/R_c - d_m))^3$, $R_n$ is the radius of the nucleus and $R_1$ is given by

$$R_1 = \frac{\varepsilon^{*}_{ne}}{\varepsilon^{*}_{cp}} \frac{2(1-v_2)\varepsilon^{*}_{ne}+(1+2v_2)\varepsilon^{*}_{np}}{(2+v_2)\varepsilon^{*}_{ne}+(1-v_2)\varepsilon^{*}_{np}} \quad , \tag{14}$$

where $v_2 = (1-d_n/R_n)^3$, $\varepsilon^{*}_{ne}$ is the complex permittivity of the nuclear envelope and $\varepsilon^{*}_{np}$ is the complex permittivity of the nucleoplasm.

Through preceding models the complex permittivity of the cell suspension can be related to the dielectric properties of cellular structures as shown in Figure 12.
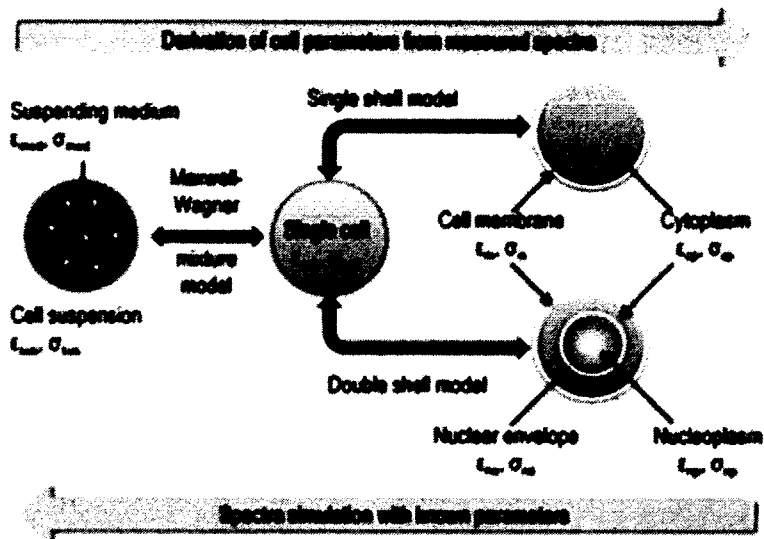
**Figure 12.** Connection between the dielectric properties of a cell suspension and the cellular dielectric parameters through the Maxwell-Wagner mixture model and the single/double shell model. The complex permittivity of each phase consists of relative permittivity and conductivity, which are assumed frequency independent for cellular structures.

Some of the parameters of the model can be assumed to be constants. Relative permittivities of supernatant and cytoplasm are fixed values of 78 and 60, respectively. Variations of these numbers have been shown to have little effect on the fitting [116]. The membrane thickness was chosen as 7 nm, following suggestions of previous studies [27]. Although this choice might give rise to a systematic error, the value is not expected to change due to exposures. In comparison, the cell size might be prone to changes due to the osmotic pressure or as a result of PEF exposures. No cell swelling or shrinkage was observed for unexposed cells or cells exposed to microsecond pulses within 30 minutes. Notably, the average size of cells exposed to nanosecond pulsed electric fields was generally already larger when the first dielectric spectrum was recorded, i.e. 5 minutes after exposure. However, the size did not increase any further subsequently. Accordingly,

the cell radius for control and μsPEF-exposed cells was accounted for by measurements taken on the microscope and was found to be on average 5.3 μm for control and μsPEF-exposed cells and 5.6 μm for nsPEF-exposed cells.

Complex permittivities of cellular structures are determined through individual values for relative permittivity and conductivity as described by equation (6). In a first approximation, these values can be assumed to be constants in the relevant frequency range from 10 kHz to 100 MHz. Hence, the complex permittivity of a cell is determined by equation (9) and the equivalent complex permittivity for the cell suspension by equation (10). Also taking into account the effect of electrode polarization by equation (7), a fit for the apparent permittivity of the suspension can be derived and compared with the measured spectrum. From the discrepancy between calculated and measured spectrum, new values for the conductivity and permittivity of the cell can be determined and the process repeated until the best fit is found for a measured point in the spectrum. A non-linear least-squares regression analysis is used to determine the best-fit parameters, i.e., the unknown parameters in equations (9)-(13). The entire fitting procedure is divided into 4 stages in order to reduce the uncertainties in fitted parameters. During the first stage, the electrode polarization impedance parameters $K$ and $\eta$ are determined by fitting the apparent dielectric spectrum of the cell suspension into equations (7)-(9). During the second stage, the values of $K$ and $\eta$ are fixed and the apparent dielectric spectrum of the cell suspension is fitted into equations (10)-(14). This way the conductivity of the supernatant is determined with the narrowest 95% confidence interval among all fitting parameters and its value fixed for the next stage. During the third stage, the relative permittivity and conductivity of the plasma membrane are determined with the narrowest

95% confidence intervals and are fixed for the next round of fitting. Eventually the dielectric properties of remaining cellular structures are fitted. This four-stage fitting strategy allows narrower confidence intervals in fitted parameters than determining all the fitting parameters simultaneously.

## 3.3 Materials

### 3.3.1 Choice of Biological Materials

The dielectric properties of several biological samples were studied. They vary by origin and characteristics. 1. Jurkat cells, a human T-lymphocyte leukemia cell line, have been extensively studied with regard to the biological effects of nanosecond pulsed electric fields. Therefore, a large number of studies are documented and biological responses can be directly related to results obtained in our study. Furthermore, the cells grow in suspension and consequently offer a mostly spherical and well-defined morphology - an ideal selection for comparison with theoretical studies, in which this geometry is often preferred. Other research groups have also investigated both the dielectric properties of these cells and their response to pulsed electric fields [103, 117-119]. 2. Murine melanoma B16F10 cells are a well established model for skin cancer. Although this is an adherent cell line, it can be suspended and become spherical by standard methods (trypsinization). 3. Hepa 1-6 cells, a mouse liver hepatoma cell line, were chosen as a second attached-growing cell line. 4. Erythrocyte ghosts were prepared from pig erythrocytes. Erythrocyte ghosts are perfectly spherical and do not have organelles inside the cell. In other words, erythrocyte ghosts can be regarded as a sphere of homogeneous electrolyte encapsulated by a layer of plasma membrane. Thus erythrocyte ghosts are an ideal candidate for the single shell model and were investigated

by dielectric spectroscopy in a number of studies [120, 121]. 5. Pig whole blood was investigated as a type connective tissue with physiological conductivity. An advantage of blood is that the measuring sensor for cell suspensions (Figure 11) can be employed without any modification since blood is a cell suspension as well. In addition the dielectric spectra of blood were widely studied and documented [122-124]. 6. Potato, a homogeneous solid tissue, can be easily processed into desired geometry which is convenient for dielectric spectroscopy as well as PEF-exposures. Several groups have explored the electrical properties and PEF-induced structural and physiological changes of potatoes [109, 125, 126]. We used potato tissue to demonstrate that PEF-induced dielectric changes in solid tissue can be measured by means of TDR dielectric spectroscopy.

### 3.3.2 Cell Culture

Jurkat, B16F10 and Hepa 1-6 cells used in this study were obtained from ATCC (Manassas, VA). Jurkat cells were cultured in RPMI-1640 medium (Mediatech Cellgro, VA) with L-glutamine supplemented with 10% fetal bovine serum and 2% penicillin/streptomycin. B16F10 cells and Hepa 1-6 cells were grown in DMEM medium (Mediatech Cellgro, VA) with L-glutamine supplemented with 10% fetal bovine serum and 2% penicillin/streptomycin (Mediatech Cellgro, VA).

### 3.3.3 Preparation of Samples

Before TDR dielectric spectroscopy or PEF-exposures the cultured cells were centrifuged for 5 minutes at 200 g and then washed three times with a low-conductivity sucrose/glucose bu□er (229 mM sucrose, 16 mM glucose, 1 μM $CaCl_2$, and 5 mM $NaH_2PO_4/Na_2HPO_4$) in deionized water. The pH of the low-conductivity buffer was adjusted to 7.4 adding 5% HCl. The low-conductivity buffer significantly reduced the

electrode polarization effect compared with the culture medium, while maintaining isotonic osmotic-pressure (280 mOsmol). The volume fraction of cell suspension was adjusted to about 10% before each experiment. The exact cell volume fraction was determined by hematocrit tubes and the extracellular space was corrected as described in other studies [127-129]. A small aliquot of the cell suspension was diluted by 100 times and cell counts were done by a hemocytometer which gave an estimate of initial cell concentration. The supernatant of a cell suspension was extracted by centrifugation for 5 minutes at 200 g.

Fresh heparinized pig whole blood was obtained from Dr. Barbara Y. Hargrave (Department of Biological Sciences, Old Dominion University). TDR dielectric spectroscopy and PEF-exposures were conducted no more than 2 hours after receiving the blood sample. Pig erythrocyte ghosts were prepared following the procedures of Steck and Kant [130]. Blood sample was centrifuged for 5 min at 300 g. After removal of the plasma and buffy coats, the red blood cells were then washed twice in PBS. The hemolysis was initiated by mixing 1 ml of packed cells in 15 ml $NaH_2PO_4/Na_2HPO_4$ solution (5 mM/ml, pH 8.0). After 30 minutes, the ghosts were centrifuged at 20,000 g for 10 minutes and washed twice in a resealing buffer (5 mM $NaH_2PO_4/Na_2HPO_4$, 1 mM $MgSO_4$, pH 8.0) which caused immediate sealing of the plasma membrane. All above operations were performed at 4 °C. Then the ghosts were washed twice and resuspended in the low conductivity buffer with 10% volume fraction for dielectric measurement.

Idaho potatoes were purchased from local supermarket. The potato tuber was peeled and sliced into 3 mm-thick cylinder for dielectric spectroscopy and PEF-exposure.

## 3.4    Pulsed Electric Field Exposure

Two in-house-made transmission line pulse generators with characteristic impedances of 7 $\Omega$ and 10 $\Omega$ provided the 300-ns and 60-ns pulses, respectively [131]. The 100-$\mu$s pulses were generated by an electroporator (ECM 830 Harvard Apparatus, Holliston, MA). Pulse durations were determined as the time the applied voltage has risen and fallen again to half the value given by the amplitude. Jurkat Cells in suspension were exposed to PEFs between plane parallel aluminum electrodes with a gap distance of 1 mm in gene pulser cuvettes (BioRad, Hercules, CA). In all experiments, the exposure of cells to pulsed electric fields was always conducted 30 minutes after the first wash with the low conductivity buffer. For this study we limited the parameter space of exposures and developed procedures and techniques that can later also be applied to study other exposure conditions. We used 3 durations for individual pulses and total exposures of 8 pulses. The exposures to 60 ns and 300 ns pulses have been studied extensively for apoptotic responses and tumor treatment [22-28]. Exposure to 100-$\mu$s pulses was chosen as an example of a typical reversible-electroporation pulse.

In order to study the PEF-induced temporal development of cellular dielectric properties, either 8 consecutive 1.1-kV/cm electroporation-pulses of 100 $\mu$s or 8 consecutive 20-kV/cm nsPEF-pulses of 300 ns were applied with a repetition rate of about 1 Hz. The parameters for an individual pulse were chosen to deliver approximately the same energy with short and long pulses.

## 3.5    Membrane Integrity and Cell Survival

The changes in membrane integrity of Jurkat cells were examined by trypan blue exclusion assay up to 30 minutes following PEF-exposure with a 5-minute temporal

resolution. Trypan blue is a vital stain which is impermeable to intact cell membranes. Once the membrane is compromised, the interior of the cell will be stained and shows a distinctive blue color. The number of cells showing trypan blue uptake was counted by a hemocytometer.

Membrane integrity of exposed cells was also tested by the uptake of propidium iodide (an accepted membrane integrity marker) [23, 26]. PI is a nucleic acid stain that is considered to be membrane impermeable such that those cells exhibiting strong fluorescent signals were determined to be membrane compromised. Two groups of PI uptake experiments were conducted, i.e. adding PI either before or shortly (~10 seconds) after PEF-exposures. For each group of experiments, PI (Sigma-Aldrich, St. Louis, MO) was added to cell samples contained in microcentrifuge tubes with a final concentration of 1 $\mu g/ml$. Then the samples were diluted to $1\ 10^6$ cells/ml and fluorescence images were taken on an inverted microscope (IX71, Olympus, Melville, NY) with a high resolution digital B/W CCD camera (Hamamatsu ORCA-ER, Hamamatsu Photonics K.K, Hamamatsu City, Japan).

The long-term survival of Jurkat cells after exposure to selected pulse conditions was recorded. Jurkat cells were seeded at $10^5$ cells per well in 96-well plates after exposure. 24 hours after plating, cell viability was measured by CellTiter-Glo Luminescent Cell Viability Assay (Promega, Madison, WI), which determines viability by measuring ATP content of cells that is directly proportional to cell number. The luminescent signal was analyzed with a microplate luminometer (Gemini XPS, Molecular Devices, CA).

# CHAPTER 4

## RESULTS

The objective of our study was correlating structural and functional changes observed after pulsed electric field exposure with changes of the dielectric properties of cells. The relative permittivity and conductivity spectrum of cell suspensions and tissues were obtained by means of time domain reflectometry (TDR) dielectric spectroscopy and were corrected for electrode polarization. Modeling studies show that the changes in cellular dielectric parameters, e.g. plasma membrane conductivity, can significantly affect the dielectric spectrum of a cell suspension, thus allowing one to estimate pulsed electric field-induced changes in dielectric properties of cellular structures by fitting the measured dielectric spectrum into proper dielectric models, such as the Maxwell-Wagner mixture model combined with a single- or double-shell cell model. Based on such data treatment strategy, the temporal development of dielectric properties of Jurkat cells was derived following exposure to 8 pulses (applied at a repetition rate of 1 Hz) of either 300-ns duration and 20-kV/cm amplitude or of 100 μs and 1.1 kV/cm. The changes in plasma membrane integrity were assessed for different times after exposure by Trypan Blue exclusion assay together with fluorescence imaging of Propidium Iodide uptake. Further investigations show that the plasma membrane conductivity has the potential to predict the efficacy of nsPEF-related treatment.

## 4.1   Time Domain Dielectric Spectroscopy of Biological Cell Suspensions and Tissues

### 4.1.1   Time Domain Response

Figure 13a shows the time domain responses of air, deionized water, unexposed Jurkat cell suspension and corresponding supernatant. The time domain reflected signals were captured by the TDR-oscilloscope on seven successive time windows with an individual length ranging from 200 ps to 5 ms, which matches the time scale of each relaxation process. In the absence of any bound or free charges, the reflected signal for the empty sensor rises from 0.2 V to about 0.4 V in less than 100 ps and remains at 0.4 V till the end of recording time, which is consistent with the fact that no permanent dipoles contribute to the response for air. Conversely, the reflected signal for the deionized water sample is determined by water dipoles and drops to about 0.05 V at 200 ps, before exponentially increasing again within 2.7 ns to values equivalent to the response of an empty sensor. The time domain responses of electrolytic samples (cell suspensions and supernatants) is determined by more complex dipole and conduction mechanisms, and can be divided into 5 periods. On the shortest timescale ($t \leq 200$ ps) is the immediate response determined by permanent and induced dipole moments and therefore identical to the response of deionized water. Water dipole alignment is still the dominant polarization mechanism for times up to a few nanoseconds (200 ps $< t <$ 2.7 ns) and the observed exponential increase on this timescale is similar to the characteristic response recorded for deionized water, eventually reaching a value of 0.3 V. From 2.7 ns to 500 ns, the contribution of cells becomes apparent. It is important to point out that in the same time frame, the supernatant, which is an electrolytic solution without cells, shows no sign of a

contributing relaxation mechanism. From 500 ns to 60 µs, both cell suspension and supernatant exhibit an exponential increase towards the empty sensor response. For longer times (t > 60 µs), no more relaxation processes can be observed for any sample. In conclusion, differences in the dielectric characteristics of cells will be most pronounced in differences of dielectric spectra for the response recorded from 20 ns to 200 ns. Figure 13b gives a detailed view of this time frame for exposed and unexposed cell suspensions. The reflected signals of exposed cell suspensions generally showed lower signal amplitudes and were also changing at slower rates than the response of the unexposed cell suspension. Comparing the exposure conditions for nanosecond and microsecond pulsed electric fields, nsPEFs resulted in a stronger deviation from the response of control samples than µsPEFs in terms of signal amplitude and rate of change of the signal.
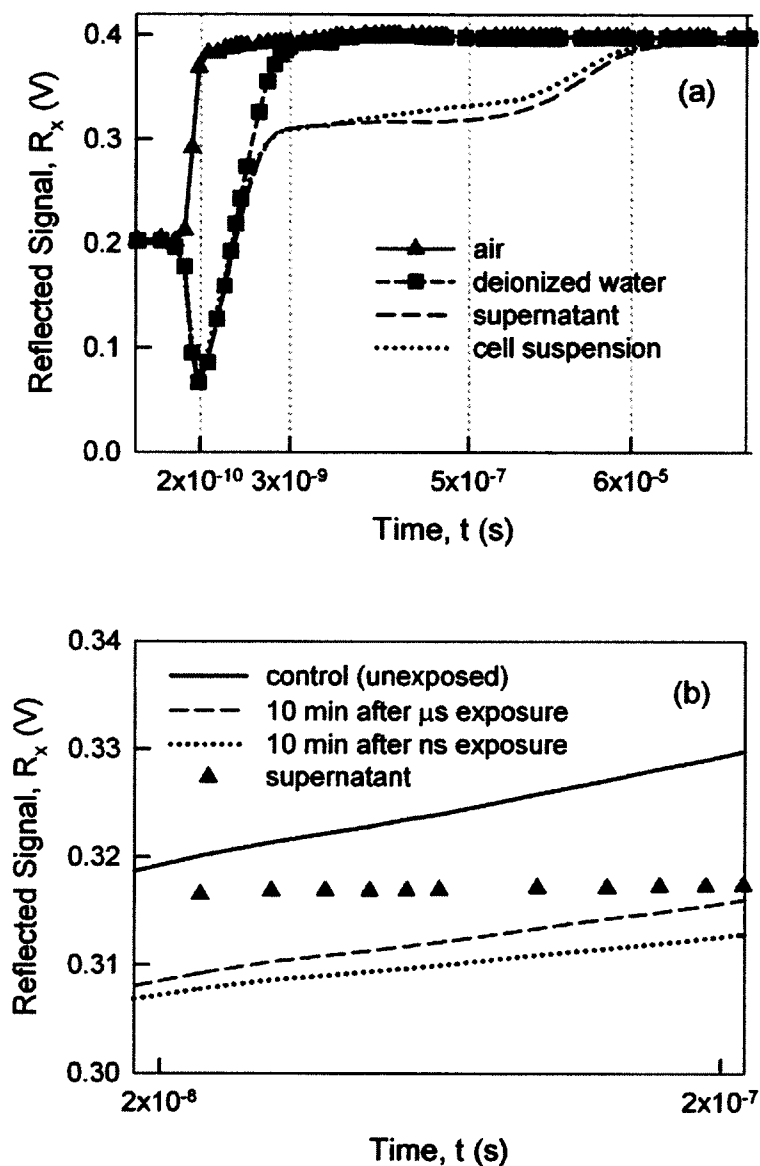
**Figure 13.** TDR responses of different samples captured on an increasing time scale. (a) Responses reconstructed from 7 consecutive segments. (b) Detailed view of the responses in the range from 20 to 200 ns, corresponding to relaxation times of β-dispersion mechanisms. The baseline of these signals is 0.2 V which is the amplitude of the incident voltage step. (For clarity, symbols are only shown for air and deionized water in (a) and for supernatant in (b). However, measurements were taken for the same time points for all samples.)

### 4.1.2  Dielectric Spectrum of Cell Suspensions and Tissues

The apparent dielectric spectra, i.e. complex permittivities derived directly from the time domain response by the Running Laplace Transform, of 3 biological samples (Jurkat cell suspension with 10% volume fraction, pig whole blood and potato) ranging from 2 kHz to 100 MHz are shown Figure 14. Both the relative permittivity and conductivity spectra show frequency-dependent characteristics. At low frequencies (f < 100 kHz), the relative permittivity of all samples increases significantly with decreasing frequency, which is a sign of electrode polarization effect. On the other hand, the conductivities decrease with decreasing frequency but the changes are less remarkable. The low frequency conductivity is about 0.55 S/m for pig blood and about 0.065 S/m for Jurkat cell suspension and potato. From 100 kHz to 10 MHz, the so-called $\beta$-dispersion becomes the dominant effect in both Jurkat cell suspension and potato dielectric spectra, i.e. falling in the relative permittivity spectrum and rising in the conductivity spectrum. The dielectric spectra of pig blood also exhibit the $\beta$-dispersion from 1 MHz to 100 MHz. At frequencies lower than the $\beta$-dispersion range, the relative permittivity of potato is the highest ($\sim2 \ 10^5$) which corresponds to the strongest polarization effect. Jurkat cell suspension has the lowest relative permittivity value ($\sim1.1 \ 10^3$) due to the low cell volume fraction (10%). At higher frequencies (f > 10 MHz), the permittivities of all samples approach to a constant value (78), which is the dielectric constant of water. The conductivity of Jurkat cell suspension and potato rises to 0.1 S/m and 0.7 S/m, respectively. The conductivity of blood reaches 1 S/m which is close to the conductivity of physiological media.
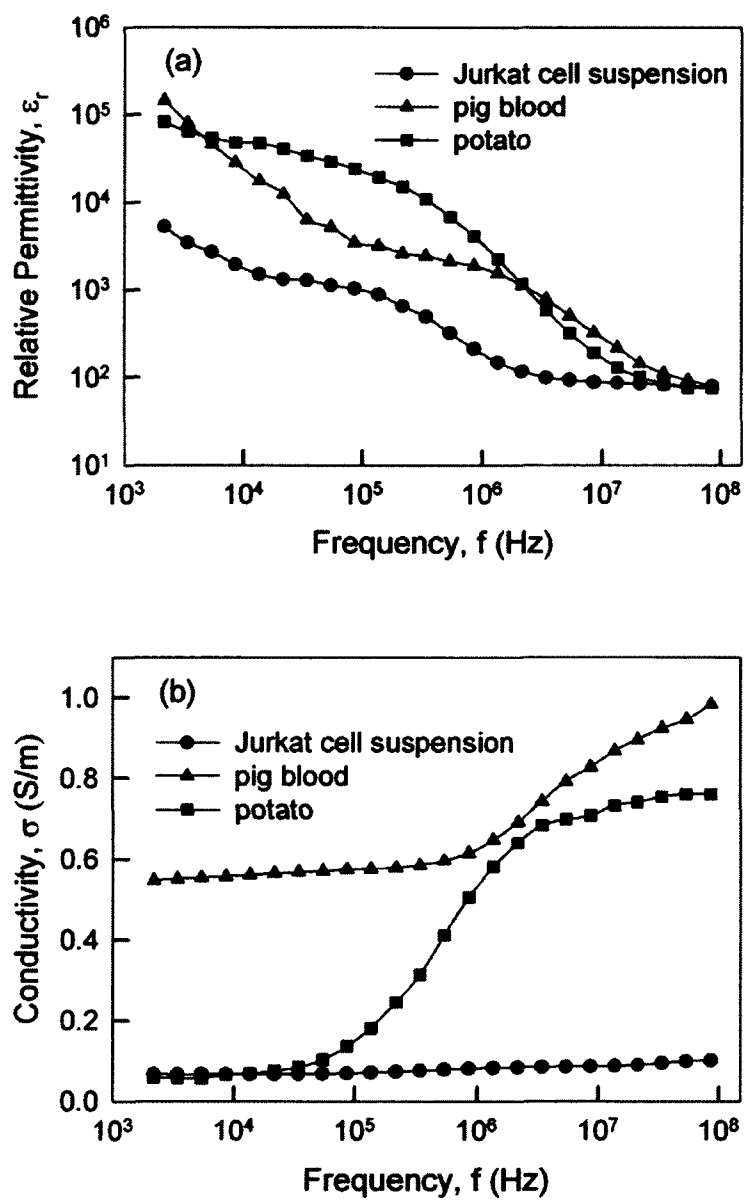
**Figure 14.** Apparent relative permittivity (a) and conductivity (b) spectrum of three different biological samples from 2 kHz to 100 MHz. The dielectric spectrum of each sample was derived from corresponding time domain response by performing the Running Laplace Transform.

### 4.1.3 Effect of Electrode Polarization on the Dielectric Spectra of Conductive Electrolyte

Theoretically an electrolyte such as a NaCl solution has no dielectric relaxation within the audio/radio frequencies. Hence its intrinsic relative permittivity and conductivity should be frequency-independent from 1 kHz to 100 MHz. However the ions in a NaCl solution form electric double layers at the measuring electrode/liquid interface, i.e. electrode polarization effect. The contribution from electrode polarization effect often overlaps with the dielectric response of conductive samples and may obscure the identification of some intrinsic relaxation mechanisms from the measured dielectric spectra. Figure 15 shows the apparent relative permittivity and conductivity spectrum of four NaCl solutions with dc conductivities ranging from 0.02 S/m to 0.5 S/m. Both the relative permittivity and conductivity spectrum are significantly affected by electrode polarization effect, especially at lower frequencies. For the NaCl solution of 0.02 S/m, its relative permittivity reaches $5 \cdot 10^4$ at 1 kHz which is 3 orders higher than the bulk dielectric constant of water (80). As frequency increases, the relative permittivity keeps decreasing and stabilizes around 80 beyond 150 kHz. The conductivity of this NaCl solution remains unaffected from 10 kHz to 100 MHz and drops less than 5% when frequency decreases to 1 kHz. As the dc conductivity of the NaCl solution increases, the influence of electrode polarization becomes more and more dominant at low frequencies and extends to even higher frequency range (as shown in Figure 15). For the NaCl solution of 0.5 S/m, the relative permittivity rises to $3 \cdot 10^6$ at 1 kHz and does not return to 80 until 20 MHz. The conductivity drops to 0.15 S/m at 1 kHz and rise back to 0.5 S/m at

100 kHz. The results also show that influence of electrode polarization effect is more significant in the relative permittivity spectrum than in the conductivity spectrum.
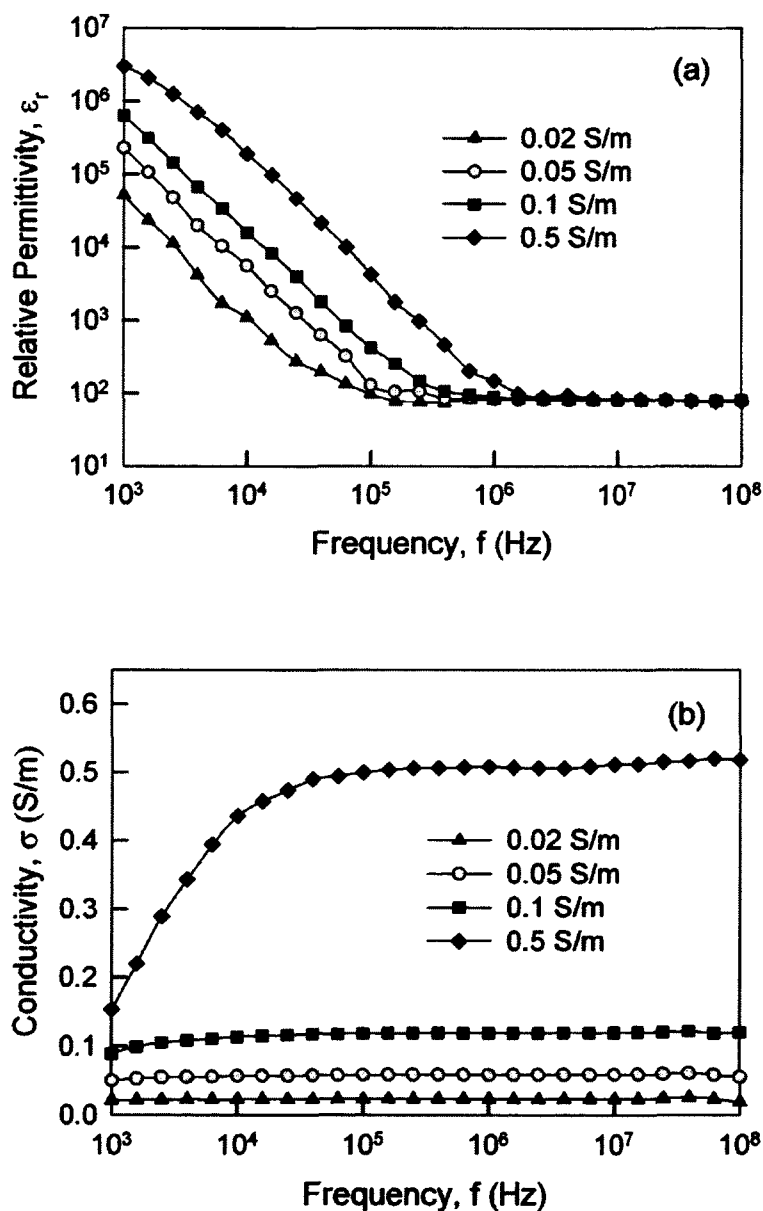


**Figure 15.** Effect of electrode polarization on the relative permittivity (a) and conductivity (b) spectrum of NaCl solutions with dc conductivities ranging from 0.02 S/m to 0.5 S/m. The dielectric spectrum of each sample was derived from corresponding time domain response by the Running Laplace Transform. The effect of electrode polarization becomes increasingly dominant with decreasing frequency and increasing dc conductivity.

### 4.1.4 Electrode Polarization Correction

Dielectric spectra for the frequency range from 1 kHz to 100 MHz, corresponding to the range of dielectric spectra in the time domain that is characterized by relaxation processes of cells, are shown for control samples and their supernatant equivalents in Figure 16. The apparent recorded spectra are not yet corrected for electrode polarization. The effect becomes increasingly dominant for decreasing frequencies ($f < 100$ kHz) and increasingly masks the more subtle contributions of other mechanisms, i.e., those due to the dielectric properties of cells. Applying the corrections described by equations (4)-(7), the spectra have been corrected. The corrected spectra indicate that the electrode polarization affected the relative permittivity and the conductivity spectrum up to 1 MHz and 100 kHz, respectively. In the audio/radio frequency range, the relative permittivity and ionic conductivity of the supernatant are constant, suggesting the absence of dispersion mechanisms. Conversely, cell suspension spectra show a decreasing relative permittivity and increasing conductivity as the frequency increases as is expected for the $\beta$-dispersion brought forth by cells.
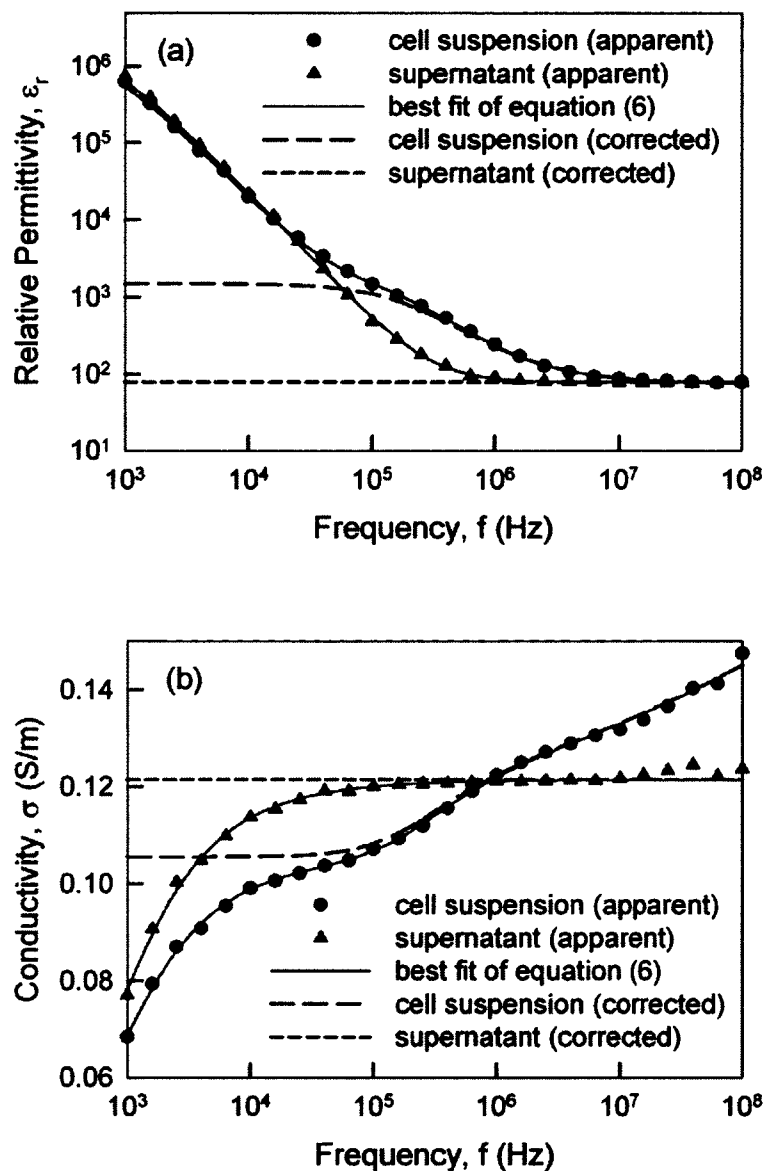
**Figure 16.** Apparent and corrected relative permittivity (a) and conductivity (b) spectra of cell suspension and corresponding supernatant from 1 kHz to 100 MHz. The dielectric spectrum was derived from the time domain response as shown in Figure 10a. At lower frequencies, electrode polarization significantly affects the dielectric spectrum, resulting in an apparent increase in permittivity and decrease in conductivity. As frequency increases, the effect of electrode polarization diminishes. The best-fit curves are determined by fitting apparent dielectric spectra to equations (4)-(7). With these results, i.e. best fit parameters, corrected dielectric spectra are then derived from the Maxwell-Wagner model combined with a single shell cell model.

### 4.1.5 Dielectric Parameters of Cellular Structures

After correction of electrode polarization effect, the dielectric parameters of cellular structures are derived by fitting the relative permittivity and the conductivity spectrum simultaneously into a combination of the Maxwell-Wagner mixture model and the single/double shell model. Some of the parameters are fixed during the fitting procedure and values are chosen as suggested previous studies [49]. Based on this fitting procedure, 4 different cell lines (pig erythrocyte ghost, Jurkat cells, B16F10 cells, Hepa 1-6 cells) were investigated in this study and corresponding cellular dielectric parameters listed in Table 3, where $\varepsilon_m$ is the plasma membrane permittivity, $\sigma_m$ is the plasma membrane conductivity, $\varepsilon_{ne}$ is the nuclear envelope permittivity, $\sigma_{ne}$ is the nuclear envelope conductivity, $\sigma_{cp}$ is the cytoplasm conductivity, $\sigma_{np}$ is the nucleoplasm conductivity, $\varepsilon_{cp}$ is the cytoplasm permittivity, $\varepsilon_{np}$ is the nucleoplasm permittivity, $d_m$ is the thickness of the plasma membrane, $d_n$ is the thickness of the nuclear envelope, $R_n$ is the radius of the nucleus and $R_c$ is the radius of the cell. Values from previous studies are also listed for comparison [50].

The plasma membrane conductivity and permittivity of erythrocyte ghosts is significantly lower than that of eukaryotic cells. Jurkat cells have higher plasma membrane conductivity but much lower plasma membrane permittivity than B16F10 cells and Hepa 1-6 cells. The plasma membrane conductivity and permittivity of B16F10 cells and Hepa 1-6 cells do not have significant differences. The erythrocyte ghosts were prepared in a low conductivity medium thus have a very low cytoplasm conductivity (0.028 S/m). The cytoplasm conductivities of other 3 cell lines are significantly different from each other. The nuclear envelope conductivity of Jurkat cells is significantly higher

than B16F10 cells and Hepa 1-6 cells. The nuclear envelope permittivities of B16F10 cells and Hepa 1-6 cells are significantly higher than that of Jurkat cells, and are not significantly different from each other. The nucleoplasm conductivity of B16F10 is significantly lower than that of Jurkat cells and Hepa 1-6 cells.

**Table 3.** Dielectric Parameters of Cellular Structures

| | $\sigma_m$ $10^{-6}$ S/m | $\varepsilon_m$ | $\sigma_{cp}$ S/m | $\sigma_{ne}$ $10^{-3}$ S/m | $\varepsilon_{ne}$ | $\sigma_{np}$ S/m |
|---|---|---|---|---|---|---|
| Ghost | 8.7±3.1 | 6.0±0.3 | 0.028±0.001 | | | |
| Jurkat | 31.4±1.5 | 8.3±0.2 | 0.43±0.01 | 1.8±0.2 | 53.8±6.1 | 0.82±0.06 |
| B16F10 | 21.2±2.6 | 23.3±1.0 | 0.20±0.03 | 1.0±0.1 | 136±11.6 | 0.41±0.01 |
| Hepa 1-6 | 20.6±5.0 | 25.8±1.3 | 0.36±0.01 | 0.4±0.05 | 145±4.7 | 0.72±0.02 |
| T-normal* | 27.4±6.2 | 11.1±1.4 | 0.65±0.13 | 8.8±0.6 | 85.6±16.7 | 1.26±0.27 |
| B-normal* | 56±29 | 12.8±1.6 | 1.31±0.08 | 11.1±7.2 | 106±35 | 2.04±0.29 |

Other parameters fixed during the fitting procedure: $\varepsilon_{cp}$ =60, $\varepsilon_{np}$ = 120, $d_m$ = 7 nm, $d_{ne}$ = 40 nm, $R_n$ = 0.8 R $_c$
*The values for human T-normal and B-normal cells are from reference [50].

## 4.2 Effect of Cellular Dielectric Parameters on the Dielectric Spectra of Cell Suspensions

### 4.2.1 Effect of Plasma Membrane Conductivity

Intense pulsed electric fields permeabilize the plasma membrane and consequently significantly increase the plasma membrane conductivity $(\sigma_m)$. If the dielectric properties of different cell-constituents and the supernatant are known, it is possible to calculate the dielectric spectrum of a cell suspension in the $\beta$-dispersion range from a single/double shell model together with the Maxwell-Wagner mixture model. Figure 17 shows the effect of increasing plasma membrane conductivity on the dielectric spectra of a

eukaryotic cell suspension. Altogether 15 parameters have to be included in the analysis as tabulated in Table 4. During the simulation, the plasma membrane conductivity was increased by 2 orders, from $1\ 10^{-5}$ S/m to $1\ 10^{-3}$ S/m, while all other parameters stay fixed as constant. The results show that the low frequency relative permittivity significantly decreases with increasing plasma membrane conductivity, dropping from 1100 ($\sigma_m = 1\ 10^{-5}$ S/m) to 150 ($\sigma_m = 1\ 10^{-3}$ S/m). The low frequency conductivity increases with increasing plasma membrane conductivity, rising from 87.1 mS/m ($\sigma_m = 1\ 10^{-5}$ S/m) to 107.2 mS/m ($\sigma_m = 1\ 10^{-3}$ S/m). Conversely, the high frequency spectrum is insensitive to the changes in plasma membrane conductivity for both relative permittivity and conductivity. In general, the increase in plasma membrane conductivity reduces the dielectric increment of $\beta$-dispersion and shifts the onset of $\beta$-dispersion to higher frequencies. Further analysis shows that these changes in the dielectric spectrum of the cell suspension are large enough to be detected by time domain dielectric spectroscopy.

**Table 4.** Fitting Parameters Used in Double Shell Model

| $\varepsilon_m$ | $\sigma_{cp}$ S/m | $\varepsilon_{cp}$ | $\sigma_{ne}$ $10^{-3}$ S/m | $\varepsilon_{ne}$ | $\sigma_{np}$ S/m | $\varepsilon_{np}$ |
|---|---|---|---|---|---|---|
| 8.0 | 0.4 | 60 | 2.0 | 40 | 0.8 | 120 |
| $\sigma_{sup}$ S/m | $\varepsilon_{sup}$ | $R_c$ μm | $R_n$ μm | $d_m$ nm | $d_n$ nm | $p$ |
| 0.1 | 78 | 5 | 4 | 7 | 40 | 0.1 |

The plasma membrane conductivity ($\sigma_m$) was fixed at $1\ 10^{-5}$ S/m for studying the effect of nuclear envelope conductivity on suspension dielectric spectra.
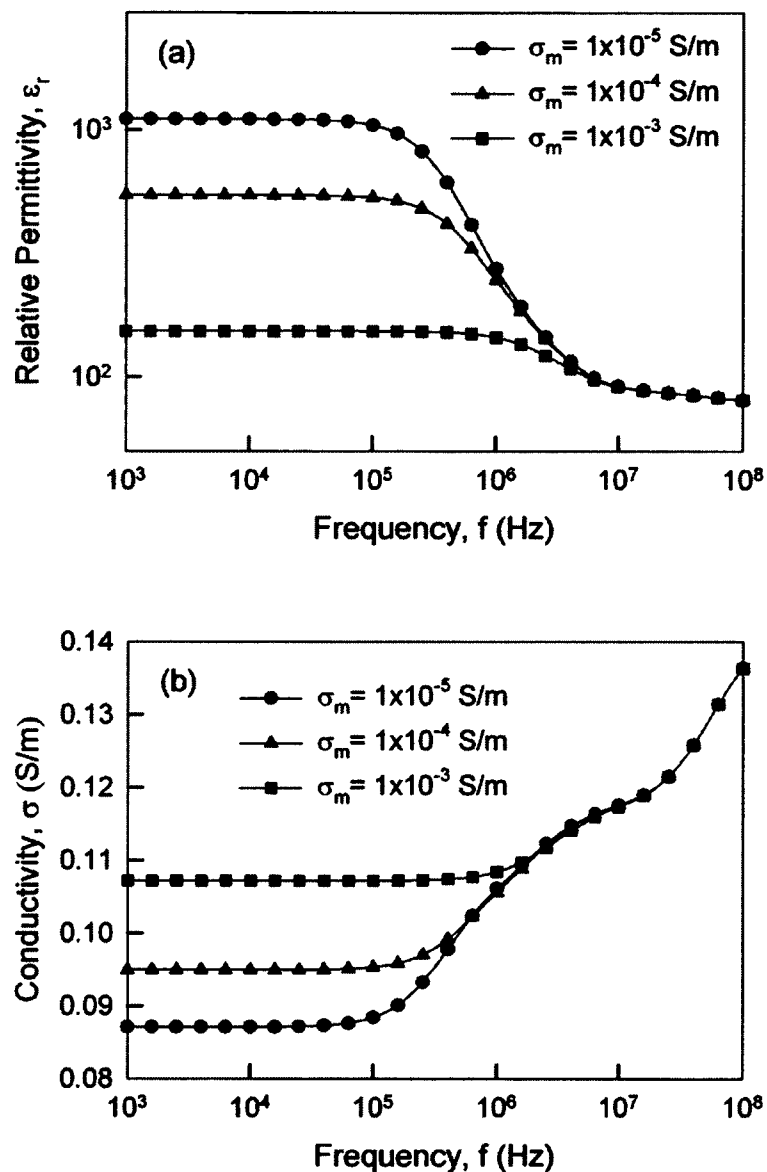
**Figure 17.** Effect of plasma membrane conductivity on the relative permittivity (a) and conductivity (b) spectrum of a eukaryotic cell suspension. The suspension dielectric spectra were generated by a combination of Maxwell-Wagner mixture model and a double-shell model. The fitting parameters are listed in **Table 4**. The effect of electrode polarization was not considered in the simulation.

### 4.2.2 Effect of Nuclear Envelope Conductivity

Previous studies have shown that intense nanosecond pulses affect intracellular structures such the nucleus. Therefore changes in the dielectric properties of the nucleus, e.g. nuclear envelope conductivity ($\sigma_{ne}$), can be expected for a double shell model. Figure 18 shows the effect of nuclear envelope conductivity on the dielectric spectra of a eukaryotic cell suspension. All parameters used in the analysis are listed in Table 4. During the simulation, the nuclear envelope conductivity was increased by 2 orders, from $2 \ 10^{-3}$ S/m to $2 \ 10^{-1}$ S/m, while all other parameters remain fixed. The simulation shows that the changes in nuclear envelope conductivity affect $\beta$-dispersion but the changes are less pronounced comparing to those induced by plasma membrane conductivity. The relative permittivity and conductivity at both low frequencies ($f < 100$ kHz) and high frequencies ($f > 10$ MHz) are insensitive to the changes in nuclear envelope conductivity. When the nuclear envelope conductivity increases from $2 \ 10^{-3}$ S/m to $2 \ 10^{-2}$ S/m, the changes in the dielectric spectra are significant. Both the permittivity and conductivity spectrum become less sensitive to further increases in nuclear envelope conductivity from $2 \ 10^{-2}$ S/m to $2 \ 10^{-1}$ S/m.
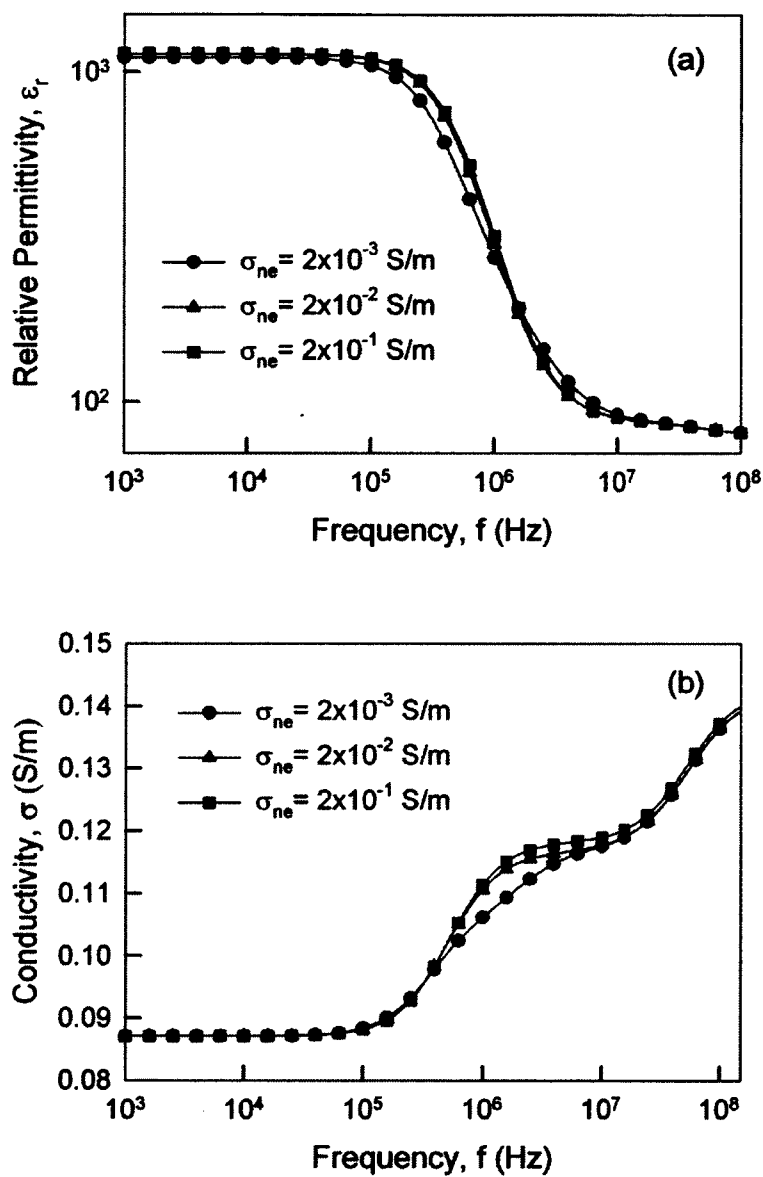
**Figure 18.** Effect of nuclear envelope conductivity on the relative permittivity (a) and conductivity (b) spectrum of a eukaryotic cell suspension. The suspension dielectric spectra were generated by a combination of Maxwell-Wagner mixture model and a double-shell model. The fitting parameters are listed in Table 2. The effect of electrode polarization was not considered in the simulation.

## 4.3 Dielectric Evolution of Jurkat Cells after Exposure to Pulsed Electric Fields

### 4.3.1 Changes in Supernatant Conductivity

Figure 19 shows the development of the supernatant conductivities of control, μsPEF-exposed and nsPEF-exposed cell suspensions. The time line was established by the first measurement on the control sample (t = 0). Exposures to pulsed electric fields were conducted at the same time with respect to subsequent dielectric measurements. A one-way ANOVA test showed that the conductivity for any pulsed electric field treatment is significantly different from the other two groups (P < 0.05). For all conditions the supernatant conductivity linearly increases with time for all measurements beyond 5 minutes. The rate of change is similar in all three cases. For control cells, the increase is consistent with a change from time zero. However, the exposed cell suspensions had already reached significantly higher supernatant conductivity values compared to the control within the first 5 minutes after exposure. The increase in supernatant conductivity after nsPEF exposure was twice as high as after μsPEF exposure.
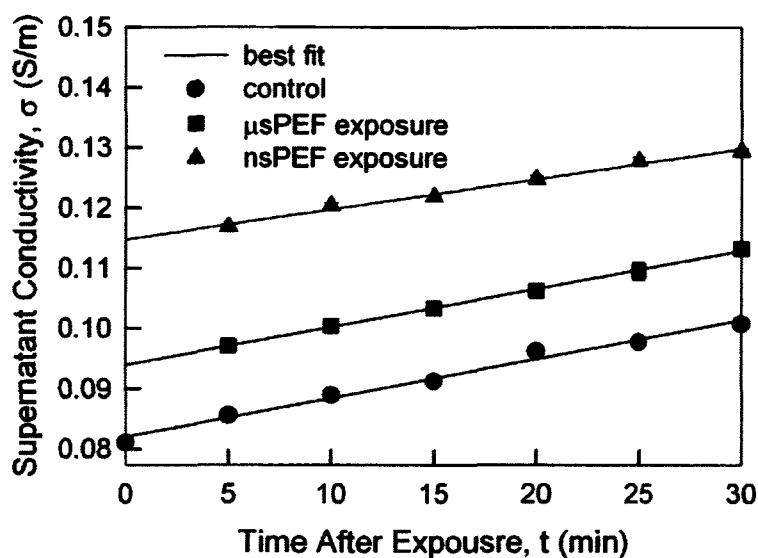
**Figure 19.** The temporal development of the supernatant conductivities of Jurkat cell suspensions with 10% volume fraction after exposure to eight 1.1 kV/cm, 100 μs pulses or eight 20 kV/cm, 300 ns pulses. Error bars, which represent standard deviations, are often smaller than the symbols displayed in the graph.

## 4.3.2 Changes in Plasma Membrane Conductivity and Permittivity

With the corrected dielectric spectra, changes in cell membrane conductivity and permittivity after PEF exposure were derived from a single shell model. Figure 20 shows the resulting temporal development of the plasma membrane conductivities and relative permittivity for control and exposed cells. Initial values (t = 0) for conductivity and relative permittivity of unexposed cells are 31 S/m and 8.3, respectively. The statistical analysis (ANOVA) confirms that the plasma membrane conductivities and relative permittivities of exposed cells are significantly different from those of control cells (P < 0.05). The membrane conductivity of control cells increased over 30 minutes to 3 times the initial value. The increase for μsPEF is slightly higher, reaching 4 times higher than pre-exposure values after 30 minutes. In comparison, the membrane conductivity after

nsPEF exposure already rises to about 9 times the pre-exposure value within 5 minutes and continues to increase to about 11 times the initial value.

**Table 5.** Results of Linear Regression Analysis, Determining Membrane Conductivity and Permittivity Immediately Following PEF Exposures

| | Intercept (t=0 min) | Rate of change | $R^2$ |
|---|---|---|---|
| $\sigma_{sup}$ of control | 82.0 mSm$^{-1}$ | 6.5x10$^{-4}$ mSm$^{-1}$s$^{-1}$ | 0.986 |
| $\sigma_{sup}$ after µs-exposure | 93.9 mSm$^{-1}$ | 6.3x10$^{-4}$ mSm$^{-1}$s$^{-1}$ | 0.999 |
| $\sigma_{sup}$ after ns-exposure | 115mSm$^{-1}$ | 5.0x10$^{-4}$ mSm$^{-1}$s$^{-1}$ | 0.989 |
| $\sigma_m$ of control | 32 µSm$^{-1}$ | 1.5 µSm$^{-1}$s$^{-1}$ | 0.883 |
| $\sigma_m$ after µs-exposure | 49 µSm$^{-1}$ | 2.5 µSm$^{-1}$s$^{-1}$ | 0.997 |
| $\sigma_m$ after ns-exposure | 263 µSm$^{-1}$ | 2.7 µSm$^{-1}$s$^{-1}$ | 0.781 |
| $\varepsilon_m$ of control | 8.2 | 0.02 s$^{-1}$ | 0.507 |
| $\varepsilon_m$ after µs-exposure | 9.3 | 0.05 s$^{-1}$ | 0.894 |
| $\varepsilon_m$ after ns-exposure | 15.2 | 0.16 s$^{-1}$ | 0.799 |

$\sigma_{sup}$: supernatant conductivity, $\sigma_m$: membrane conductivity, $\varepsilon_m$: relative membrane permittivity

In 30 minutes, the membrane permittivity of unexposed cells does not change. The relative membrane permittivity of µsPEF-exposed cells increased to 11.4 within 30 minutes. For nsPEF-exposure, the value already increases to 16 within the first 5 minutes, and in the next 25 minutes, the membrane permittivity continues to increase to 20. The development follows the same trend as observed for the supernatant conductivities pointing towards their correlation. The results show that a strong change in membrane conductivities and relative membrane permittivities is already established in the first 5 minutes after exposure for nsPEF. The increase observed for µsPEF is only moderate in comparison. The observed continuing increase of values, in all cases develops at slower, fairly linear and similar rates. Consequently, a regression analysis and extrapolation of

measurements allows conclusions on changes immediately following exposure. The results for respective slopes and intercepts for "time zero", i.e., values expected for membrane conductivity and permittivity, are shown in Table 5.
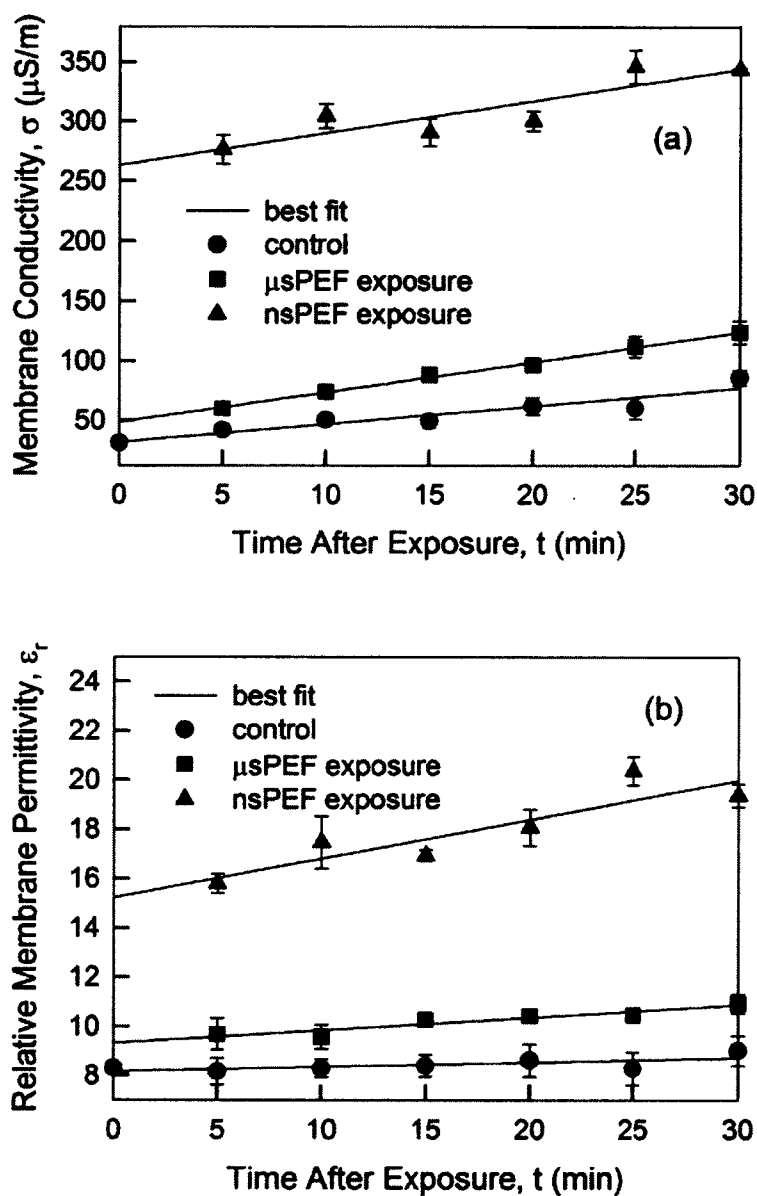
**Figure 20.** Development of plasma membrane conductivities (a) and relative membrane permittivities (b) of Jurkat cells after exposure to eight 1.1-kV/cm, 100-μs pulses or eight 20-kV/cm, 300-ns pulses. Error bars indicate standard deviations. Changes in both conductivity and permittivity are much stronger for nsPEF.

### 4.3.3 Changes in Cytoplasm Conductivity

Changes in cytoplasm conductivities for control and PEF-exposed cells were derived from a double shell model, as shown in Figure 21. The cytoplasm conductivity of control cells remained around 0.43 S/m during 30 minutes experiment time. For µsPEF-exposed cells, the conductivity value dropped to 0.41 S/m 5 minutes after exposure. No significant changes were observed for later times. The cytoplasm conductivity after nsPEF exposure dropped to 0.25 S/m after 5 minutes, which is more than 40% decreases compared to the pre-exposure value. From 5 minutes to 30 minutes, the cytoplasm conductivity gradually decreased to 0.22 S/m with a constant changing rate. The exposure to nsPEFs caused significant changes to cytoplasm conductivity in comparison with control and µsPEF-exposed cells (P < 0.01).
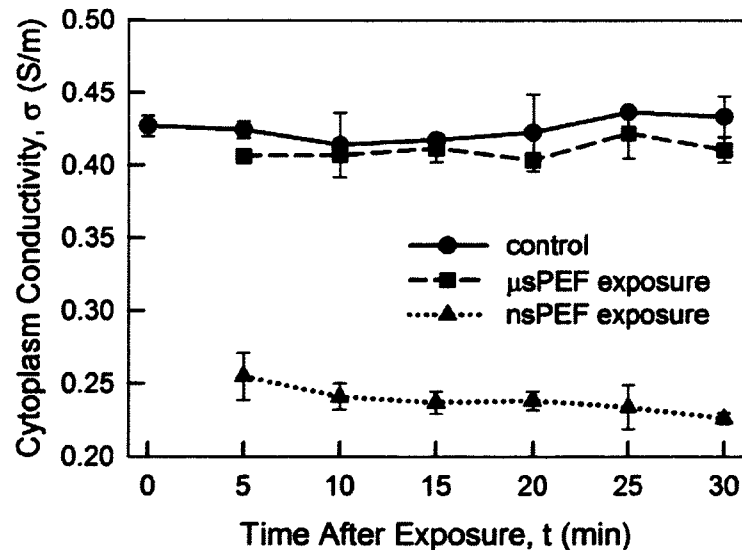


**Figure 21.** The temporal development of the cytoplasm conductivities of Jurkat cells after exposure to eight 1.1-kV/cm 100-µs pulses or eight 20-kV/cm 300-ns pulses. Error bars indicate standard deviations.

### 4.3.4 Changes in Nuclear Envelople Conductivity

Changes in nuclear envelope conductivities for control and exposed cells were derived from a double shell model, as shown in Figure 22. For both control and μsPEF-exposed cells within 30 minutes measuring period, the nuclear envelope conductivities remained about 2.0 ms/m. The nuclear envelope conductivity after nsPEF exposure rose to about 2.7 mS/m after 5 minutes. For the next 25 minutes, the nuclear envelope conductivity remained steady around this value. The statistical analysis (ANOVA) showed that the nuclear envelope conductivities of cells after μs-exposure were not significantly different from that of control cells ($P > 0.05$). Conversely, nsPEFs induced significant changes in comparison with control cells ($P < 0.05$).
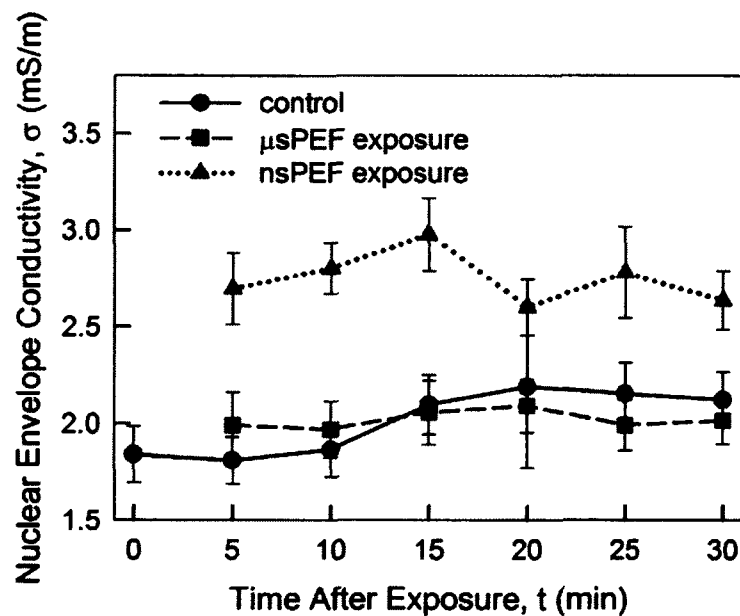


Figure 22. The temporal development of the nuclear envelope conductivities of Jurkat cells after exposure to eight 1.1-kV/cm 100-μs pulses or eight 20-kV/cm 300-ns pulses. The nsPEFs cause significant increases in the nuclear envelope conductivity whereas μsPEFs have no effects on the nuclear envelope conductivity. Error bars indicate standard deviations.

### 4.3.5 Changes in Nucleoplasm Conductivity

Figure 23 shows the temporal development of nucleoplasm conductivity of control and exposed cells obtained from a double shell model. The pre-exposure value for nucleoplasm conductivity was 0.81 S/m, which is about 2 times the cytoplasm conductivity. For control cells, the nucleoplasm conductivities remained unchanged within 30 minutes. The nucleoplasm conductivities of μsPEF-exposed cells were slightly lower than that of control cells. However, statistical analysis showed that the differences were not significant ($P > 0.05$). Significant changes ($P < 0.01$) were induced by exposure to nsPEFs, which decreased the nucleoplasm conductivity to 0.54 S/m after 5 minutes. At 10 minutes, the conductivity further dropped to 0.49 S/m. From 10 minutes to 30 minutes, continuous reduction was still seen with a constant decreasing rate.
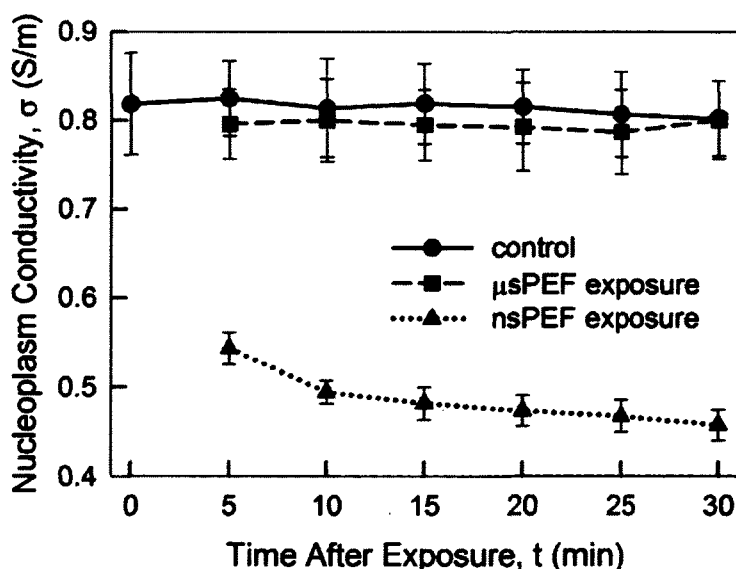


**Figure 23.** The temporal development of the nucleoplasm conductivities of Jurkat cells after exposure to eight 1.1-kV/cm 100-μs pulses or eight 20-kV/cm 300-ns pulses. Error bars indicate standard deviations.

## 4.4 Pulsed Electric Field Induced Changes in Plasma Membrane Integrity and Cell Survival

### 4.4.1 Temporal Development of Plasma Membrane Integrity after Exposure

The plasma membrane integrity of Jurkat cells after PEF exposure was examined by Trypan Blue Uptake (TBU), labeling cells with severely damaged membrane. The results are shown in Figure 24. For control cells, i.e., cells that were treated similarly to other samples but not exposed to an electric field, the fraction of cells showing trypan blue uptake is consistent at about 10% and no significant changes are observed within 30 minutes. The response is similar for µsPEF-exposed cells and differences in trypan blue uptake compared to control cells are not statistically significant, as was confirmed by an ANOVA analysis with $P > 0.05$. For nsPEF-exposed cells, the fraction taking up trypan blue increases from 10% to 40% after 5 minutes. After 10 minutes, the fraction of cell taking up trypan blue increases to 70% and remains stable for the next 20 minutes. Notably, exposure to nanosecond pulsed electric fields results in a significant number of dead cells over time, while cell viability seems not to be affected for microsecond applications within the first 30 minutes following exposure.

Fraction of Cells with TBU (%)

control
μsPEF exposure
nsPEF exposure

Time After Exposure, t (min)
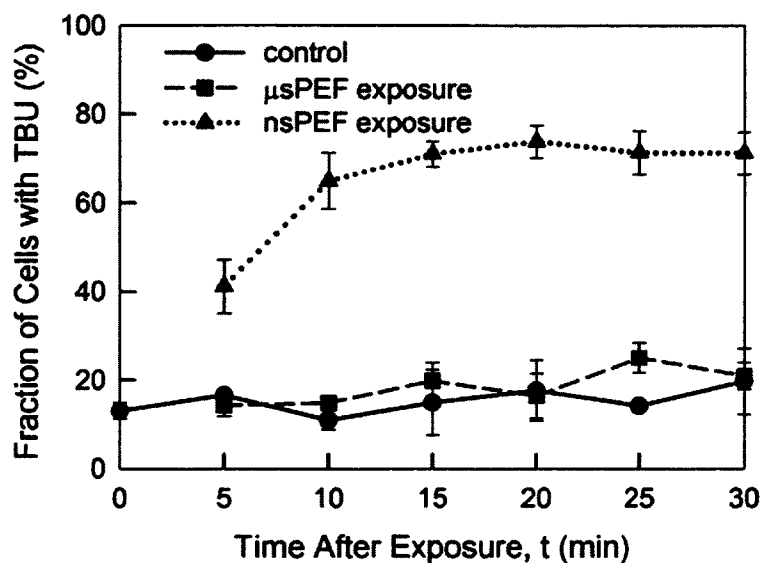
**Figure 24.** Fraction of cell showing Trypan Blue Uptake (TBU) as a function of time after exposure to eight 1.1 kV/cm, 100 μs pulses or eight 20 kV/cm, 300-ns pulses. Error bars represent standard deviations. (Each experiment was repeated at least 3 times.)

### 4.4.2 Poration of Plasma Membrane Determined by Propidium Iodide

Propidium Iodide (PI) was added to Jurkat celll suspensions before (Figure 25) or after (Figure 26) exposure to pulsed electric fields to detect the existence of membrane pores. Figure 25 shows the uptake of PI by Jurkat cells 2 minutes and 15 minutes after exposure to eight 1.1 kV/cm, 100 μs pulses or eight 20 kV/cm, 300-ns pulses. PI was added to cell suspensions before exposure to pulses. Cells show significant amount of PI uptake after exposure to eight 1.1 kV/cm, 100 μs pulses (Figure 25a and 25c), which is strong evidence of electroporation of plasma membrane. On the other hand, few cells show sign of PI uptake 2 minutes after exposure to eight 20 kV/cm, 300 ns pulses (Figure 25c). The percentage of cells taking up PI increased remarkably 15 minute after exposure, as shown in Figure 25d. Figure 26 shows the uptake of PI by Jurkat cells under the same exposure

conditions with PI added 10 seconds after exposure. The delayed addition of PI significantly affected the outcome of microsecond exposures, most cells did not take up PI at either 2 minute (Figure 26a) or 15 minute (Figure 26c) following exposure. Conversely, similar PI uptake pattern was observed for cells exposed to nanosecond pulses (Figure 26b and d).

**8 pulses: 1.1 kV/cm, 100 μs**          **8 pulses: 20 kV/cm, 300 ns**
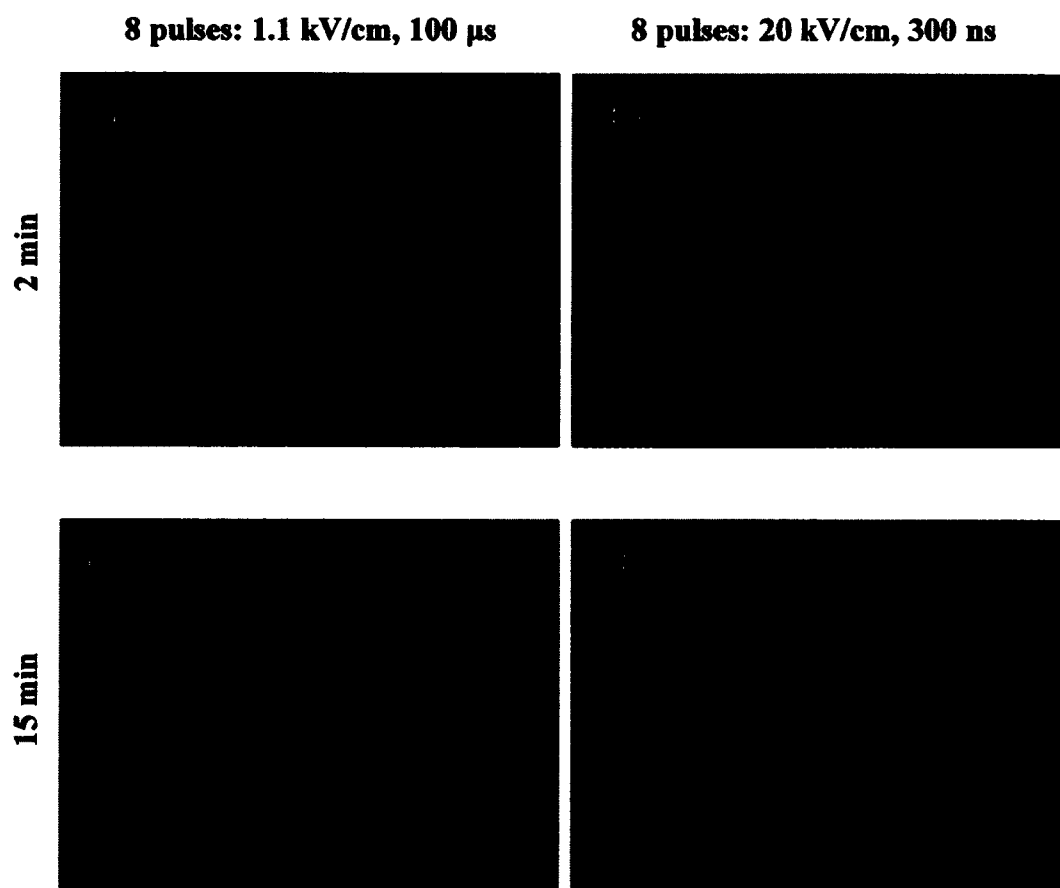


**Figure 25.** Uptake of PI by Jurkat cells 2minutes (a) and 15 minutes (c) after exposure to eight 1.1 kV/cm, 100 μs pulses or 2minutes (b) and 15 minutes (d) after exposure to eight 20 kV/cm, 300-ns pulses. PI was added to cell suspensions before exposure to pulses. The cell suspensions were diluted to about $1\ 10^{6}$ cell/ml before images were taken.

**8 pulses: 1.1 kV/cm, 100 μs**     **8 pulses: 20 kV/cm, 300 ns**
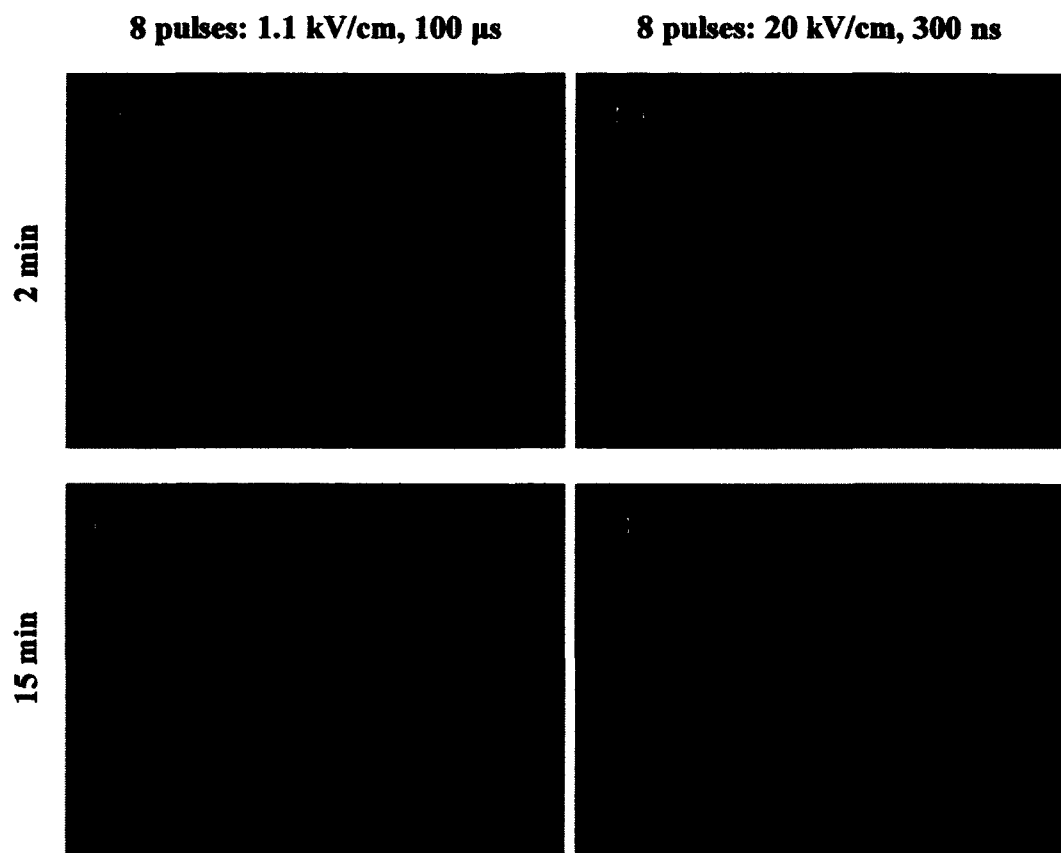


**Figure 26.** Uptake of PI by Jurkat cells 2minutes (a) and 15 minutes (c) after exposure to eight 1.1 kV/cm, 100 μs pulses or 2minutes (b) and 15 minutes (d) after exposure to eight 20 kV/cm, 300-ns pulses. PI was added to cell suspensions within 10 seconds after exposure to pulses. The cell suspensions were diluted to about 1 106 cell/ml before images were taken.

## 4.4.3    Short-term Plasma Membrane Conductivity and Long-term Cell Survival

Figure 27a shows the plasma membrane conductivity (normalized to control) of Jurkat cells determined 30 minutes after exposure to 8 pulses of different pulse width and pulse amplitude. The 24-hour cell survival of corresponding exposure condition is shown in Figure 27b. Different exposure conditions induced significantly different responses in plasma membrane conductivity and 24-hour cell survival. For cells exposed to PEFs with same pulse width but different pulse amplitude, higher electric field strength caused

higher plasma membrane conductivity and lower cell survival. For cells exposed to PEFs with same pulse amplitude but different pulse width, longer pulse duration resulted in higher plasma membrane conductivity and lower cell survival. For cells exposed to PEFs with same electrical energy (60 ns with 45 kV/cm, 300 ns with 20 kV/cm, 100 $\mu$s with 1.1 kV/cm), 300ns-PEF has the most significant effects in increasing plasma membrane conductivity and reducing 24-hour cell survival. The results show that higher short-term plasma membrane conductivity corresponds to lower long-term cell survival.
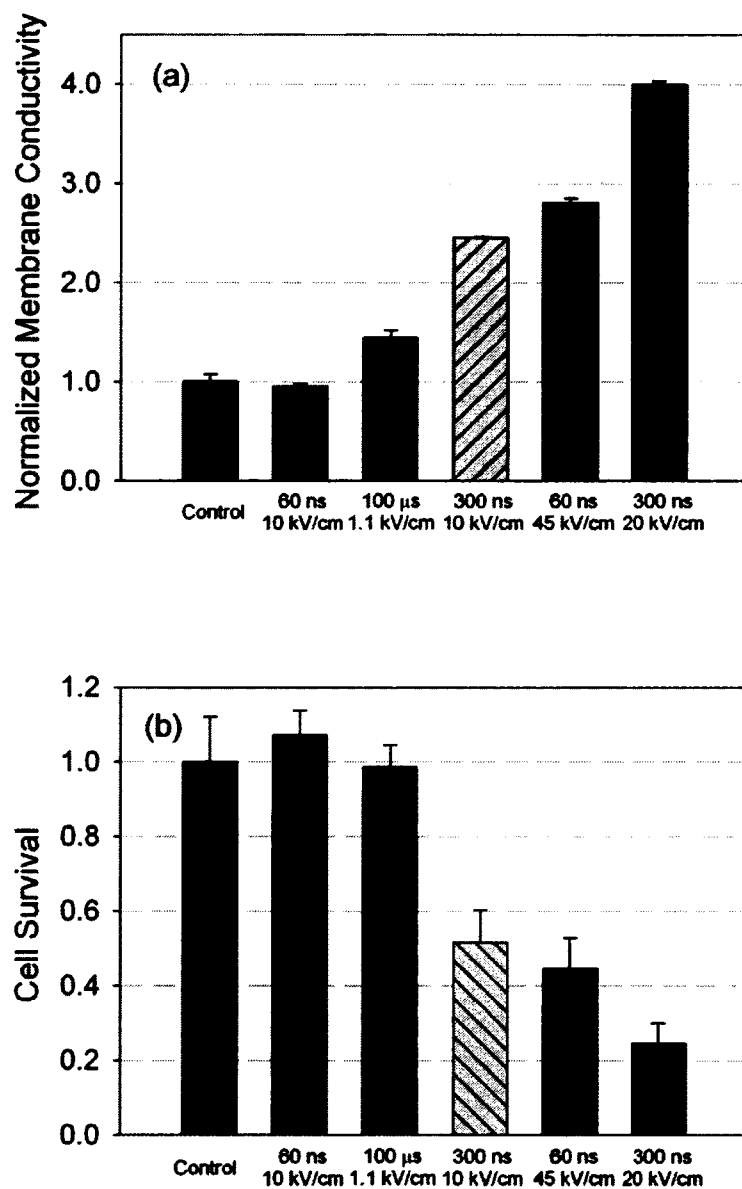
**Figure 27.** Plasma membrane conductivity measured 30 minutes (a) and cell survival rate measured 24 hours (b) for Jurkat cells after exposure to 8 pulses of various pulse width and amplitude. Higher short-term plasma membrane conductivity corresponds to lower long-term cell survival. Error bars are calculated by standard deviation.

## 4.5 Nanosecond Pulsed Electric Field Induced Changes in Dielectric Properties of Tissues

### 4.5.1 Effect of nsPEFs on the Dielectric Properties of Pig Blood

Figure 28 shows the dielectric spectra of pig whole blood before and 5 minutes after exposure to eight 30 kV/cm, 300 ns pulses from 1 kHz to 400 MHz. Both spectra were fitted into a Cole-Cole relaxation model. The parameters for the best fit are listed in Table 6. The low-frequency relative permittivities of both unexposed and exposed blood were dominated by electrode polarization effect. The $\beta$-dispersion in both unexposed and exposed pig blood spectrum ranges from 1 MHz to 100 MHz. Five minutes after exposure to nanosecond pulses, the low frequency conductivity ($\sigma_{dc}$) of blood decreased from 0.6 S/m to 0.47 S/m. The low frequency relative permittivity spectrum decreased from 2382 to 1621. The relaxation time ($\tau$) decreased from 80.7 ns to 35.1 ns. The high frequency relative permittivity ($\varepsilon_h$) did not change significantly after exposure.

**Table 6.** Best-fit Parameters of Cole-Cole Relaxation Model for the Dielectric Spectra in Figure 28.

|  | $\varepsilon_l$ | $\sigma_{dc}$ S/m | $\tau$ ns | $\alpha$ | $\varepsilon_h$ |
|---|---|---|---|---|---|
| Blood (control) | 2133 | 0.66 | 68.1 | 0.87 | 59.5 |
| Blood (pulsed) | 1627 | 0.55 | 32.4 | 0.92 | 61.5 |
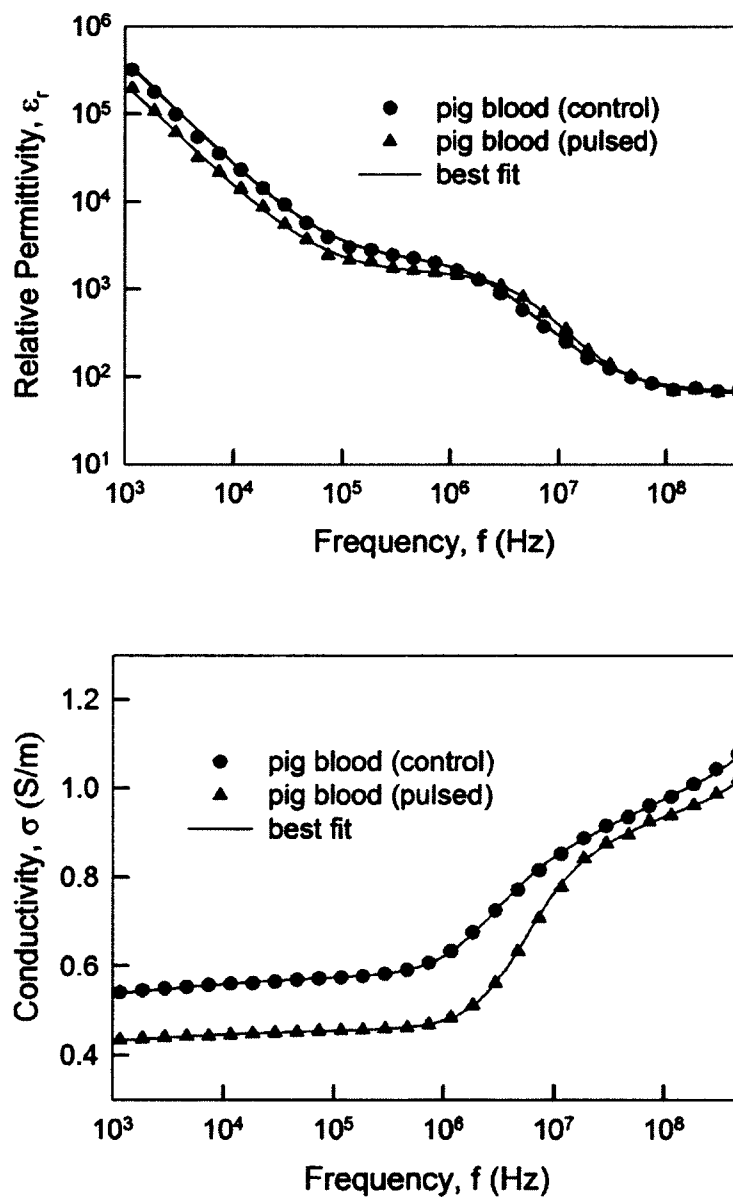
**Figure 28.** The relative permittivity (a) and conductivity (b) spectrum of pig whole blood before and 5 minutes after exposure to eight 30 kV/cm, 300 ns pulses.

### 4.5.2 Effect of nsPEFs on the Dielectric Properties of Potato

The dielectric spectra of a sliced potato disk (0.2 cm thick), measured by an open-ended measuring sensor, before and after exposure to eight 20 kV/cm, 300 ns pulses are shown in Figure 29. Both the relative permittivity and conductivity spectrum of unexposed potato show a strong $\beta$-dispersion from 100 kHz to 100 MHz. The exposure to nanosecond pulses significantly increased the conductivity of potato in the low frequency range. The relative permittivity spectrum of exposed potato presents a sign of electrode polarization at low frequencies (f < 10 kHz) due to increased conductivity. The effect of nanosecond-exposure becomes negligible in both the relative permittivity and conductivity spectrum when frequency is higher than 10 MHz.
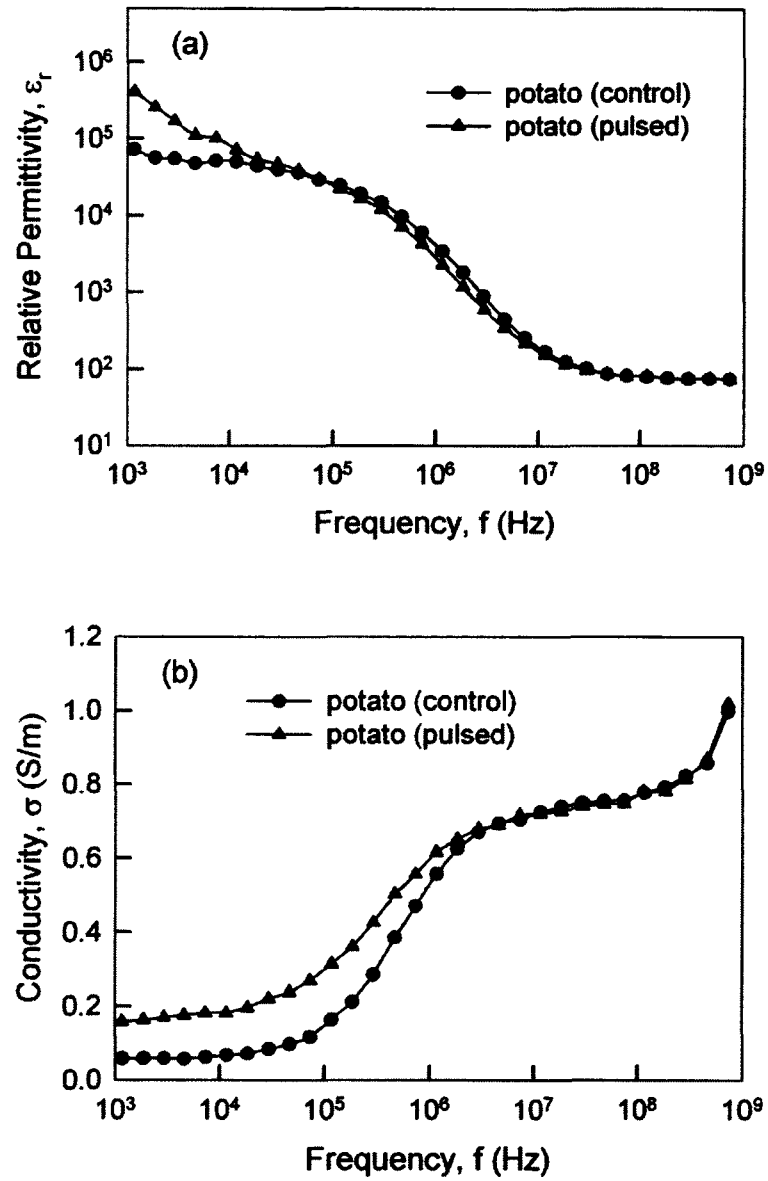
**Figure 29.** The relative permittivity (a) and conductivity (b) spectrum of potato before and 5 minutes after exposure to eight 20 kV/cm, 300 ns pulses.

# CHAPTER 5

## DISCUSSION

The response of cells and tissues following the exposure to a pulsed electric field is generally discussed as the poration of the cell membranes and the development of the changes in membrane permeability. It is supposed that the efficacy of drug uptake and gene transfer achieved through reversible electroporation techniques can be related to exposure parameters, such as pulse duration, pulse amplitude, pulse number and repetition rate. These same pulse parameters can also be used to characterize the ablation of tissues by irreversible electroporation. Many experiments have shown that exposures to nanosecond pulsed electric fields cause biological responses distinctively different from results obtained with longer pulses [18, 24, 26]. Differences are explained by the potential of shorter, intense pulses to affect and manipulate subcellular structures. Simultaneously, the characteristic for the permeabilization of membranes (inner and outer) is very different from exposures to longer pulses. The specific changes to the cell morphology and function will be reflected in respective changes of the dielectric properties. Consequently, measurements of conductivity and permittivity of cellular structures can be used to describe and compare different exposure regimens and ultimately even predict the fate of cells or the efficacy of the treatment parameters. This motivates our study: investigate changes in the dielectric properties of biological cells after nsPEF exposure and relate these changes to conformational and functional changes.

## 5.1 Methodological Development

Measurements of dielectric parameters generally employ techniques of dielectric spectroscopy in the frequency or the time domain. Whereas the first method requires

scanning of samples for different frequencies, the second approach delivers results of all frequencies in a single measurement. Since this reduces the possibility that cell properties might change during the diagnostic or even be affected by it, this procedure is often preferred. However, we had to develop and modify the method to consider specific requirements arising from the analysis of cells and tissues exposed to pulsed electric fields. To account for the multiple dielectric relaxation processes of the cell suspensions and tissues, we adjusted the sampling rate of the measurement according to the respective time scales of the different mechanisms contributing to the overall dielectric response. Our method was adapted from a technique developed and used by Hagar to determine the fraction of water in concrete samples and it relies on non-linear data sampling [111]. The non-uniform sampling technique preserves the details of each relaxation process without significantly increasing the total sampling time. A typical measurement is shown in Figure 13. Unfortunately, in this research TDR dielectric spectroscopy could not be conducted during exposure, since the TDR oscilloscope is very sensitive to high voltages. Also using a TDR dielectric spectroscopy system, Pliquett et al. developed a exposure/measuring sample holder and a fast mechanical switching system that allowed dielectric measurement of Jurkat cell suspensions only 10 ms after ns-exposure with a 100 ms temporal resolution [104]. In this study dielectric measurement and PEF-exposures were conducted with different sample holder. It takes about 5 minutes to transfer exposed cell suspensions from the electroporation cuvette to the measuring sensor and stabilize the temperature with our current experimental setup and protocol. Hence in the study of PEF effects on Jurkat cells, we chose to observe the dielectric response and cell membrane integrity from 5 minutes to 30 minutes after exposure.

Future improvements of the method aim to close the time lag between exposure and dielectric measurements.

To ensure the viability of cells, they must be suspended in electrolytic solutions with certain ions present. A particularly difficult problem with conductive samples is the polarization of the sampling electrodes, which dominates the dielectric spectra in the frequency range from 1 kHz to several hundred kHz in our measurements. The influence of electrode polarization becomes stronger and extends to higher frequency as the conductivity of the sample increases, as shown in Figure 15. The effect of electrode polarization on dielectric spectra competes with the $\beta$-dispersion response, which is the manifestation of the Maxwell-Wagner effect at the interface between cell and electrolyte. Modifying the material especially the surface property of the measuring electrode, e.g. plating a layer of platinum black, has been shown to significantly reduce the magnitude of electrode polarization. We also plated our measuring sensor for cell suspensions with platinum black. However, it does not completely remove electrode polarization. Different numerical correction methods have been developed to further separate contributions from electrode polarization and the sample [132]. Feldman has shown that the typical substitution method and single exponential correction method cannot remove the electrode polarization effect entirely [132]. The substitution method, which requires obtaining the supernatant by centrifuging the cell suspension, is especially not suitable for this study. We found that centrifugation significantly increased the supernatant conductivity of nsPEF-exposed cell suspensions, mostly due to poration of cell membranes. Alternatively, we have used a correction method suggested by Bordi et al. [114], which was reported to completely remove electrode polarization by modeling it as

a constant-phase-angle (CPA) element in series with the sample. Although the dielectric relaxations of different samples can already be distinguished in their time domain responses and Sun et al. have shown theoretically that the dielectric properties of cells can be derived in time domain directly [133], the correction of electrode polarization in time domain has not been reported yet to the best of our knowledge. The CPA-electrode polarization correction technique can also only be applied to frequency domain spectra so far. Hence the recorded time domain responses were brought into the frequency domain by a running Laplace Transform which was specifically designed for the non-uniformly sampled time domain signal [110]. To extract parameters for electrode polarization (K and $\eta$ in equation (7), an analytical model representing the bulk dielectric spectrum of the sample is required for numerical fitting of the dielectric spectra. For a conductive electrolyte, such as the supernatant of a cell suspension, both the permittivity and conductivity are constant from 1 kHz to 100 MHz. For a cell suspension or a tissue, a Cole-Cole relaxation function (equation 8) is usually used to describe the $\beta$-dispersion. The combination of platinum black plating and CPA-electrode polarization correction allowed us to study the $\beta$-dispersion of low-conductivity cell suspension as well as tissues with physiological conductivity such as pig blood and potato. Figure 16 shows an example of corrected dielectric spectra of a cell suspension modeled by a Cole-Cole function with this correction.

The derivation of dielectric parameters for cell constituents from the dielectric spectra obtained for a cell suspension requires further efforts. In our analysis, we generally followed the theoretical analysis by Ermolina [116]. Accordingly, information for individual cells – as a whole – is linked to the cell suspension by applying a Maxwell-

Wagner mixture model, which requires knowledge about the volume fraction of cells in the suspension as a critical parameter. The derivation of values for cell components, such as the membrane or the nucleus, necessitates further assumptions, in particular, about the geometry of the investigated cells. A fundamental model assumes the cells to be spheres with a shell of different dielectric properties. Consequently, this single shell model is particularly appropriate for cells without nucleus such as erythrocyte ghosts. Since the dielectric properties of erythrocyte ghosts are very well studied, it makes an excellent standard model for verification purpose. For eukaryotic cells, i.e. cells having a nucleus, a more complicated dielectric cell model – double shell model- was employed in this study. Through this model the conductivity of intracellular structures such cytoplasm, nuclear envelope and nucleoplasm was derived. For cells exposed to intense pulsed electric fields, the specific changes to the plasma membrane, such as formation of pores, will be inevitably reflected in changes of plasma membrane conductivity. The simulation results in Figure 17 show that both the relative permittivity and conductivity spectrum of a cell suspension will change significantly if the plasma membrane conductivity increases. Therefore the changes in plasma membrane conductivity can be obtained by measuring the dielectric spectra of a cell suspension before and after PEF-exposure and fitting the spectra into above mentioned Maxwell-Wagner mixture model and double shell model. In addition to plasma membrane conductivity, the dielectric changes in supernatant, cytoplasm and nucleus following PEF-exposures can also be estimated this way. It is worth noting that the sensitivity of suspension dielectric spectra to nuclear envelope conductivity is lower than that to plasma membrane conductivity. Hence the changes in

nuclear envelope conductivity induced by nsPEF-exposures were determined with a higher uncertainty.

However, for changes induced by pulsed electric fields, other complications have to be taken into account. Often very low conductivity buffers have been employed to minimize the electrode polarization effect for dielectric spectroscopy of cell suspensions, especially when the Maxwell-Wagner mixture model is used to derive dielectric parameters of cells. The low conductivity of the buffer has been reported to induce Maxwell stress on the cell membrane which causes deformation of the cells during PEF-exposure [134]. Such electro-deformation force occurs in a few nanoseconds after the onset of pulsed electric field and contributes significantly to the enlargement of "electroleaks" in the plasma membrane induced by pulsed electric fields [135, 136]. In addition, cells might leak ions due to the low ionic strength of the extracellular environment and, as a result, the conductivity of the cell suspension and the supernatant are changing with time even without exposure. In our experiments, we also compromised on a buffer of relatively low conductivity and found a slow but continuous conductivity increase in unexposed and exposed cell suspensions, suggesting ion leakage from cells (Figure 19). In return, this result suggests that the dielectric properties of the plasma membrane are depending and changing due to the buffer itself. The low conductivity buffer also has been reported to affect other cell characteristics, including ion channel regulation, membrane potential, membrane fluidity and pH of the cytoplasm [137]. In general, many details on the relation between the characteristics of the buffer and the dielectric properties of cells are not well understood yet and all experiments can therefore only distinguish between exposed and unexposed cells for the same environment. As the discussion shows, the

interaction between pulsed electric fields and cell membranes can also not be assessed independently from the properties of the buffer. Likewise, the subsequent development after exposure to a pulsed electric field will depend on the buffer itself as well [138]. In our experiments we have therefore consequently distinguished between the effects induced by the buffer alone and the changes that are caused by an exposure under these conditions. Accordingly, we have not relied on fixed conductivity of the buffer itself for the different regimens but taken into account the changes in the conductivity of the supernatant for the different exposure conditions and the unexposed control. Previous studies have usually disregarded the effect and relied on constant values for the supernatant conductivity instead.

As a result of the combination of these efforts, we now have a method available that allows us to measure and follow the changes in the dielectric parameters of cell constituents in a low-conductivity buffer. For dielectric spectroscopy of tissues the cell volume fraction is usually very high (> 30%) thus the intensity of $\beta$-dispersion is much stronger than that of Jurkat cell suspensions used this study. Therefore we were also able to detect the changes in the bulk dielectric parameters of tissues in spite of much higher ionic conductivity. The approach further permits us complete control over every step of the analysis, while investigations that our group conducted in the past had to rely on the output of an integrated measurement system and were limited to low conductive samples [27, 34].

## 5.2 Dielectric Measurements

With TDR dielectric spectroscopy, we measured different types of samples including cell suspensions and tissues (Figure 14). Despite the influence of electrode polarization at

low frequencies, the existence of $\beta$-dispersion in all samples is still evident due to the careful design of the measuring sensor. Substantial differences in relaxation frequency and dielectric increment are seen in both the permittivity and conductivity spectra, which can be attributed to differences in cell volume fraction, cell size, conductivity of extracellular environment and cell dielectric properties. Noteworthy the relative permittivity of all samples approaches to a constant value (~80) as frequency reaches 100 MHz, suggesting that most content of these samples is water. The relative permittivity and conductivity of the ghost membrane are in good agreement with values reported in literature [121], which confirms the validity and accuracy of our method (Table 3). We have also compared results obtained with our method for three types of cancer cells with reports in the literature for the same or similar cells and investigations using a similar technique [27, 34, 50, 127, 139]. Our results again agree well with reported values. For all cell lines the nucleoplasm conductivity is consistently higher than the cytoplasm conductivity, suggesting that the nuclear envelope is capable of regulating ion flux or is less viscous than cytoplasm. The higher conductivity of nuclear envelope corresponds to the fact that the pores in nuclear envelope are larger than the ion channels in plasma membrane. The nuclear envelope consists of two concentric membranes thus the relative permittivity is much higher than that of the plasma membrane. Our results show that the dielectric properties of cells are cell-type specific. The differences in cell dielectric parameters may be indications of different lipid/protein composition, membrane morphology and ion/molecule concentration among cell lines. The initial charging of membranes relies on the dielectric properties of cells. As a consequence, the diversity in

cell dielectric properties will result in cell-specific membrane changing and might be related to subsequent cell fate.

In order to track the time course of dielectric changes after exposure to intense pulsed electric fields, we chose Jurkat cells, which are spherical cells and fit the modeling requirements. In addition, a wealth of data exists on the effects induced with pulsed electric fields for Jurkat cells. A comparison of differences of exposures with pulsed electric fields of nanosecond duration and of microsecond duration was conducted. The temporal development membrane integrity after PEF-exposures was tested by both trypan blue and propidium iodide. The long term cell survival under various exposure conditions was recorded. Previous investigation had shown significant differences in the biological response, in particular, for cell survival [18, 24]. For the exposure to µsPEFs we chose parameters considered 'typical' for gene transfer [140]. Under these conditions, a temporary increase of membrane permeability is expected, which should correspond to an increase in membrane conductivity. Modeling and simulation studies predict that the poration is limited to the poles of the cells (with respect to the direction of the applied electric field) [17]. Conversely, the same simulations for the application of nsPEFs predict a poration of the entire cell envelope with much smaller but also more numerous pores. Compared with longer pulsed electric fields, subcellular membranes are presumably also affected in a similar fashion.

As discussed before, the plasma membrane dielectric properties were determined with higher confidence. Therefore we focused on membrane conductivity and permittivity of cells exposed to µsPEF and nsPEF and the conductivity of their supernatants starting 5 minutes after exposure and continuing for 25 minutes until 30 minutes post exposure. The

development of all parameters can be described by a linear increase with time (Table 5). Equivalent parameters differ strongly at the 5-min time point, but show relatively similar rates of change in further development. Notable differences are observed in membrane conductivities after exposure to either μsPEF or nsPEF, with membrane conductivities of unexposed samples increasing at a much slower rate. A faster rate of change is also observed for the permittivities of cell membranes after exposure to nsPEFs. The increase in membrane conductivity corresponds to a similar change in supernatant conductivities, although at orders of magnitude lower rates. The measurements show a linear increase for unexposed controls, starting from a value equivalent to the media conductivity without any cells present. Conversely, exposed cell suspensions show much higher initial supernatant conductivities that cannot be extrapolated to values for media without cells. However, the extrapolated values for μsPEFs are still only slightly higher compared to the increase observed for nsPEFs. The plasma membrane conductivity of Jurkat cells 30 minutes after various nsPEF-exposures were selected to compare with the corresponding 24-hour cell survival (Figure 27). The results indicate that the increase in plasma membrane conductivity leads to decrease in long term cell survival. Ivorra et al. also observed similar relationship between low-frequency tissue conductivity (mainly determined by plasma membrane conductivity) and cell viability after exposure to irreversible electroporation pulses [98]. Thus the plasma membrane conductivity may have the potential as a marker to predict the efficacy of nsPEF-related treatment.

## 5.3 Microsecond Exposures

Although we were not able to conduct measurements immediately after exposure, the extrapolation of the data allows us – to some degree – to draw conclusions on initial

values of dielectric parameters. For the exposure of 8 consecutive pulses (applied at 1 Hz) of 1.1-kV/cm amplitude and 100-µs duration, we found an increase in membrane conductivity of only 18 µS/m (43%) five minutes after exposure to pulses of 100 µs as compared to the unexposed control. The extrapolated value for the 'immediate' change in membrane conductivity (at t = 0) is 48.7 µS/m, which is equivalent to a slightly higher initial increase of 55% compared to the control group. This 'immediate' increase in membrane conductivity is considerably lower than expected from the previously described model of limited poration by a 10-µs, 1-kV/cm electroporation pulse, which predicts an increase in membrane conductivity of 3 orders of magnitude for the pole areas [141, 142]. However, experimental studies on both cell suspensions and cell pellets suggest that the elevated membrane conductivity decreases quickly after removal of the electroporation pulses. Kinosita et al. measured the conductivity increase of erythrocyte suspensions after exposure to an 80-µs pulse (3.7 kV/cm) and found the relative increase in suspension conductivity 1 ms after exposure was considerably smaller than that at the end of the 80-µs pulse [44]. This decrease in cell suspension conductivity was attributed to the recovery of membrane in the µs range. Schmeer et al. also observed a rapid decrease in cell pellet conductivity measured shortly (on the scale of seconds) after exposure to a 1-ms electroporation pulse [143]. Similar fast recovery was also found on planar lipid bilyaers by Melikov with a mean pore life-time of 3 ms [144]. The rapid recovery of membrane from electroporation has been predicted by modeling and simulation studies on cell membranes. Gowrishankar calculated a membrane conduction recovery time of 0.16 ms for electroporation conditions [17]. Much longer resealing times of 1.5 s were suggested by Krassowska's and DeBruin [31]. Therefore, the extrapolated

membrane conductivity may only reflect the residual or recovering membrane conductivity rather than the peak values of membrane conductivity that could be achieved with reversible electroporation conditions. Although multiple exposures will increase the membrane permeability further, only a remnant of perturbation might still be discovered after 5 minutes. Pavlin and Miklavcik have related the increase caused by consecutive pulses to a growing probability for the formation of larger pores as compared to smaller ones, which would then allow the uptake of large molecules into the cell [94]. They calculated pore relaxation times of 10 ms and hypothesize that after 100 ms only a few long-lived pores might have survived, which might still be sufficient to explain a substantial uptake of molecules. Although the times are shorter than monitored by our measurements, a long-lasting and persistent effect on the membrane conductivity is also implicated in our experiments (Figure 20a). A slightly greater rate of change in conductivity for μsPEF-exposure might actually indicate a lingering increased permeability. This might be the result of the pore resealing process as suggested by Pavlin and Miklavcic [94].

That transient pores of sufficient size, i.e., allowing larger molecules to pass through, had actually formed shortly after our microsecond exposures (i.e., reversible electroporation has occurred) was confirmed by exposing cells in the presence of propidium iodide (PI) - a membrane integrity marker for large molecule permeabilization. Cells did not take up the dye when it was added 2 minutes (or later) after μs-field exposure, but more than 50% cells were permeable to PI when the dye was added before exposure (Figure 25, 26). The measurements are consistent with the nonexistent uptake of trypan blue for these times. The molecule is larger than propidium iodide and is

presumed to enter only dying cells with severely compromised membrane integrity. Despite the initial and continuing increase in membrane conductivity following μsPEF exposure, cells do not take up trypan blue between 5 and 30 minutes after exposure. The temporal development of cytoplasm conductivity also suggests no significant membrane poration after 5 minutes. The conductivities of nuclear envelope and nucleoplasm after μs-exposure were not significantly different from that of unexposed controls (Figure 22, 23), suggesting that the reversible electroporation pulses used in this study did not affect the nucleus.

Our dielectric measurements are not spatially resolved and are instead averages for the entire cell and investigated ensemble of cells. On one hand, the predicted increase in conductivity at the pole caps could therefore even be much higher. On the other hand, for an exposure to multiple electric field pulses, a homogeneous exposure of cells and spatially averaged values for conductivities seem more plausible due to the individual dynamic of the cell membrane (fluidity) and the movement of cells in suspension itself [145]. In conclusion, conductivities measured 5 minutes after exposure will not be representative of peak values of an electroporated cell. Depending on the dynamics of the resealing process, the extrapolation from our delayed measurements will likewise underestimate the immediate membrane conductivity and disagree with modeling prediction. Hence, our measurements offer an estimate for the change in membrane conductivity after exposure.

In general, dielectric measurements for several minutes after μs-exposure closely follow the transient biological response of cells that eventually determine the fate of cells [138]. This was confirmed by the long term cell survival measurement. As such, the

method might offer an immediate assessment of the efficacy of different treatment parameters.

## 5.4 Nanosecond Exposures

The changes in cell dielectric parameters achieved by the exposure to nanosecond pulses are distinctively higher than for the exposure to the longer microsecond pulses. Parameters for the pulsed electric field exposure were chosen to deliver the same energy per pulse for nanosecond and microsecond exposures. Therefore the observed differences are not a mere dose response. Five minutes after the exposure to 8 pulses of 300 ns duration and 20 kV/cm amplitude (applied with a repetition rate of 1 Hz), a membrane conductivity of 276 µS/m is observed, i.e., about 4.5 times higher than for the µsPEF exposure and 7 times higher compared to the equivalent value obtained for the unexposed control. The conductivity of cytoplasm and nucleoplasm both dropped about 40% and the conductivity of nuclear envelope increased by 50%. The extrapolation of the measurements suggests that during, or immediately following the nsPEF regimen, membrane conductivities reached 263 µS/m. Pliquett et al. observed an increase in membrane conductivity by a factor of no more than 2 within 30 second after exposure to 300-ns pulses using a TDR method [104]. With the same technique Garner et al. found a membrane conductivity decrease after exposure to 10-ns pulses and no significant changes in membrane permittivity [27]. This difference could be the result of variations in pulse duration and amplitude or because of the double shell model that was used in this study. Again, measured conductivities might only be a representative average if pore resealing times are actually short and on the same millisecond timescale as some predictions for µsPEF. However, no conclusive studies have been conducted on the

resealing time of the predicted much smaller pores that are formed by nanosecond exposures. In fact, measurements on the uptake of smaller ions, such as calcium, and electrophysiological investigations on membrane conductivity, suggest recovery times of several tens of seconds or even minutes. Scarlett et al. reported a recording with a temporal resolution of 15 ms, which indicated that in the presence of external calcium, a maximum in intracellular calcium levels are achieved 22 s after exposure to a 60 ns, 100 kV/cm pulse. Conversely, in the absence of extracellular calcium, which allows only for the release of calcium from internal stores, the peak is reached after 2 s [21]. Pakhomov et al., using a whole-cell patch clamp technique, measured membrane resistance and membrane potential of several cell lines, including Jurkat cells, as early as 1 minute after exposure to a 60 ns pulse of 12 kV/cm. Following the development of these parameters for up to 15 minutes, he only found a gradual recovery [20]. Subsequent studies of exposures to a single 60-ns (> 6 kV/cm) or 600-ns (> 1 kV/cm) pulse suggest that pores created under these conditions stay open for times that could extend up to several minutes [107]. Albeit, the membrane conductivities obtained from these patch clamp studies are in the range of tens of nS/m which are much smaller than values derived from measurements – ours and other groups -- using dielectric spectroscopy. The difference could be caused by different measuring techniques or different suspending media used during measurements and needs to be explored further. Although the earliest observation times of 1 s or even 100 ms, might still be too late to capture immediate membrane changes, the difference between $\mu$s- and ns-exposures is striking. The data on changes in dielectric properties of nucleus after ns-exposure are scarce. Our results show that the nucleoplasm conductivity significantly decreases after ns-exposure and keeps dropping

thereafter. Similar changes have been reported by Garner et al. on HL-60 cells after exposure to 10-ns pulses [27]. Previous study has shown that nanosecond pulses of both 10-ns and 60-ns duration cause an increase in the permeability of the nuclear envelope of HL-60 cells [25]. We also observed increase in nuclear envelope conductivity after ns-exposure. However it is possible that the observed changes in the dielectric properties of nucleus were results of secondary effects instead of primary effects induced by ns-exposures considering the time delay of our measurements. It is likely the decrease in nucleoplasm conductivity was the result of an increased permeability of nuclear envelope which had led to ion diffusion from the nucleoplasm to the cytoplasm. Altogether the evidence suggests that pore evolution processes are different for the shorter exposures, resulting in much higher membrane conductivities and long lasting permeability. As such, our measurements are able to follow the pore evolution process for nsPEF exposure more accurately than for microsecond pulses.

An increase in conductivity by 3 orders of magnitude at the end of a 10 us pulse was predicted by theoretical studies [142]. Exposures to nsPEFs were also predicted to create $10^3$ - $10^4$ more membrane pores than conventional electroporation protocols [17]. Depending on the pore size, the higher number of pores corresponds to an increase in conductivity. Although our results are lower than predicted by these estimates for the comparison of both conditions, they generally confirm the predicted difference. The development of membrane and supernatant conductivities for 30 minutes after exposure demonstrates the same linear increase as is observed for the longer pulsed electric field conditions, including only slightly different rates of change. That the evolution of pores created under nanosecond exposure conditions is different from microsecond exposures is

also shown by the slow progressive uptake of trypan blue (Figure 24). The experiments indicate that initially pores are too small to allow the passage of larger molecule and pores of sufficient size form over several minutes instead. The results are consistent with observations on the uptake of propidium iodide. Contrary to the exposure to μsPEFs, cells did not take up the dye 2 minutes after exposure (Figure 24). In earlier experiments no uptake was observed within several milliseconds after exposure [21, 23]. This further confirms that no large pores have formed (and resealed) within the first 2 minutes after the field was applied. However, unlike for μsPEF exposures, after several minutes, cells start to become increasingly permeable to trypan blue (Figure 24) and propidium iodide (Figure 25). Combined, our measurements on membrane conductivity and dye uptake indicate that for cells that were exposed to nanosecond pulsed electric fields, smaller pores that would originally not allow larger molecules to pass evolve into pores supporting such transport over several minutes. The gradual uptake of trypan blue therefore might or might not indicate that a cell is dead, particularly for times shortly after exposures.

Although the dielectric properties of blood have been extensively studied for several decades [122-124, 146], to the best of our knowledge, the effect of nanosecond pulsed electric fields on these properties has not been investigated yet. As shown in Figure 28, significant changes occur in both permittivity and conductivity spectra of pig whole blood after nanosecond exposure. In spite of the high conductivity of the blood plasma (1.12 S/m), the $\beta$-dispersion of blood can still be readily identified thanks to the measuring sensor plated with platinum-black. Hence we were able to obtain reliable blood dielectric parameters (as shown in Table 6) by fitting the dielectric spectra into a

Cole-Cole function with the electrode polarization modeled as a CPA-element. In this way, the relationship between these dielectric parameters and the conformational changes in blood cells could be investigated. In this study the volume fraction of erythrocytes in pig whole blood is about 38% which is consistent with values reported in other studies [147, 148]. The volume fraction of white blood cells and platelets, on the other hand, is negligibly small (much less than 1%). Therefore it is reasonable to consider the blood sample as a suspension of erythrocytes while the dielectric contribution from other cells ignored. Among the dielectric parameters obtained from the Cole-Cole function, the relaxation time ($\tau$) and broadening parameter ($\alpha$) are highly specific to the erythrocyte shape as reported by Hayashi et al. [149] which, to the best of our knowledge, is the only systematic study on the sensitivity of dielectric properties to the morphology of erythrocytes. The relaxation time and broadening parameter of healthy rabbit blood, meaning erythrocytes are discocytes, reported by Hayashi are 64 ns and 0.85. The counterparts of unexposed pig blood determined in our study are 68 ns and 0.87 which are in good agreement. Observation by microscopy shows that these pig erythrocytes maintained biconcave shape before nanosecond exposure. Five minutes after exposure to eight 30 kV/cm, 300 ns pulses, $\tau$ decreased to 32 ns and $\alpha$ increased to 0.92. According to Hayashi's study, such changes indicate that the erythrocytes are transforming from discocytes to spherocytes (spherical erythrocytes). The values for $\tau$ and $\alpha$ determined in their study for spherocytes are 30 ns and 0.94. This shape change is further confirmed by our observation that most erythrocytes were significantly enlarged 5 minutes after exposure. The significant drop in low frequency relative permittivity ($\varepsilon_l$) from 2133 to 1624 after nanosecond exposure is most likely a synergistic effect of a decrease in

membrane permittivity ($\varepsilon_m$) and an increase in membrane conductivity ($\sigma_m$). The decrease in cell suspension dc conductivity ($\sigma_{dc}$) has been reported in a number of studies for exposure to electroporation pulses [44, 84, 94, 96]. Osmotic swelling of erythrocytes due to formation of membrane pores reduces the extracellular space for ions to transport which inevitably leads to reduction of dc conductivity. We also observed ongoing swelling of erythrocytes, even formation of ghost cells, 5 minutes after nanosecond exposure therefore the formation of long-lived nanopores in erythrocyte membrane seems to be the only plausible explanation. In comparison, a significant increase in conductivity is seen for the potato sample after exposure to nanosecond pulses. Similar increase in potato conductivity was also observed by Silve et al. using 100-ns pulses [109]. The different conductivity change in comparison with blood can be attributed the existence of cell walls in potato cells which prevented osmotic swelling. Hence the increase in potato conductivity is expected as a result of ion leakage and membrane poration. Unfortunately we were not able to achieve a satisfactory fitting using the Cole-Cole relaxation function for the dielectric spectrum of potato in this study. As compared to mammalian cells, plant cells have very different structures, e.g. the cell wall, which might require different dielectric relaxation functions to describe the dielectric spectrum. Further efforts are needed to obtain the dielectric parameters from potato dielectric spectrum, which will permit revealing the conformational changes induced by nanosecond pulses.

## 5.5 Supraporation Evolution

Pulsed electric fields of nanosecond duration have been shown experimentally and theoretically to promote initially only the formation of smaller pores, which would allow only smaller ions, such as calcium, to pass [21, 150, 151]. Accordingly, these pores

would be revealed by an increase in conductivity but not by traditional membrane integrity markers. The almost one order of magnitude higher conductivity of the cell membrane seems in generally good agreement with expectations from simulation studies on supraporation [17]. Again, absolute comparisons have to take into account pore resealing times, which might be very different for both exposure regimens.

Interestingly, the increasing uptake of trypan blue within the first 15 minutes after exposure has no effect on the observed linear increase in membrane conductivity during this period, i.e., the increasing permeability to larger molecules does not lead to a superimposed increase in membrane conductivity. It is therefore unlikely that the observed strict linear increase in conductivity is an incidental effect of averaging across number of trypan blue positive (i.e., porated) cells and trypan blue negative (i.e., membrane-uncompromised) cells. In fact, the rate of change is very similar for nsPEFs and µsPEFs. This could indicate that the development of morphological changes for later times after exposure is already independent of the original membrane changes and determined by relaxation mechanisms that involve physiological activity. The similarity of slopes suggests that the same mechanisms, i.e., changes to the membrane morphology, are responsible for a further increase in conductivity after the initial response during the application of pulsed electric fields. Accordingly, the eventual observed uptake of trypan blue might already be the result of secondary mechanisms [138].

One could suppose that larger pores might actually form by mergers of smaller pores rather than by the expansion of smaller pores. In this way, the total porated membrane area is maintained. The process agrees with life times of smaller pores, on the order of minutes, as is suggested by the delayed uptake of PI. By comparison, the growth of

smaller pores would correspond to a significant increase in membrane conductivity unless the growth is balanced by pore resealing. This interpretation, however, seems challenged by the long lifetime of smaller pores. Conversely, the rates by which small pores expand and reseal could serendipitously balance. Strikingly, the larger pores eventually formed under our conditions after nanosecond exposure do not seem to reseal again; unlike their microsecond-induced complements. This is also shown by the gradually increasing number of cells taking up propidium iodide, while for μsPEF, this number decreases.

The hypothesis of merging smaller nanosecond-induced pores is also consistent with the recorded changes in permittivity. Similar to the conductivities, the development of measured values for permittivities is approximately linear, particularly for the first 15 minutes after exposure. For nsPEF-exposed cells we have not observed a significant change in cell size, e.g., swelling. Hence the permittivity increase might be accounted for by membrane areas that are replaced by water-filled pores through the membrane. That no deviation from linearity is observed during the formation process of larger pores further indicates that the entire membrane area replaced by such conduits is basically unchanging. From the comparison with unexposed controls we can calculate that about 13% of the membrane area must be replaced by water to result in the observed increase of permittivity. Derivation of the area replaced by water channels from conductivity data is more challenging since the conductivities in these passages could lie between supernatant and cytoplasm conductivities. Corresponding estimates of surface area replaced by water conduits are between 0.2% and 0.046%. The large discrepancy between estimates from permittivity and conductivity measurement two orders of magnitude could suggest that

not all water-filled membrane defects are actually permeable, even for small ions. In general, the variations in plasma membrane permittivity could also be due to changes in membrane thickness and dielectric composition [152]. Alterations in membrane surface morphology have been reported as a factor inducing changes in membrane permittivity [153]. At the current stage, we cannot rule out the possibility that such changes are induced by pulsed electric fields. The membrane roughness and structure itself might be altered due to the exposure. Further investigations are necessary to clarify the mechanisms behind the permittivity changes.

# CHAPTER 6

## CONCLUSION

### 6.1    Summary

In this research, the changes in dielectric properties of biological cells and tissues induced by intense pulsed electric fields, in particular nanosecond pulsed electric fields, of varying pulse duration and pulse amplitude were investigated. A comprehensive approach, combining TDR dielectric spectroscopy, electrode polarization correction and appropriate dielectric models, was developed to derive the dielectric characteristics of selected cells and tissues. On the basis of measured dielectric properties, simulations through dielectric mixture & cell models were performed to confirm the feasibility of evaluating PEF-induced dielectric changes in cellular structures, such as plasma membrane and nuclear envelope, by means of dielectric spectroscopy. The dielectric evolution of Jurkat cells, following exposures to 8 consecutive pulses of either 100 $\mu$s or 300 ns with the same dose of electrical energy, was tracked with a 5-minute temporal resolution (up to 30 minutes). For the sake of comparison, changes in plasma membrane integrity of Jurkat cells were assessed at corresponding time scales. In addition, 24-hour viability of Jurkat cells was examined for the exposure to 100-$\mu$s, 300-ns and 60-ns pulses and compared with plasma membrane conductivity measured 30 minutes after exposure. Using a platinum black-plated measuring sensor, the dielectric spectrum of pig blood, a liquid tissue model exhibiting strong ionic conductivity, was measured and parameterized by the Cole-Cole relaxation function. Nanosecond pulsed electric fields induced changes in the Cole-Cole dielectric parameters and cell morphology were

investigated. The effect of nanosecond pulsed electric fields on the dielectric properties potato, chosen as a solid tissue model, was probed with an open-ended measuring sensor.

Dielectric and impedance measurements have been used to study the PEF-cell interactions for several decades, in particular with electroporation pulses. Dielectric spectroscopy is a powerful means capable of indicating changes in cell components such as membrane permeabilization and efflux of intracellular ions in response to pulsed electric fields. In particular, the mechanisms that are essential for the formation, development and resealing of membrane pores can be investigated by tracking the dielectric evolution of cells and tissues with corresponding time scales. The feasibility of evaluating and predicting the outcome of pulsed electric field-cell (tissue) interactions by means of dielectric spectroscopy has been suggested by many studies as well. In general, dielectric spectroscopy has shown promising potentials in PEF-related basic research and biomedical applications thanks to its high speed and non-intrusion. However, the experimental evidences regarding the effects of nanosecond pulsed electric fields on the dielectric properties of cells and tissues have remained scarce. The connection between experiments and simulations has not been fully established yet. The research of this dissertation aimed to fill this gap and promote the utilization of dielectric spectroscopy in nsPEF-related research and applications. The major findings of this research are summarized as follows:

1. The dielectric characteristics of cells exhibit remarkable cell specificity, which is a strong indication of cell-type-dependent charging behavior under the same exposure condition. Simulation studies may benefit from these findings and will be able to predict cell-specific membrane pore evolutions.

2. We have shown for the first time an increase in the conductivity of nuclear envelope together with a strong increase in plasma membrane conductivity after exposure to nanosecond pulsed electric fields, based on a double shell model. Significant differences have been observed in cell dielectric characteristics for exposures to nanosecond and microsecond pulsed electric fields, despite delivery of the same energy.

3. The plasma membrane conductivity is an indicator of plasma membrane integrity for Jurkat cells when exposed to nanosecond pulsed electric fields. A strong correlation between the 24-hour cell survival and the 30-minute plasma membrane conductivity has been observed as well. For the assessment of membrane permeabilization, dielectric spectroscopy might permit the immediate evaluation or even prediction of nsPEF-related treatment conditions in the future.

4. For nanosecond exposures, the pores or defects occurred in the plasma membrane can be long-lived. The measurements further suggest that smaller pores might merge into larger pores permeable to trypan blue and propidium iodide molecules.

5. Nanosecond pulsed electric fields induce significant changes in dielectric properties of tissues. Dielectric parameters obtained from the Cole-Cole relaxation model exhibit strong correlation with the conformational changes in cells. To the best of our knowledge, this study is the first of its kind to track the dielectric evolution of blood after nanosecond exposures by means of dielectric spectroscopy. Previous studies on cell suspensions were either conducted with the current-voltage method, which only provides an "instant conductivity," or limited to a non-physiological low-ionic strength environment.

## 6.2    Future Directions

The research of this dissertation demonstrated that the dielectric characteristics of biological cells and tissues, and the effects of nanosecond pulsed electric fields on these properties can be obtained by means of TDR dielectric spectroscopy. Based on the methodology developed in this research, some possible directions for future studies are proposed.

1. Provide dielectric properties of cells and tissue for basic research and biomedical applications. Dielectric spectroscopy of concentrated cell suspension provide well defined average values of dielectric properties for cellular structures, which can be used to design pulse parameters that can target a specific type of cells, such as cancer, or separate different cells using dielectrophoresis. The tissue dielectric properties can be used in PEF-related surgery planning. Optimum exposure conditions according to the dielectric properties of individual patient may be designed for patient-specific treatment.

2. Provide real-time feedback and predict efficacy for PEF-related treatment based on changes in dielectric properties of cells and tissues between and after application multiple pulses. This would allow dynamic adjustment of pulse parameters, e.g. pulse width, pulse amplitude and repetition rate, during PEF treatment.

3. Single cell dielectric spectroscopy. Measuring sensors designed with microfludics technology will allow examination of the dielectric properties of individual cells. Combining with other diagnostic techniques such as fluorescence microscopy, single cell dielectric spectroscopy may become a powerful tool to investigate the interaction between individual cells to pulsed electric fields.

4. New imaging modality. With the open-ended measuring sensor, dielectric spectroscopy may be used to developed new imaging modality based on the dielectric properties of tissues both in vitro and in vivo.

5. Dielectric spectroscopy can also be extended to study the response of biological cells and tissues to other types of physical or chemical stimuli, e.g. non-thermal atmospheric plasmas.

# REFERENCES

[1]     E. Neumann, S. Kakorin, and K. Toensing, "Fundamentals of electroporative delivery of drugs and genes", Bioelectrochemistry and Bioenergetics, Vol. 48, pp. 3-16, 1999.

[2]     E. Neumann, S. Kakorin, and K. Toensing, "Principles of membrane electroporation and transport of macromolecules", Methods in Molecular Medicine, Vol. 37, pp. 1–35, 2000.

[3]     R. Shirakashi, C. Köstner, K. Müller, M. Kürschner, U. Zimmermann, and V. Sukhorukov, "Intracellular delivery of trehalose into mammalian cells by electropermeabilization", Journal of Membrane Biology, Vol. 189, pp. 45-54, 2002.

[4]     L. Mir, P. Moller, F. André, and J. Gehl, "Electric pulse-mediated gene delivery to various animal tissues", Advances in Genetics, Vol. 54, pp. 83-114, 2005.

[5]     L. Mir and S. Orlowski, "Mechanisms of electrochemotherapy", Advanced Drug Delivery Reviews, Vol. 35, pp. 107-118, 1999.

[6]     N. Olaiz, F. Maglietti, C. Suárez, F. Molina, D. Miklavčič, L. Mir, and G. Marshall, "Electrochemical treatment of tumors using a one-probe two-electrode device", Electrochimica Acta, Vol. 55, pp. 6010–6014, 2010.

[7]     S. Dev, D. Rabussay, G. Widera, G. Hofmann, G. Inc, and C. San Diego, "Medical applications of electroporation", IEEE Transactions on Plasma Science, Vol. 28, pp. 206-223, 2000.

[8]     G. Hofmann, S. Dev, G. Nanda, and D. Rabussay, "Electroporation therapy of solid tumors", Critical Reviews in Therapeutic Drug Carrier Systems, Vol. 16, pp. 523-569, 1999.

[9]     D. Rabussay, "Applicator and electrode design for in vivo DNA delivery by electroporation", Methods in Molecular Biology, Vol. 423, pp. 35-59, 2008.

[10]    R. Heller, R. Gilbert, and M. Jaroszeski, "Clinical applications of electrochemotherapy", Advanced Drug Delivery Reviews, Vol. 35, pp. 119-129, 1999.

[11]    M. Jaroszeski, L. Heller, R. Gilbert, and R. Heller, "Electrically mediated plasmid DNA delivery to solid tumors in vivo", Methods in Molecular Biology, Vol. 245, pp. 237-244, 2004.

[12]    S. Roux, C. Bernat, B. Al-Sakere, F. Ghiringhelli, P. Opolon, A. Carpentier, L. Zitvogel, L. Mir, and C. Robert, "Tumor destruction using electrochemotherapy followed by CpG oligodeoxynucleotide injection induces distant tumor responses", Cancer Immunology, Immunotherapy, Vol. 57, pp. 1291-1300, 2008.

[13]    G. Sersa, D. Miklavčič, M. Cemazar, Z. Rudolf, G. Pucihar, and M. Snoj, "Electrochemotherapy in treatment of tumours", European Journal of Surgical Oncology (EJSO), Vol. 34, pp. 232-240, 2008.

[14]    B. Rubinsky, Irreversible Electroporation: Springer Verlag, 2010.

[15]    S. Jayaram, G. Castle, and A. Margaritis, "Kinetics of sterilization of Lactobacillus brevis cells by the application of high voltage pulses", Biotechnology and Bioengineering, Vol. 40, pp. 1412-1420, 1992.

[16]  B. Al-Sakere, F. André, C. Bernat, E. Connault, P. Opolon, R. Davalos, B. Rubinsky, and L. Mir, "Tumor ablation with irreversible electroporation", PLoS One, Vol. 2, p. e1135, 2007.

[17]  T. Gowrishankar, A. Esser, Z. Vasilkoski, K. Smith, and J. Weaver, "Microdosimetry for conventional and supra-electroporation in cells with organelles", Biochemical and Biophysical Research Communications, Vol. 341, pp. 1266-1276, 2006.

[18]  J. Deng, K. H. Schoenbach, E. Stephen Buescher, P. S. Hair, P. M. Fox, and S. J. Beebe, "The effects of intense submicrosecond electrical pulses on cells", Biophysical Journal, Vol. 84, pp. 2709-2714, 2003.

[19]  W. Frey, J. White, R. Price, P. Blackmore, R. Joshi, R. Nuccitelli, S. Beebe, K. Schoenbach, and J. Kolb, "Plasma membrane voltage changes during nanosecond pulsed electric field exposure", Biophysical Journal, Vol. 90, pp. 3608-3615, 2006.

[20]  A. Pakhomov, J. Kolb, J. White, R. Joshi, S. Xiao, and K. Schoenbach, "Long lasting plasma membrane permeabilization in mammalian cells by nanosecond pulsed electric field (nsPEF)", Bioelectromagnetics, Vol. 28, pp. 655-663, 2007.

[21]  S. Scarlett, J. White, P. Blackmore, K. Schoenbach, and J. Kolb, "Regulation of intracellular calcium concentration by nanosecond pulsed electric fields", Biochimica et Biophysica Acta (BBA) - Biomembranes, Vol. 1788, pp. 1168-1175, 2009.

[22]    E. Buescher, R. Smith, and K. Schoenbach, "Submicrosecond intense pulsed electric field effects on intracellular free calcium: mechanisms and effects", IEEE Transactions on Plasma Science, Vol. 32, pp. 1563-1572, 2004.

[23]    N. Chen, K. Schoenbach, J. Kolb, R. Swanson, A. Garner, J. Yang, R. Joshi, and S. Beebe, "Leukemic cell intracellular responses to nanosecond electric fields", Biochemical and Biophysical Research Communications, Vol. 317, pp. 421-427, 2004.

[24]    S. Beebe, P. Fox, L. Rec, K. Somers, R. Stark, and K. Schoenbach, "Nanosecond pulsed electric field (nsPEF) effects on cells and tissues: apoptosis induction and tumor growth inhibition", in Pulsed Power Plasma Science, PPPS-2001. Digest of Technical Papers, Vol. 1, pp. 211-215, 2001,

[25]    R. Nuccitelli, U. Pliquett, X. Chen, W. Ford, R. Swanson, S. Beebe, J. Kolb, and K. Schoenbach, "Nanosecond pulsed electric fields cause melanomas to self-destruct", Biochemical and Biophysical Research Communications, Vol. 343, pp. 351-360, 2006.

[26]    K. Schoenbach, S. Beebe, and E. Buescher, "Intracellular effect of ultrashort electrical pulses", Bioelectromagnetics, Vol. 22, pp. 440-448, 2001.

[27]    A. Garner, G. Chen, N. Chen, V. Sridhara, J. Kolb, R. Swanson, S. Beebe, R. Joshi, and K. Schoenbach, "Ultrashort electric pulse induced changes in cellular dielectric properties", Biochemical and Biophysical Research Communications, Vol. 362, pp. 139-144, 2007.

[28]    C. Grosse and H. Schwan, "Cellular membrane potentials induced by alternating fields", Biophysical Journal, Vol. 63, pp. 1632-1642, 1992.

[29]  T. Kotnik and D. Miklavčič, "Analytical description of transmembrane voltage induced by electric fields on spheroidal cells", Biophysical Journal, Vol. 79, pp. 670-679, 2000.

[30]  T. Kotnik and D. Miklavčič, "Theoretical evaluation of voltage inducement on internal membranes of biological cells exposed to electric fields", Biophysical Journal, Vol. 90, pp. 480-491, 2006.

[31]  K. DeBruin and W. Krassowska, "Modeling electroporation in a single cell. I. Effects of field strength and rest potential", Biophysical Journal, Vol. 77, pp. 1213-1224, 1999.

[32]  K. DeBruin and W. Krassowska, "Modeling electroporation in a single cell. II. Effects of ionic concentrations", Biophysical Journal, Vol. 77, pp. 1225-1233, 1999.

[33]  M. Pavlin, M. Kandušer, M. Reberšek, G. Pucihar, F. Hart, R. Magjarevićcacute, and D. Miklavčič, "Effect of cell electroporation on the conductivity of a cell suspension", Biophysical Journal, Vol. 88, pp. 4378-4390, 2005.

[34]  A. Garner, N. Chen, J. Yang, J. Kolb, R. Swanson, K. Loftin, S. Beebe, R. Joshi, and K. Schoenbach, "Time domain dielectric spectroscopy measurements of HL-60 cell suspensions after microsecond and nanosecond electrical pulses", IEEE Transactions on Plasma Science, Vol. 32, pp. 2073-2084, 2004.

[35]  R. P. Joshi and K. H. Schoenbach, "Electroporation dynamics in biological cells subjected to ultrafast electrical pulses: A numerical simulation study", Physical Review E, Vol. 62, pp. 1025-1033, 2000.

[36] R. Joshi, Q. Hu, and K. Schoenbach, "Modeling Studies of Cell Response to Ultrashort, High-Intensity Electric Fields - implications for Intracellular Manipulation", IEEE Transactions on Plasma Science, Vol. 32, pp. 1677-1686, 2004.

[37] L. Mir, "Application of electroporation gene therapy: past, current, and future", Methods in Molecular Biology, Vol. 423, pp. 3-17, 2008.

[38] J. Maxwell, *A treatise on electricity and magnetism*: Clarendon, 1892.

[39] P. Debye, *Polar molecules*: The Chemical Catalog Company, inc., 1929.

[40] H. Schwan, "Electrical properties of tissue and cell suspensions", Advances in Biological and Medical Physics, Vol. 5, p. 147, 1957.

[41] K. Wagner, "Explanation of the dielectric fatigue phenomenon on the basis of Maxwell's concept", Arkiv für Electrotechnik, 1914.

[42] J. P. H. Burt, R. Pethig, P. R. C. Gascoyne, and F. F. Becker, "Dielectrophoretic characterisation of Friend murine erythroleukaemic cells as a measure of induced differentiation", Biochimica et Biophysica Acta (BBA) - General Subjects, Vol. 1034, pp. 93-101, 1990.

[43] M. Hibino, M. Shigemori, H. Itoh, K. Nagayama, and K. Kinosita, "Membrane conductance of an electroporated cell analyzed by submicrosecond imaging of transmembrane potential", Biophysical Journal, Vol. 59, pp. 209-220, 1991.

[44] K. Kinosita Jr and T. Y. Tsong, "Voltage-induced conductance in human erythrocyte membranes", Biochimica et Biophysica Acta (BBA) - Biomembranes, Vol. 554, pp. 479-497, 1979.

[45] K. Asami, T. Yonezawa, H. Wakamatsu, and N. Koyanagi, "Dielectric spectroscopy of biological cells", Bioelectrochemistry and Bioenergetics, Vol. 40, pp. 141-145, 1996.

[46] U. Kaatze and Y. Feldman, "Broadband dielectric spectrometry of liquids and biosystems", Measurement Science and Technology, Vol. 17, pp. 17-35, 2006.

[47] C. Gabriel, S. Gabriel, and E. Corthout, "The dielectric properties of biological tissues: I. Literature survey", Physics in Medicine and Biology, Vol. 41, pp. 2231-2250, 1996.

[48] F. Kremer, "Dielectric spectroscopy зit esterday, today and tomorrow", Journal of Non-Crystalline Solids, Vol. 305, pp. 1-9, 2002.

[49] Y. Feldman, I. Ermolina, and Y. Hayashi, "Time domain dielectric spectroscopy study of biological systems", IEEE Transactions on Dielectrics and Electrical Insulation, Vol. 10, pp. 728-753, 2003.

[50] I. Ermolina, Y. Polevaya, Y. Feldman, B. Ginzburg, and M. Schlesinger, "Study of normal and malignant white blood cells by time domaindielectric spectroscopy", IEEE Transactions on Dielectrics and Electrical Insulation, Vol. 8, pp. 253-261, 2001.

[51] R. Pethig and D. Kell, "The passive electrical properties of biological systems: their significance in physiology, biophysics and biotechnology", Physics in Medicine and Biology, Vol. 32, pp. 933-970, 1987.

[52] H. Fricke, "The electric capacity of suspensions with special reference to blood", Journal of General Physiology, Vol. 9, pp. 137-152, 1925.

[53] O. Schanne and E. Ceretti, *Impedance measurements in biological cells*: John Wiley & Sons, 1978.

[54] D. Kell and C. Harris, "Dielectric spectroscopy and membrane organisation", Electromagnetic Biology and Medicine, Vol. 4, pp. 317-348, 1985.

[55] K. Cole, "Membranes, Ions (1978) and Impulses," ed: University of California Press, Berkeley, 1972.

[56] K. Cole and R. Baker, "Longitudinal impedance of the squid giant axon", Journal of General Physiology, Vol. 24, pp. 771-788, 1941.

[57] A. Hodgkin and A. Huxley, "Currents carried by sodium and potassium ions through the membrane of the giant axon of Loligo", The Journal of Physiology, Vol. 116, p. 449, 1952.

[58] R. Pethig, "Dielectric properties of biological materials: biophysical and medical applications", IEEE Transactions on Electrical Insulation, pp. 453-474, 1984.

[59] M. Stuchly, "Dielectric Properties of Biological Substances- Tabulated", Journal of Microwave Power, Vol. 15, pp. 19-26, 1980.

[60] H. Schwan and K. Foster, "RF-field interactions with biological systems: electrical properties and biophysical mechanisms", Proceedings of the IEEE, Vol. 68, pp. 104-113, 1980.

[61] K. Foster and H. Schwan, "Dielectric properties of cells and tissues: a critical review", Critical Reviews in Biomedical engineering, Vol. 17, pp. 25-104, 1989.

[62] S. Gabriel, R. Lau, and C. Gabriel, "The dielectric properties of biological tissues: II. Measurements in the frequency range 10 Hz to 20 GHz", Physics in Medicine and Biology, Vol. 41, pp. 2251-2270, 1996.

[63]  S. Gabriel, R. Lau, and C. Gabriel, "The dielectric properties of biological tissues: III. Parametric models for the dielectric spectrum of tissues", Physics in Medicine and Biology, Vol. 41, pp. 2271-2294, 1996.

[64]  E. Grant, R. Sheppard, and G. South, *Dielectric behaviour of biological molecules in solution*: Clarendon Press, Oxford, 1978.

[65]  R. Pethig, "Dielectric and Electronic Behavior of Biological Materials," ed: Wiley, New York, 1979.

[66]  S. Grimnes and O. Martinsen, *Bioimpedance and bioelectricity basics*: Academic press, 2008.

[67]  S. Beebe, P. Fox, L. Rec, K. Somers, R. Stark, and K. Schoenbach, "Nanosecond pulsed electric field (nsPEF) effects on cells and tissues: apoptosis induction and tumor growth inhibition", IEEE Transactions on Plasma Science, Vol. 30, pp. 286-292, 2002.

[68]  S. Beebe, J. White, P. Blackmore, Y. Deng, K. Somers, and K. Schoenbach, "Diverse effects of nanosecond pulsed electric fields on cells and tissues", DNA and Cell Biology, Vol. 22, p. 785, 2003.

[69]  K. Schoenbach, B. Hargrave, R. Joshi, J. Kolb, R. Nuccitelli, C. Osgood, A. Pakhomov, M. Stacey, R. Swanson, and J. White, "Bioelectric effects of intense nanosecond pulses", IEEE Transactions on Dielectrics and Electrical Insulation, Vol. 14, pp. 1088-1109, 2007.

[70]  M. Stacey, P. Fox, S. Buescher, and J. Kolb, "Nanosecond pulsed electric field induced cytoskeleton, nuclear membrane and telomere damage adversely impact cell survival", Bioelectrochemistry, Vol. 82, pp. 131-134, 2011.

[71]   P. Vernier, Y. Sun, L. Marcu, S. Salemi, C. Craft, and M. Gundersen, "Calcium bursts induced by nanosecond electric pulses", Biochemical and Biophysical Research Communications, Vol. 310, pp. 286-295, 2003.

[72]   J. White, P. Blackmore, K. Schoenbach, and S. Beebe, "Stimulation of Capacitative Calcium Entry in HL-60 Cells by Nanosecond Pulsed Electric Fields", Journal of Biological Chemistry, Vol. 279, pp. 22964-22972, 2004.

[73]   D. Tieleman, H. Leontiadou, A. Mark, and S. Marrink, "Simulation of Pore Formation in Lipid Bilayers by Mechanical Stress and Electric Fields", Journal of the American Chemical Society, Vol. 125, pp. 6382-6383, 2003.

[74]   Q. Hu, R. Joshi, and K. Schoenbach, "Simulations of nanopore formation and phosphatidylserine externalization in lipid membranes subjected to a high-intensity, ultrashort electric pulse", Physical Review E, Vol. 72, p. 031902, 2005.

[75]   Q. Hu, S. Viswanadham, R. Joshi, K. Schoenbach, S. J. Beebe, and P. Blackmore, "Simulations of transient membrane behavior in cells subjected to a high-intensity ultrashort electric pulse", Physical Review E, Vol. 71, p. 031914, 2005.

[76]   D. Tieleman, "The molecular basis of electroporation", BMC Biochemistry, Vol. 5, p. 10, 2004.

[77]   M. Tarek, "Membrane Electroporation: A Molecular Dynamics Simulation", Biophysical Journal, Vol. 88, pp. 4045-4053, 2005.

[78]   Z. Levine and P. Vernier, "Life Cycle of an Electropore: Field-Dependent and Field-Independent Steps in Pore Creation and Annihilation", Journal of Membrane Biology, Vol. 236, pp. 27-36, 2010.

[79] M. Ziegler and P. Vernier, "Interface Water Dynamics and Porating Electric Fields for Phospholipid Bilayers", The Journal of Physical Chemistry B, Vol. 112, pp. 13588-13596, 2008.

[80] K. Kinosita Jr and T. Tsong, "Voltage-induced pore formation and hemolysis of human erythrocytes", Biochimica et Biophysica Acta (BBA) - Biomembranes, Vol. 471, p. 227, 1977.

[81] K. Kinosita and T. T. Tsong, "Hemolysis of human erythrocytes by transient electric field", Proceedings of the National Academy of Sciences, Vol. 74, pp. 1923-1927, May 1, 1977 1977.

[82] J. Teissie and T. Y. Tsong, "Evidence of voltage-induced channel opening in Na/K ATPase of human erythrocyte membrane", Journal of Membrane Biology, Vol. 55, pp. 133-140, 1980.

[83] I. Abidor, A. Barbul, D. Zhelev, P. Doinov, I. Bandrina, E. Osipova, and S. Sukharev, "Electrical properties of cell pellets and cell electrofusion in a centrifuge", Biochimica et Biophysica Acta (BBA) - Biomembranes, Vol. 1152, pp. 207-218, 1993.

[84] I. Abidor, L. Li, and S. Hui, "Studies of cell pellets: II. Osmotic properties, electroporation, and related phenomena: membrane interactions", Biophysical Journal, Vol. 67, pp. 427-435, 1994.

[85] U. Pliquett, R. Langer, and J. C. Weaver, "Changes in the passive electrical properties of human stratum corneum due to electroporation", Biochimica et Biophysica Acta (BBA) - Biomembranes, Vol. 1239, pp. 111-121, 1995.

[86]    U. Pliquett and J. C. Weaver, "Electroporation of human skin: simultaneous measurement of changes in the transport of two fluorescent molecules and in the passive electrical properties", Bioelectrochemistry and Bioenergetics, Vol. 39, pp. 1-12, 1996.

[87]    T. R. Gowrishankar, U. W. E. Pliquett, and J. C. Weaver, "Changes in Skin Structure and Electrical Properties following High Voltage Exposure", Annals of the New York Academy of Sciences, Vol. 888, pp. 183-194, 1999.

[88]    R. Vanbever, U. F. Pliquett, V. Preat, and J. C. Weaver, "Comparison of the effects of short, high-voltage and long, medium-voltage pulses on skin electrical and transport properties", Journal of Controlled Release, Vol. 60, pp. 35-47, 1999.

[89]    S. A. Gallo, A. R. Oseroff, P. G. Johnson, and S. W. Hui, "Characterization of electric-pulse-induced permeabilization of porcine skin using surface electrodes", Biophysical Journal, Vol. 72, pp. 2805-2811, 1997.

[90]    S. Gallo, A. Sen, M. Hensen, and S. Hui, "Temperature-dependent electrical and ultrastructural characterizations of porcine skin upon electroporation", Biophysical Journal, Vol. 82, pp. 109-119, 2002.

[91]    S. Narasimha Murthy, A. Sen, Y. L. Zhao, and S. W. Hui, "Temperature influences the postelectroporation permeability state of the skin", Journal of Pharmaceutical Sciences, Vol. 93, pp. 908-915, 2004.

[92]    R. V. Davalos, B. Rubinsky, and D. M. Otten, "A feasibility study for electrical impedance tomography as a means to monitor tissue electroporation for molecular medicine", Biomedical Engineering, IEEE Transactions on, Vol. 49, pp. 400-403, 2002.

[93]   M. Pavlin and D. Miklavčič, "Effective conductivity of a suspension of permeabilized cells: a theoretical analysis", Biophysical Journal, Vol. 85, pp. 719-729, 2003.

[94]   M. Pavlin and D. Miklavčič, "Theoretical and experimental analysis of conductivity, ion diffusion and molecular transport during cell electroporation--Relation between short-lived and long-lived pores", Bioelectrochemistry, Vol. 74, pp. 38-46, 2008.

[95]   M. Pavlin, V. Leben, and D. Miklavčič, "Electroporation in dense cell suspension—Theoretical and experimental analysis of ion diffusion and cell permeabilization", Biochimica et Biophysica Acta (BBA) - General Subjects, Vol. 1770, pp. 12-23, 2007.

[96]   M. Pavlin, M. Kanduaer, M. Reberaek, G. Pucihar, F. X. Hart, Magjarevi cacute, Ratko, and D. Miklavčič, "Effect of Cell Electroporation on the Conductivity of a Cell Suspension", Biophysical Journal, Vol. 88, pp. 4378-4390, 2005.

[97]   A. Ivorra, L. Miller, and B. Rubinsky, "Electrical impedance measurements during electroporation of rat liver and muscle", in 13th International Conference on Electrical Bioimpedance and the 8th Conference on Electrical Impedance Tomography, Vol. 17, pp. 130-133, 2007,

[98]   A. Ivorra and B. Rubinsky, "In vivo electrical impedance measurements during and after electroporation of rat liver", Bioelectrochemistry, Vol. 70, pp. 287-295, 2007.

[99]   A. Golberg, S. Laufer, H. Rabinowitch, and B. Rubinsky, "In vivo non-thermal irreversible electroporation impact on rat liver galvanic apparent internal resistance", Physics in Medicine and Biology, Vol. 56, pp. 951-963, 2011.

[100]  Y. Granot, A. Ivorra, E. Maor, and B. Rubinsky, "In vivo imaging of irreversible electroporation by means of electrical impedance tomography", Physics in Medicine and Biology, Vol. 54, pp. 4927-4943, 2009.

[101]  R. Benz and U. Zimmermann, "The resealing process of lipid bilayers after reversible electrical breakdown", Biochimica et Biophysica Acta (BBA) - Biomembranes, Vol. 640, pp. 169-178, 1981.

[102]  G. Chen, N. Chen, A. Garner, J. Kolb, R. Swanson, S. Beebe, R. Joshi, and K. Schoenbach, "Conductivity in Jurkat cell suspension after ultrashort electric pulsing", presented at the 3rd International workshop on biological effect of EMFs, Kos, Greece, 2004.

[103]  U. Pliquett, R. Joshi, V. Sridhara, and K. Schoenbach, "High electrical field effects on cell membranes", Bioelectrochemistry, Vol. 70, pp. 275-282, 2007.

[104]  U. Pliquett and K. Schoenbach, "Changes in electrical impedance of biological matter due to the application of ultrashort high voltage pulses", IEEE Transactions on Dielectrics and Electrical Insulation, Vol. 16, pp. 1273-1279, 2009.

[105]  U. F. Pliquett and K. H. Schoenbach, "Changes in electrical impedance of biological matter due to the application of ultrashort high voltage pulses", IEEE Transactions on Dielectrics and Electrical Insulation, Vol. 16, pp. 1273-1279, 2009.

[106] A. Pakhomov, R. Shevin, J. White, J. Kolb, O. Pakhomova, R. Joshi, and K. Schoenbach, "Membrane permeabilization and cell damage by ultrashort electric field shocks", Archives of Biochemistry and Biophysics, Vol. 465, pp. 109-118, 2007.

[107] B. Ibey, S. Xiao, K. Schoenbach, M. Murphy, and A. Pakhomov, "Plasma membrane permeabilization by 60- and 600-ns electric pulses is determined by the absorbed dose", Bioelectromagnetics, Vol. 30, pp. 92-99, 2009.

[108] B. Ibey, D. Mixon, J. Payne, A. Bowman, K. Sickendick, G. Wilmink, W. P. Roach, and A. Pakhomov, "Plasma membrane permeabilization by trains of ultrashort electric pulses", Bioelectrochemistry, Vol. 79, pp. 114-121, 2010.

[109] A. Silve, A. Ivorra, and L. Mir, "Detection of permeabilisation obtained by micropulses and nanopulses by means of bioimpedance of biological tissues", in Proceedings of the 5th European Conference on Antennas and Propagation (EUCAP), pp. 3164-3167, 2011,

[110] N. Hager III, "Broadband time domain reflectometry dielectric spectroscopy using variable time scale sampling", Review of Scientific Instruments, Vol. 65, p. 887, 1994.

[111] N. Hager III and R. Domszy, "Monitoring of cement hydration by broadband time-domain-reflectometry dielectric spectroscopy", Journal of Applied Physics, Vol. 96, p. 5117, 2004.

[112] O. Gottmann, U. Kaatze, and P. Petong, "Coaxial to circular waveguide transition as high-precision easy-to-handle measuring cell for the broad band dielectric

spectrometry of liquids", Measurement Science and Technology, Vol. 7, pp. 525-534, 1996.

[113] A. Gregory and R. Clarke, "A review of RF and microwave techniques for dielectric measurements on polar liquids", IEEE Transactions on Dielectrics and Electrical Insulation, Vol. 13, pp. 727-743, 2006.

[114] F. Bordi, C. Cametti, and T. Gili, "Reduction of the contribution of electrode polarization effects in the radiowave dielectric measurements of highly conductive biological cell suspensions", Bioelectrochemistry, Vol. 54, pp. 53-61, 2001.

[115] K. Cole and R. Cole, "Dispersion and absorption in dielectrics I. Alternating current characteristics", The Journal of Chemical Physics, Vol. 9, p. 341, 1941.

[116] I. Ermolina, Y. Polevaya, and Y. Feldman, "Analysis of dielectric spectra of eukaryotic cells by computer modeling", European Biophysics Journal, Vol. 29, pp. 141-145, 2000.

[117] P. Vernier, A. Li, L. Marcu, C. Craft, and M. Gundersen, "Ultrashort pulsed electric fields induce membrane phospholipid translocation and caspase activation: differential sensitivities of Jurkat T lymphoblasts and rat glioma C6 cells", IEEE Transactions on Dielectrics and Electrical Insulation, Vol. 10, pp. 795-809, 2003.

[118] E. Garon, D. Sawcer, P. Vernier, T. Tang, Y. Sun, L. Marcu, M. Gundersen, and H. Koeffler, "In vitro and in vivo evaluation and a case report of intense nanosecond pulsed electric field as a local therapy for human malignancies", International Journal of Cancer, Vol. 121, pp. 675-682, 2007.

[119] U. Pliquett, T. Nacke, and K. Schoenbach, "High frequency and low concentration – limitation for impedance measurements", in 13th International Conference on Electrical Bioimpedance and the 8th Conference on Electrical Impedance Tomography, Vol. 17, pp. 12-15, 2007,

[120] H. Kaneko, K. Asami, and T. Hanai, "Dielectric analysis of sheep erythrocyte ghost. Examination of applicability of dielectric mixture equations", Colloid & Polymer Science, Vol. 269, pp. 1039-1044, 1991.

[121] R. Lisin, B. Zion Ginzburg, M. Schlesinger, and Y. Feldman, "Time domain dielectric spectroscopy study of human cells. I. Erythrocytes and ghosts", Biochimica et Biophysica Acta (BBA) - Biomembranes, Vol. 1280, pp. 34-40, 1996.

[122] H. Schwan, "Electrical properties of blood and its constitutents: Alternating current spectroscopy", Annals of Hematology, Vol. 46, pp. 185-197, 1983.

[123] H. Beving, L. Eriksson, C. Davey, and D. Kell, "Dielectric properties of human blood and erythrocytes at radio frequencies (0.2–10 MHz); dependence on cell volume fraction and medium composition", European Biophysics Journal, Vol. 23, pp. 207-215, 1994.

[124] M. Wolf, R. Gulich, P. Lunkenheimer, and A. Loidl, "Dielectric spectroscopy of human blood", Biochimica et Biophysica Acta (BBA) - General Subjects, Vol. 1810, pp. 727-740, 2011.

[125] F. Hart and B. Bodakian, "The dielectric spectra of heated potatoes", Journal of Materials Science Letters, Vol. 14, pp. 1214-1217, 1995.

[126] F. Galindo, P. Vernier, P. Dejmek, A. Vicente, and M. Gundersen, "Pulsed electric field reduces the permeability of potato cell wall", Bioelectromagnetics, Vol. 29, pp. 296-301, 2008.

[127] Y. Polevaya, I. Ermolina, M. Schlesinger, B. Z. Ginzburg, and Y. Feldman, "Time domain dielectric spectroscopy study of human cells:: II. Normal and malignant white blood cells", Biochimica et Biophysica Acta (BBA) - Biomembranes, Vol. 1419, pp. 257-271, 1999.

[128] M. Ginzburg and B. Z. Ginzburg, "Distribution of non-electrolytes in halobacterium cells I. Halobacterium marismortui", Biochimica et Biophysica Acta (BBA) - General Subjects, Vol. 584, pp. 398-406, 1979.

[129] A. Zmiri and B. Z. Ginzburg, "Extracellular space and cellular sodium content in pellets of Dunaliella parva (Dead Sea, 75)", Plant Science Letters, Vol. 30, pp. 211-218, 1983.

[130] T. L. Steck and J. A. Kant, "Preparation of impermeable ghosts and inside-out vesicles from human erythrocyte membranes", in Methods in Enzymology. Vol. Volume 31, L. P. Sidney Fleischer, Ed., ed: Academic Press, 1974, pp. 172-180.

[131] J. Kolb, S. Kono, and K. Schoenbach, "Nanosecond pulsed electric field generators for the study of subcellular effects", Bioelectromagnetics, Vol. 27, pp. 172-187, 2006.

[132] Y. Feldman, E. Polygalov, I. Ermolina, Y. Polevaya, and B. Tsentsiper, "Electrode polarization correction in time domain dielectric spectroscopy", Measurement Science and Technology, Vol. 12, pp. 1355-64, 2001.

[133] T. Sun, S. Gawad, N. Green, and H. Morgan, "Dielectric spectroscopy of single cells: time domain analysis using Maxwell's mixture equation", Journal of Physics D: Applied Physics, Vol. 40, pp. 1-8, 2007.

[134] J. Teissie, M. Golzio, and M. Rols, "Mechanisms of cell membrane electropermeabilization: a minireview of our present (lack of?) knowledge", Biochimica et Biophysica Acta (BBA) - General Subjects, Vol. 1724, pp. 270-280, 2005.

[135] V. Sukhorukov, H. Mussauer, and U. Zimmermann, "The effect of electrical deformation forces on the electropermeabilization of erythrocyte membranes in low-and high-conductivity media", Journal of Membrane Biology, Vol. 163, pp. 235-245, 1998.

[136] K. Müller, V. Sukhorukov, and U. Zimmermann, "Reversible electropermeabilization of mammalian cells by high-intensity, ultra-short pulses of submicrosecond duration", Journal of Membrane Biology, Vol. 184, pp. 161-170, 2001.

[137] I. Bernhardt, "Alteration of cellular features after exposure to low ionic strength medium", in Cell Electrophoresis, ed: CRC Press. Inc., 1994, pp. 163-179.

[138] W. Baldwin, B. Gregory, C. Osgood, K. Schoenbach, and J. Kolb, "Membrane Permeability and Cell Survival After Nanosecond Pulsed-Electric-Field Exposure—Significance of Exposure-Media Composition", IEEE Transactions on Plasma Science, Vol. 38, pp. 2948-2953, 2010.

[139]  A. Di Biasio and C. Cametti, "On the dielectric relaxation of biological cell suspensions: The effect of the membrane electrical conductivity", Colloids and Surfaces B: Biointerfaces, Vol. 84, pp. 433-441, 2011.

[140]  J. Teissie, N. Eynard, B. Gabriel, and M. Rols, "Electropermeabilization of cell membranes", Advanced drug Delivery Reviews, Vol. 35, pp. 3-19, 1999.

[141]  D. Stewart Jr, T. Gowrishankar, and J. Weaver, "Transport lattice approach to describing cell electroporation: use of a local asymptotic model", IEEE Transactions on Plasma Science, Vol. 32, pp. 1696-1708, 2004.

[142]  D. A. Stewart Jr, T. Gowrishankar, and J. C. Weaver, "Transport lattice approach to describing cell electroporation: use of a local asymptotic model", IEEE Transactions on Plasma Science, Vol. 32, pp. 1696-1708, 2004.

[143]  M. Schmeer, T. Seipp, U. Pliquett, S. Kakorin, and E. Neumann, "Mechanism for the conductivity changes caused by membrane electroporation of CHO cell-pellets", Physical Chemistry Chemical Physics, Vol. 6, pp. 5564-5574, 2004.

[144]  K. C. Melikov, V. A. Frolov, A. Shcherbakov, A. V. Samsonov, Y. A. Chizmadzhev, and L. V. Chernomordik, "Voltage-induced nonconductive pre-pores and metastable single pores in unmodified planar lipid bilayer", Biophysical Journal, Vol. 80, pp. 1829-1836, 2001.

[145]  K. Schoenbach, R. Joshi, S. Beebe, and C. Baum, "A scaling law for membrane permeabilization with nanopulses", IEEE Transactions on Dielectrics and Electrical Insulation, Vol. 16, pp. 1224-1235, 2009.

[146]  H. F. Cook, "Dielectric Behaviour of Human Blood at Microwave Frequencies", Nature, Vol. 168, pp. 247-248, 1951.

[147] C. Ramirez, E. Miller, D. Ullrey, and J. Hoefer, "Swine Hematology from Birth to Maturity. III. Blood Volume of the Nursing Pig", Journal of Animal Science, Vol. 22, pp. 1068-1074, 1963.

[148] B. Gradinski-Vrbanac, Z. Stojevic, S. Milinkovic-Tur, T. Balenovic, J. Pirsljin, and M. Zdelar-Tuk, "In vitro susceptibility of duck, chicken and pig erythrocyte lipids to peroxidation", Veterinarni Medicina-UZPI, Vol. 47, 2002.

[149] Y. Hayashi, I. Oshige, Y. Katsumoto, S. Omori, A. Yasuda, and K. Asami, "Dielectric inspection of erythrocyte morphology", Physics in Medicine and Biology, Vol. 53, p. 2553, 2008.

[150] P. Vernier, Y. Sun, M. Chen, M. Gundersen, and G. Craviso, "Nanosecond electric pulse-induced calcium entry into chromaffin cells", Bioelectrochemistry, Vol. 73, pp. 1-4, 2008.

[151] J. A. White, P. F. Blackmore, K. H. Schoenbach, and S. J. Beebe, "Stimulation of capacitative calcium entry in HL-60 cells by nanosecond pulsed electric fields", Journal of Biological Chemistry, Vol. 279, p. 22964, 2004.

[152] P. Gascoyne, R. Pethig, J. Satayavivad, F. F. Becker, and M. Ruchirawat, "Dielectrophoretic detection of changes in erythrocyte membranes following malarial infection", Biochimica et Biophysica Acta (BBA) - Biomembranes, Vol. 1323, pp. 240-252, 1997.

[153] X. Wang, Y. Huang, P. Gascoyne, F. Becker, R. Hölzel, and R. Pethig, "Changes in Friend murine erythroleukaemia cell membranes during induced differentiation determined by electrorotation", Biochimica et Biophysica Acta (BBA) - Biomembranes, Vol. 1193, pp. 330-344, 1994.

# VITA

## EDUCATION

- **Ph.D.** in Electrical and Computer Engineering                    *May 2012*
  Old Dominion University, Norfolk, VA, USA;

- **M.S.** in Biomedical Engineering                    *Jan 2007*
  Peking University, Beijing, China;

- **B.S.** in Electrical Engineering                    *Jun 2004*
  Xiamen University, Xiamen, China;

## SELECTED PUBLICATIONS

**J. Zhuang**, W. Ren, Y. Jing, J.F. Kolb, "Dielectric Evolution of Mammalian Cell Membranes after Exposure to Pulsed Electric Fields," IEEE Transactions on Dielectrics and Electrical Insulation, Vol. 19, no. 2, pp. 609-622, 2012.

D. Lv, **J. Zhuang**, H. Chen, J. Wang, Y. Xu, X. Yang, J. Zhang, X. Wang, and J. Fang, "Dynamic Contrast-Enhanced Magnetic Resonance Images of the Kidney," IEEE Engineering in Medicine and Biology Magazine, vol. 27, pp. 36-41, 2008.

**J. Zhuang**, K.H. Schoenbach, J.F. Kolb, "Time Domain Dielectric Spectroscopy of Biological Cells after Pulsed Electric Field Exposure," Proc. 2011 IEEE Conference on Electrical Insulation and Dielectric Phenomena, Oct 16-19, 2011, Cancun, Mexico, 44-47.

**J Zhuang**, K.H. Schoenbach, J.F. Kolb, "Modification of Dielectric Characteristics of Cells by Intense Pulsed Electric Field," Proc. 18th IEEE International Pulsed Power Conference, Jun 19-23, 2011, Chicago, IL, USA, in print.

J.F. Kolb, **J. Zhuang**, X. Chen, "Pulsed Discharges in Tissue," Proc. 18th IEEE International Pulsed Power Conference, Jun 19-23, 2011, Chicago, IL, USA, in print.

**J. Zhuang**, W.H. Baldwin, K.H. Schoenbach, J.F. Kolb, "Pulsed Electric Field Induced Changes in Dielectric Properties of Biological Cells," Proc. 2010 IEEE International Power Modulator and High Voltage Conference, May 23-27, 2010, Atlanta, GA, USA, 200 – 203.

**J. Zhuang**, W.H. Baldwin, K.H. Schoenbach, J.F. Kolb, "Pulsed Electric Field Induced Changes in Dielectric Properties of Biological Cells," Proc. 2009 IEEE International Pulsed Power Conference, June 29 - July 2, 2009, Washington, DC, USA, 1008 – 1013.